Thèse d'habilitation à diriger des recherches
Contribution en Signal, Image et Instrumentation pour l'Astronomie

Annexe C. Etude d'étoiles Am binaires spectroscopiques

Habilitation thesis, "Accreditation to supervise research"
Contribution to Signal, Image & Instrumentation in Astronomy

Appendix C. Study of spectroscopic binary Am-type stars

Jean-Louis Prieur

Version March 31, 2014

Mots clés:
Etoiles: Am, paramètres fondamentaux, marées
Binaires: spectroscopiques, orbites
Techniques: spectroscopie, vitesses radiales

Keywords:
Stars: Am, fondamental parameters, tides
Binaries: spectroscopic, orbits
Techniques: spectroscopy, radial velocities

Contents

Chapter I

Objectives and methods

I.1 Presentation of the program

From 1999, I collaborated with the "Spectroscopic Binaries" group of Observatoire Midi-Pyrénées. I present here the results we obtained concerning the study of Am-type binary stars. It is the last part of an extensive program whose purpose was to study to determine the frequency and properties of binaries in this stellar family (hot stars with metallic lines of Am-type).

This program was devoted to the search and the consequent study of spectroscopic binaries (SB) in a large sample (about one hundred objects) of chemically peculiar stars of type Am.

Many Am stars are known to belong to binary systems and it seems that multiplicity plays a key role, although poorly understood, in the formation of Am stars. Some basic questions still to be addressed are: do all Am stars belong to binary systems and what is the influence of tidal effects in those binary systems? The origin of their peculiarities could be a chemical segregation in the atmosphere caused by radiative diffusion favoured by a slow rotational velocity (Michaud al., 1983). Whereas spin breaking is difficult to explain for isolated stars, an efficient process exists for close binary systems. Indeed tidal effects tend to synchronize the spin and the orbital velocities, which generally corresponds to a strong breaking of the initial spin velocities.

As presented in the first paper of this series (Ginestet & Carquillat, 1998), our program started in 1992 and aimed at determining the binarity rate among a large sample of Am stars (about one hundred objects) and, when possible, computing their orbital elements in order to derive orbital and physical parameters of the systems and study the occurrence of circularized and synchronized orbits. The main goals of this investigation were:

(i) to discover new spectroscopic binaries among Am stars and determine their orbits and physical properties,

(ii) to estimate the ratio of SBs and stars with constant radial velocity (RV) in the sample,

(iii) to provide new material about tidal interaction and the related question of the implication of binaries in Am phenomenon.

Our sample of 91 Am stars, was mainly constituted from the Third Catalogue of Am Stars with Known Spectral Types (Hauck, 1986). Our main purpose was to bring some observa-

tional arguments about the implication of binaries in Am phenomenon. To do so, we wanted to:

(i) search for all the SBs in this sample and derive the rate of Am stars belonging to SBs,

(ii) monitor the radial velocities of SBs found in the sample and determine their orbital parameters and physical properties of the stellar components,

(iii) study the importance of tidal interaction in those systems, that may lead to the circularisation of the orbits and to the spin-orbit synchronization.

Our program concerns a large sample of Am-type stars, described in Ginestet & Carquillat (1998), that was mainly selected from the "Third catalogue of Am stars with known spectral types" (Hauck, 1986). When we started this study, none of the 91 stars of our sample had known SB orbital elements. Most of the orbits were then determined and published by our team (J.-M. Carquillat, N. Ginestet, A. Pédoussaut and J.-L. Prieur) or in collaboration with colleagues of Marseille (France), Cambridge (U.K.) and Geneva (Swiss). Marseille (M. Imbert), Cambridge (R.F. Griffin) and Geneva (S. Udry and J.-Y. Debernardi).

The results of this study were published in a series of eight papers (see Table I.1). Papers I to IV concerned the most peculiar binaries first detected in the sample, such as double-lined (SB2) and multiple systems. Paper V was devoted to the radial velocity study of eight single-lined (SB1) short-period ($P \leq 10$ days) spectroscopic binaries, namely HD 341, 55822, 61250, 67317, 93991, 162950, 224890, and 225137. Paper VIII dealt with statistics about the whole programme.

Table I.1: Series of the papers devoted to the search for binarity among our sample of Am-type stars.

Name	Stars	Reference
Am-PaperI	HD 125273	Ginestet & Carquillat (1998)
Am-PaperII	HD 81976, HD 98880	Carquillat et al. (2001)
Am-PaperIII	HD 7119	Carquillat et al. (2002)
Am-PaperIV	HD 100054 B, HD 187258	Ginestet et al. (2003)
Am-PaperV	HD 341, 55822, 61250, 67317, 93991 162950, 224890, 225137	Carquillat et al. (2003b)
Am-PaperVI	HD 19342, 19910, 36360, 102925, 126031, 127263, 138406, 155714, 195692, 199360	Carquillat et al. (2004)
Am-PaperVII	HD 3970, 35035, 93946, 151746, 153286, 204751, 224002	Prieur et al. (2006b)
Am-PaperVIII	HD 32893, 60489, 109762, 111057, 113697, 204918, 219675 and BD+44°4512	Carquillat & Prieur (2007c)

Am-PaperI *"Contribution à l'étude de la binarité des étoiles de type Am: I. HD 125273, binaire spectroscopique à raies doubles"*
Ginestet N., Carquillat J.-M., 1998, A&AS 130, 415

Am-PaperII *"Contribution to the search for binaries among Am stars. II. HD 81876 and HD 98880, double-lined spectroscopic binaries."*
Carquillat J.-M., Ginestet N., Prieur J.-L., 2001, Astron. & Astrophys., 369, 908–914

Am-PaperIII *"Contribution to the search for binaries among Am stars. III. HD 7119, a double-lined spectroscopic binary and a triple system"*
Carquillat J.-M., Ginestet N., Prieur J.-L., Udry S., 2002, MNRAS, 336, 1043–1048

Am-PaperIV *"Contribution to the search for binaries among Am stars. IV. HD 100054 B and HD 187258"*
Ginestet N., Prieur J.-L., Carquillat J.-M., Griffin R.F., 2003, MNRAS, 342, 61–68.

Am-PaperV *"Contribution to the search for binaries among Am stars. V. Orbital elements of eight short-period spectroscopic binaries"*
Carquillat J.-M., Ginestet N., Prieur J.-L., Debernardi Y., 2003b, MNRAS, 346, 555–564.

Am-PaperVI *"Contribution to the search for binaries among Am stars. VI. Orbital elements of ten new spectroscopic binaries, implications on tidal effects"*
Carquillat J.-M., Prieur J.-L., Ginestet N., Oblak E., Kurpinska-Winiarska M., 2004, MNRAS, 352, 708–720.

Am-PaperVII *"Contribution to the search for binaries among Am stars. VII. Spectroscopical orbital elements of seven new spectroscopic binaries, implications on tidal effects"*
Prieur J.-L., Carquillat J.-M., Imbert M., 2006, MNRAS, 372, 703–714

Am-PaperVIII *"Contribution to the search for binaries among Am stars. VIII. New spectroscopic orbits of 8 systems and statistical study of a sample of 91 Am stars"*
Carquillat J.-M., Prieur J.-L., 2007, MNRAS, 380, 1064–1078

I.2 Am stars: brief theory

Am stars are chemically peculiar hot stars of type A whose spectra show an over-abundance of heavy elements and an under-abundance of calcium. It is now generally admitted that such anomalies are the consequence of chemical element segregation in the outer layers of those stars.

Observational studies (Abt, 1961, 1965; Abt & Levy, 1985) have shown that most Am stars belonged to close binary systems and that all Am stars have small rotational velocities, with $v_e \sin i < 100$ km.s^{-1}, smaller than the normal A stars. Abt (1961) first suggested that tidal interaction with the companion could be at the origin of the Am phenomenon, through the spin-orbit synchronism which reduces the axial rotation of the stars. Nevertheless Abt & Levy (1985) found that there existed isolated Am stars and that another process had to be invoked to explain their small rotational velocities.

According to the model proposed by Michaud (1980) and Michaud al. (1983), small rotational velocities are required to allow helium to settle gravitationally rather quickly after the star has reached the main sequence (a few 10^6 yr only), producing the vanishing of the HeII convection zone existing in A stars that blocks the diffusion of the chemical elements from the deep layers. After this disappearance, the diffusion can proceed higher in the star, at the bottom of the H-HeI convection zone, where Ca is in the Ar configuration (i.e. CaII) and so has a small g_{rad}, causing an under-abundance of Ca that is observed in the spectra of the Am stars. This model is also called "superficial model", since the separation of chemical elements occurs close to the surface of the star and implies that only a small proportion of the star would have anomalous abundances during the main sequence ($\sim 10^{-10}\ M_\star$).

A modified version of this model called "evolution model" was recently proposed by Richer et al. (2000) and Michaud al. (2005) in which the separation of elements occurs deeper in the star, at a radius where Ca is in the Ne configuration (i.e. CaX), which also corresponds to a small value of g_{rad}(Ca), causing Ca under-abundances. In this case, anomalous abundances would affect a larger fraction of the stellar mass while the star is on the main sequence ($\sim\ 10^{-5}\ M_\star$), and thus would survive after the turn-off. Thus, contrarily to the superficial model, the evolution model would naturally explain the existence of evolved Am stars, similar to o Leo found by Griffin (2002).

Note that hydrodynamical codes based on those two models tend to produce too large abundance anomalies, when only atomic diffusion is considered. There is a need of introducing a competing process whose nature has been a matter of debate in the last thirty years. A possibility would be to improve the treatment of turbulence with the introduction of anisotropy in the vertical transport as suggested by a recent work by Talon et al. (2006) who manages to reproduce observed Am spectra with a self-consistent model.

I.3 CORAVEL measurements

Although this programme was initiated with conventional spectrographs in the years 1980, most of observations were done after 1992 with the CORAVEL instrument (Baranne, 1979). mounted at the Cassegrain focus of the 1-m Swiss telescope at the *Observatoire de Haute-Provence* (OHP). After 2000, many measurements were also obtained with another version of the CORAVEL instrument, that is mounted on the coudé focus of the 91-cm telescope at the Cambridge Observatories, thanks to the collaboration of R.F. Griffin. (e.g. Ginestet et al. (2003); Carquillat et al. (2004); Carquillat & Prieur (2007c))

CORAVEL is a spectrophotometer that allows measurements of heliocentric radio-velocities (RVs) by performing a cross-correlation of the stellar spectrum with a physical mask placed in the focal plane of the spectrograph (Baranne, 1979). Although CORAVEL was designed to be efficient for observing cool stars, with spectral types later than F4, it also permits to measure RVs of hotter stars which rotate slowly ($v_e \sin i < 40$ km.s^{-1}) and exhibit metallic lines in their spectrum, such as Am stars.

Fig. II.4 shows an example of the correlation dips observed for the primary and secondary components of HD 7119. In the case of the OHP observations, Gaussian functions are fitted to the cross-correlation dips to derive radial velocities (Baranne, 1979); Cambridge traces are cross-correlated with functions derived from one that was empirically established from observations of practically non-rotating stars by convolving it with a broadening function to mimic stellar rotation. The mean internal standard error of the measurements depends upon the depth and the width of the correlation dip. The latter is strongly correlated with the rotational velocity $v_e \sin i$. A smaller rotational velocity induces a sharper CORAVEL correlation dip, which in turn leads to a more accurate computed radial velocity. In fact, as shown by Benz & Mayor (1981), the projected equatorial velocity $v_e \sin i$ of each detected stellar component can be derived from the analysis of the CORAVEL correlation dips.

Some measurements have to be discarded when the correlation dips are blended. For example in the case of HD 7119, the width of these dips was about 10 km/s, and the radial velocity separation of two components had to be larger than $\sim$20 km/s to allow reliable measurements (Carquillat et al., 2001).

For SB2's, the magnitude difference of the two components can be inferred from the value of the ratio of the integrated areas of the CORAVEL dips (Lucke & Mayor, 1980). For HD 98880 for instance, we obtained $\Delta m_B = 1.25 \pm 0.1$ mag (Carquillat et al., 2001).

I.4 Orbit determination

The theory and the full description of the programs we used for computing the orbits of spectroscopic binaries are presented in Annexe B.

I.4.1 Non-linear least-squares programs

The orbital elements of the single and double lined binaries (*SB1* and *SB2*) were computed with the least-square programs `BS1.for` and `BS2.for` respectively. Those programs were written by R. Nadal in the early 1980's (Nadal et al, 1979), but I revised them completely in 1999.

For some objects, like HD 7119 (see Carquillat et al. (2002)), the residuals $(O-C)_{01}$ were very large, and not randomly distributed when plotted as a function of time. For HD 7119, their standard deviation of the residuals was $\sigma(O-C)_{01} = 1.7$ km.s^{-1}, which was more than twice the mean error of the radial velocity measurements (see Carquillat et al. (2002)). This generally reveals the presence of a perturbing third body. To handle the case of triple systems, I wrote two programs (`BS3.for` and `BS4.for`, for double or single spectrum detection, respectively) that simultaneously fit the two orbits of the visible and suspected components.

I.4.2 Initial guess of the period

Actually the main difficulty consists of finding the preliminary elements that are required for linearising the problem and starting the first iteration of the least-square minimisation performed by `BS1.for`, `BS2.for`, etc.

In the first papers of this series, the preliminary values of the periods needed by those programs, were found "manually" by a guess-and-try procedure. The selecting criterion was that the corresponding phase diagram (RV versus phase) had to look like that of a radial velocity orbit. In practice, it had to look like one of those printed in our catalogue of curves obtained with a simulation program. The other preliminary elements were then taken equal to the parameters corresponding to the most similar curve found in that catalogue.

In 2002 (for Paper V) we improved this procedure by using a new program, SB_INITIAL, that computes preliminary elements, provided that the period is approximately known. This program is based on the method proposed by Imbert (1975). A Fourier series development is calculated with a least-squares minimisation of the data in the phase diagram corresponding to the preliminary period. We limit this development to the first 4 or 6 terms and then use the relations found by Imbert that express the orbital elements as a function of the first terms of the Fourier coefficients.

In 2004 (for Paper VI), we developed a new program PERIOD_RESID that allowed an automatic determination of all preliminary elements, including the period. We only have to select the interval of possible values for the period and the step that is to be used to explore this range. For each value, the program constructs a phase diagram, determines preliminary elements with SB_INITIAL and then calls BS1 to derive more accurate orbital elements (if possible) and the r.m.s. residual of this orbit. A good (preliminary) value for the period corresponds to the value which leads to the smallest residuals, compatible with the measurement errors. We have found that this program was very efficient for all the objects we have

processed so far. On a PC, only a few minutes are generally required to find the period of an unknown system with PERIOD_RESID, and a few seconds more are needed by BS1 to obtain the final elements, the postscript curves and the LaTeX tables, that can been used in a paper like this one.

I.4.3 Circular orbits

Because of observational errors, a spectroscopic orbit with a truly circular orbit will be found to have an elliptical orbit of small, but non-zero, eccentricity.

When the eccentricity of the calculated orbit was found very close to zero, we computed another orbit assuming it was circular (by setting $e = 0$) and compared the residuals obtained in the two cases. We evaluated the validity of setting the eccentricity to zero by applying the Lucy & Sweeney (1971)'s statistical test. For example, for the short period systems HD 93946 and HD 151746 studied in Prieur et al. (2006b), this test led us to consider as significant, although very small, the eccentricity of the HD 93946 orbit and to adopt a circular orbit for HD 151746.

I.4.4 Mass function

The orbital parameters determined with spectroscopic orbits lead to the determination of the *mass function* $f(m)$. As shown in Annexe B, in the case of a single detection (*SB1*), it is:

$$f(m) \equiv \frac{M_2^3 \sin^3 i}{(M_2 + M_1)^2} = \frac{K_1^3 P (1 - e^2)^{-3/2}}{2\pi G} \tag{I.1}$$

In the case of an *SB2*, it is:

$$f(m) = \frac{M_2^3 \sin^3 i}{M_2^2 (1 + M_1/M_2)^2} = \frac{M_2 \sin^3 i}{(1 + K_2/K_1)^2} \tag{I.2}$$

where G is the gravity constant; M_1 and M_2 are the masses of the primary and secondary components, respectively; K_1 and K_2 are the amplitudes of the radial velocity oscillations in the phase diagram of those two components; e and P are the eccentricity and period of the orbit. The full description of those parameters and the demonstration of those relations are given in Annexe B.

In Paper VIII (see II.7.8), we used another version of Eq. (I.1):

$$f(m) = M_1 \sin^3 i \, \mu^3/(1 + \mu)^2 \tag{I.3}$$

where $\mu = M_2/M_1$ is the mass ratio of the components (1 = primary, 2 = secondary).

I.5 Strömgren photometry

I.5.1 Introduction

Spectrophotometric measurements around the wavelength of the Balmer discontinuity can be used for two-dimensional stellar classification as shown for instance by Barbier & Chalonge (1939). A practical implementation was proposed by Strömgren (1956); Crawford (1966)), through their "Strömgren photometric system". This system uses the filters u, v, b, y, β whose characteristics are given in Table I.2 (see also Fig. I.1).

- The u-band (ultra-violet) is located entirely below the Balmer discontinuity and above the atmospheric cutoff. Its is wide enough to fill most of the region between those two wavelengths.
- The v-band (violet) is located above the Balmer discontinuity, in the region where blanketing is strong. The Hδ line is near the center of this band.
- The b (blue) and y (yellow) bands are located above the point (around 450 nm) where blanketing absorption due to heavy elements becomes important (for stars hotter than the Sun). As a result, the $b - y$ color is rather free of blanketing effects, considerably more than the $B - V$ index of the Johnson UBV system.
- The y band is located at 550 nm, the same central wavelength as the Johnson V band. As there are generally no strong feature in the V bandpass, an y magnitude measure can be accurately transformed to the V-magnitude of the Johnson system.

For more information about the interest of those bandwidths, see Crawford (1975).
Four indices were derived from the u, v, b, y, β measurements obtained with those filters:

- $(b - y)$ to measuring Paschen continuum.
- $m_1 = (v - b) - (b - y)$ measuring line blanketing, is sensitive to metallicity $[Fe/H]$
- $c_1 = (u - v) - (v - b)$ ("color difference") indicating the magnitude of the Balmer discontinuity, is sensitive to the surface gravity g
- $\beta = \beta_{\text{narrow}} - \beta_{\text{wide}}$ measuring the strength of Hβ absorption line.

The color index $(b - y)$ is sensitive to stellar temperature T_{eff}, but it was found that β is a better parameter to use for measuring this temperature (Crawford (1975) p 956). It appears that β is the primary parameter for measuring the absolute magnitude for B-type stars and the temperature for A- and F-type stars whereas c_1 is the primary parameter for measuring the temperature for B-type stars and the absolute magnitude for A- and F-type stars (see e.g., Crawford (1979), p 1858).

When adding the V magnitude derived by the y filter measurement, one obtain five parameters $(V, (b - y), m_1, c_1, \beta)$ that were shown to fully characterize the physical description of the measured star: apparent and absolute brightness (hence its distance), temperature measure (from accurate calibrations with spectral type), and $[Fe/H]$ abundance. From a combination of these, one also gets an estimate of the age of the star, through stellar evolution model calibrations (see e.g. Fig. I.5).

	u	v	b	y	β_{narrow}	β_{wide}
λ_{cent}	350	411	467	547	485.8	485
Half-width	30	19	18	23	2.9	12.9

Table I.2: Filters used in the Strömgren photometric system (wavelengths in nm).

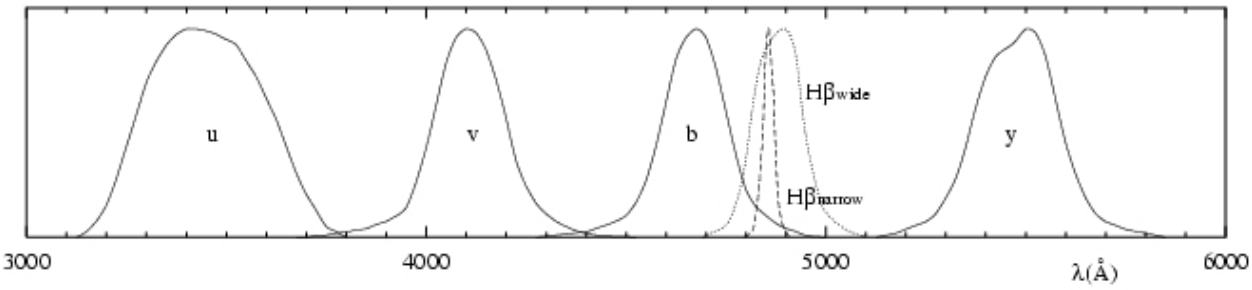

Figure I.1: Transmission of the filters u, v, b, y used in the Strömgren photometric system.

Investigations on interstellar reddening effects have established to the following relations (Crawford, 1975):

$$E(b-y) \approx 0.73\,E(B-V), \quad E(m_1) \approx -0.3\,E(b-y) \text{ and } E(c_1) \approx 0.2\,E(b-y) \quad \text{(I.4)}$$

The convention is generally to use the subscript 0 for reddening corrected indices (Crawford, 1979). Therefore, the correction of the observed measurements $(m_1)_{obs}$ and $(c_1)_{obs}$ is:

$$(m_1)_0 = (m_1)_{obs} + 0.3\,E(b-y) \quad \text{and} \quad (c_1)_0 = (c_1)_{obs} - 0.2\,E(b-y) \quad \text{(I.5)}$$

The β parameter that measures a line strength only is unaffected by interstellar reddening.

I.5.2 Metallicity index

The m_1 index is particularly useful for determining abundance differences from star to star, such as $[Fe/H]$ for example. Crawford (1975) introduced the *blanketing parameter*:

$$\delta m_1 = m_1(standard) - (m_1)_0 \quad \text{for a given } \beta$$

where $m_1(standard)$ is the m_1 index value of a star belonging to the Hyades cluster with the same β index as the observed star. This parameter is null when the observed star has the same blanketing as the Hyades stars.

In practice, we used the following notation:

$$\delta m_1(\beta) = m_{1,hyades}(\beta) - (m_1)_0 \quad \text{(I.6)}$$

where $m_{1,hyades}(\beta)$ is the expected index corresponding to the β measurement, using the calibration established for the Hyades cluster A-type stars by Crawford (1979). To estimate this value for each β measurement, we interpolated Crawford's calibration table (Tab. I.3) in the program `indices_Astars.for` (see Sect. A.1). This parameter $\delta m_1(\beta)$ used for measuring blanketing differences, has been calibrated for deriving $[Fe/H]$ (see Fig. I.2).

I.5.3 Interstellar reddening

In a manner similar to that used for δm_1, Crawford (1975) introduced the difference δc_1, but with an opposite sign:

$$\delta c_1(\beta) = (c_1)_{obs} - c_{1,hyades}(\beta) \tag{I.7}$$

where $c_{1,hyades}$ is the c_1 index value of a star belonging to the Hyades cluster with the same β index as the observed star (Tab. I.3).

From Crawford (1979)'s calibration, we can compute the expected value of $(b-y)_0$:

$$\begin{cases} (b-y)_0 = 2.946 - \beta - 0.1\,\delta c_1(\beta) - 0.25\,\delta m_1(\beta) & \text{if} \quad \delta m_1 < 0 \\ \\ (b-y)_0 = 2.946 - \beta - 0.1\,\delta c_1(\beta) & \text{if} \quad \delta m_1 > 0 \end{cases} \tag{I.8}$$

The interstellar reddening is then given by:

$$E(b-y) = (b-y) - (b-y)_0$$

This value can then be used for correcting $(m_1)_{obs}$ and $(c1)_{obs}$ with Eq. refeq:stromgren-redcorrection. This allows a new computation of δm_1 and δc_1 (Eqs. I.6 and I.7). Then we update the reddening values using Eq. I.8, and go on... It is thus necessary to perform a few iterations until all the equations of this section are satisfied simultaneously. This is done in my program `indices_Astars.for` (Sect. A.1). An example of reddening correction is given in Table I.4.

I.5.4 Luminosity

Crawford (1979) derived a calibration of the absolute M_v versus β, limited to the ZAMS A-type stars, that is shown in Table I.3.

The parameter δc_1 can then be used for checking that this calibration is valid for the measured star. If it is too large, the Balmer discontinuity c_1 that is measured is too different from that of the calibration star with the same β value. In that case, $M_v(\beta)$ is not relevant, and should not be used. Crawford (1979) found that the limit of validity of his calibration was $\delta c_1 < 0.28$.

I.5.5 Derivation of $T_{\rm eff}$, $\log g$ and $[Fe/H]$

When $ubvy, \beta$ Strömgren photometry was available for the Am-type stars we studied, we derived the quantities $T_{\rm eff}$ and $\log g$ using the $(c_1)_0$ versus β grids of Moon & Dworetsky (1985) For $\log g$ determination, we applied the correction for metallicity proposed by Dworetsky & Moon (1986) for Am stars.

The parameter $[Fe/H]$ was estimated from the δm_1 versus $[Fe/H]$ correlation, using Cayrel's calibration $[Fe/H] = 0.2 - 10\,\delta_{m1}(\beta)$ (Crawford, 1975) (see Fig. I.2).

β (mag.)	$m_1(\beta)$ (mag.)	$c_1(\beta)$ (mag.)	M_V(ZAMS,β) (mag.)
2.88	0.93	0.200	2.30
2.86	0.89	0.205	2.50
2.84	0.85	0.208	2.64
2.82	0.82	0.206	2.70
2.80	0.78	0.203	2.76
2.78	0.74	0.196	2.82
2.76	0.70	0.188	2.88
2.74	0.66	0.182	2.96
2.72	0.60	0.177	3.10

Table I.3: Calibration of Strömgren photometry: standard relations for A-type stars established for the Hyades cluster by Crawford (1979). In column 4, M_V is the V absolute magnitude of calibrating stars located in the ZAMS (Zero Age Main Sequence).

HD	β	$b-y$	$E(b-y)$	m_1	$(m_1)_0$	c_1	$(c_1)_0$	$(\delta m_1)_0$
19342	2.73	0.31	0.10	0.20	0.23	0.77	0.75	-0.05
19910	2.81	0.19	0.04	0.20	0.21	0.73	0.72	-0.01
36360	2.80	0.16	0.01	0.24	0.24	0.81	0.81	-0.04
126031	2.74	0.20	−0.01	0.23	0.23	0.66	0.67	-0.04
127263	2.83	0.14	−0.01	0.28	0.28	0.80	0.80	-0.07
155714	(2.72)	0.23	0.01	0.19	0.19	0.68	0.67	-0.01
195692	(2.78)	0.16	0.00	0.21	0.21	0.76	0.76	-0.01
199360	(2.81)	0.18	0.03	0.25	0.26	0.74	0.73	-0.06

Table I.4: Strömgren photometry β, $(b-y)$, m_1, c_1 of Am-type stars: example of reddening correction using `indices_Astars.for`. From Carquillat et al. (2004).

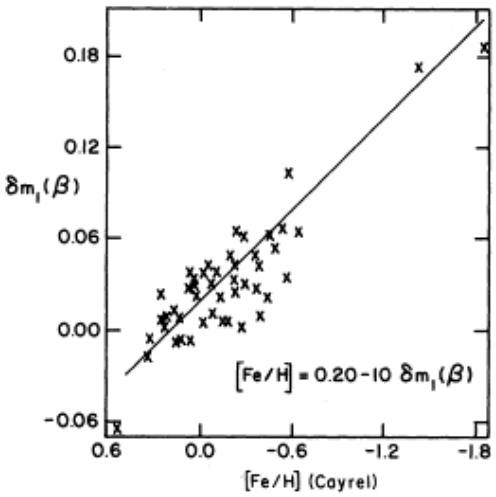

Figure I.2: Strömgren photometry: $\delta m_1(\beta)$ versus $[Fe/H]$ of F-type stars compared to Cayrel's correlation formula. From Crawford (1975).

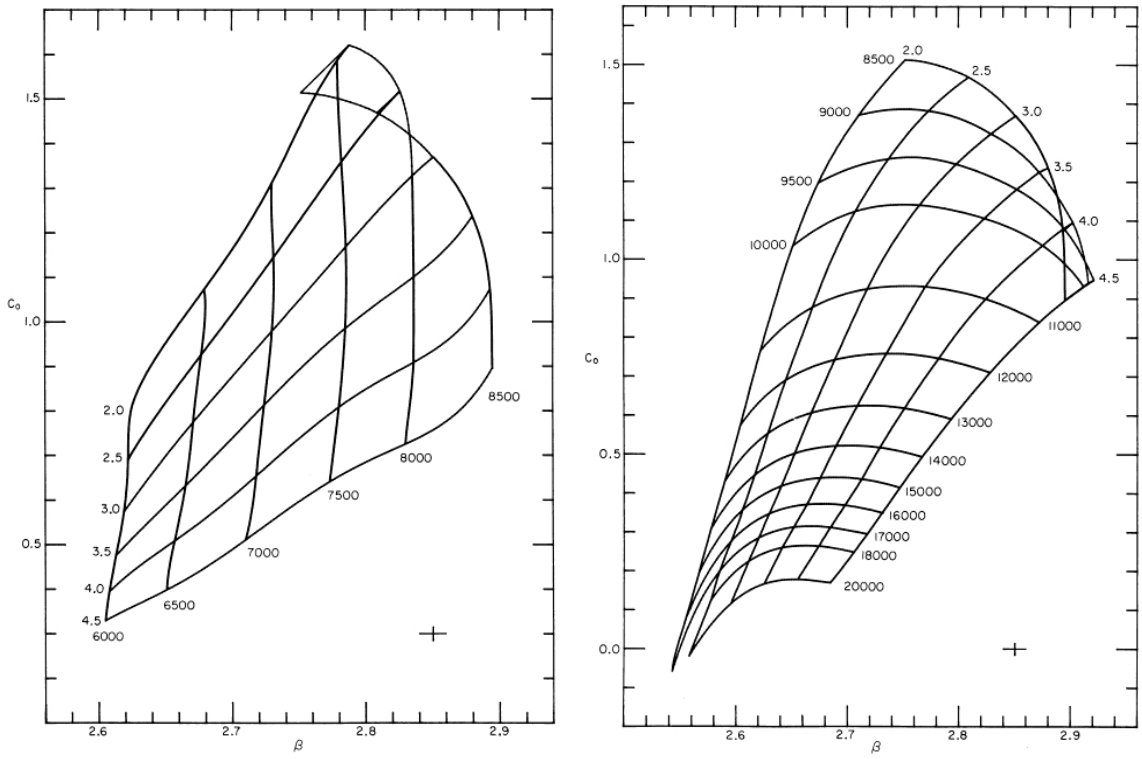

Figure I.3: Theoretical grids ($T_{\rm eff}$, $\log g$) of Kurucz' models in the Strömgren $(c_1)_0$ versus β diagram. From Moon & Dworetsky (1985).

I.6 Determination of physical parameters

I.6.1 Method used for deriving stellar physical parameters

For deriving the physical parameters for the stars we studied (e.g., in PaperV, PaperVI, and PaperVII), we proceeded as follows:

1 – From Hipparcos parallaxes π (ESA , 1997), we obtained the distances and the visual absolute magnitudes of the systems and their errors.

2 – When $ubvy, \beta$ Strömgren photometry was available, (cf. Sect. I.5), we derived $T_{\rm eff}$, $\log g$, and $[Fe/H]$ as described in Sect. I.5.5. When Strömgren photometry was not available, the effective temperature $T_{\rm eff}$ was based upon the $B-V$ index and Flower (1996)'s calibration.

3 – From M_V, we computed $M_{\rm bol}$ using the bolometric correction tabulated by Flower (1996) (see Table I.5). From $M_{\rm bol}$ and $T_{\rm eff}$ we estimated the theoretical radius of the stars, as shown in Sect. I.6.4.

4 – Finally, we reported the positions of the stars in the theoretical Hertzsprung-Russell diagram, $\log(L/{\rm L}_\odot)$ versus $\log T_{\rm eff}$, from Schaller et al. (1992), completed with the isochrones computed by Meynet et al. (1993) (e.g. Fig. II.18). The positions of the stars in this diagram lead to theoretical estimates of their masses M_1 and ages (see Sect. I.6.5).

I.6.2 Absolute luminosity

M_V from Hipparcos data only

For HD 7119 that we studied in PaperIII (Carquillat et al., 2002), Strömgren photometry was not available. For determining M_V, we only used data from Hipparcos (ESA , 1997): $V = 7.57$, $B-V = 0.34$, $\varpi = 3.38 \pm 0.93$ mas. HD 7119 is at a distance of $d = 300$ (+110, -70) pc. Using galactic charts from Lucke (1978) (see Fig. I.4), we we estimated the reddening correction due to interstellar absorption as $E(B-V) \approx 0.06$ mag for HD 7119 (first level at 0.2 mg/kpc multiplied by 0.3 kpc). The de-reddenned color index is then $B-V = 0.34 - E(B-V) = 0.28$, and the interstellar absorption is

$$\mathrm{A}_V \approx 3\,\mathrm{E}(B-V) \tag{I.9}$$

The global apparent magnitude corrected for this absorption is then:

$$m_V = V - \mathrm{A}_V = V - 3\,\mathrm{E}(B-V) \tag{I.10}$$

For HD 7119 we find $m_V = 7.39$ mag.
We have then, from Pogson's law (see Annexe B):

$$M_V = m_V + 5\log\varpi + 5 \tag{I.11}$$

The global absolute magnitude of HD 7119 is then: $M_V = 0.035$.

Photometry of the binary components from global values

Global V photometry was available for all the Am systems we studied, and in particular m_V was known. In the case of SB2's the difference of V magnitude could be determined from the CORAVEL correlation dips (Lucke & Mayor, 1980). We show in this section how we estimated the absolute V magnitudes of each component.

When M_V is known, the global bolometric magnitude of the system can be derived by applying a bolometric correction C_V (see Table I.5 from Flower (1996)):

$$M_{bol} = M_V + C_V \tag{I.12}$$

Since $L_\odot = 4.75$ (Schmidt-Kaler, 1982), the intrinsic luminosity $L/L_\odot$ is related to the absolute bolometric magnitude M_{bol} as:

$$M_{bol} = -2.5 \log L/L_\odot + 4.75 \tag{I.13}$$

Therefore:

$$\log L/L_\odot = 1.9 - 0.4 M_{bol} \tag{I.14}$$

The two components (with indices 1 and 2) contribute to this global luminosity as $L = L_1 + L_2$, and therefore:

$$M_V = -2.5 \log(L_1 + L_2) - C_V + 4.75 \quad \text{and} \quad M_{V2} - M_{V1} = -2.5 \log(L_2/L_1) \tag{I.15}$$

where L_1 and L_2 are in $L_\odot$ units

$$L_1 + L_2 = 10^{-0.4\, M_V - C_V - 4.75} \quad \text{and} \quad L_2/L_1 = 10^{-0.4\, \Delta m_V} \tag{I.16}$$

Finally:

$$L_1 = \frac{10^{-0.4\,(M_V - C_V - 4.75)}}{(1 + 10^{-0.4\,\Delta m_V})} \quad \text{and} \quad L_2 = \frac{10^{-0.4\,(M_V + \Delta mV - C_V - 4.75)}}{(1 + 10^{-0.4\,\Delta m_V})} \tag{I.17}$$

$$M_{V1} = -2.5 \log L_1 + 4.75 - C_V \quad \text{and} \quad M_{V2} = -2.5 \log L_2 + 4.75 - C_V \tag{I.18}$$

For HD 7119, $C_V = -0.1$, and $M_V = 0.035$ (see Sect. I.6.2). As we measured $\Delta m_V = 0.7$ from the CORAVEL correlation dips, those relations lead to $M_{V1} = 0.69$ and $M_{V2} = 1.39$.

M_V from $ubvy\beta$ Strömgren photometry and Hipparcos parallax

When β was available, the de-reddened indices $(b-y)_0$, $(m_1)_0$, $(c_1)_0$ and $(\delta m_1)_0$ were computed with Crawford (1975, 1979)'s formulae, as explained in Sect. I.5.3. The colour-excess was then derived with the relation established by Crawford (1975):

$$\mathrm{E}_{B-V} = \mathrm{E}_{b-y}/0.73 \tag{I.19}$$

When β was not known, E_{B-V} was estimated from Lucke (1978)'s opacity maps and the distance deduced from the parallax. Then the same relation allowed to retrieve E_{b-y} which we could use to correct the Strömgren indices for reddening effects.

The values found for E_{B-V} are then used to correct the apparent visual magnitudes m_V for the interstellar absorption $\mathrm{A}_V \approx 3\,\mathrm{E}_{B-V}$ (Eq. I.9). When the Hipparcos parallaxes ϖ were available those corrected m_V magnitudes allowed the computation of the absolute magnitudes M_V with Eq. I.11

$\log_{10} T_{\rm eff}$ (K)	4.7	4.6	4.5	4.4	4.3	4.2	4.1	4.0	3.9	3.8	3.7	3.6	3.5
C_V	-4.5	-3.9	-3.1	-2.5	-1.9	-1.4	-0.84	-0.25	+0.03	-0.01	-0.3	-1.2	-3.8
$B-V$	-0.34	-0.32	-0.30	-0.27	-0.23	-0.19	-0.13	-0.03	0.17	0.49	0.91	1.50	1.76

Table I.5: Bolometric correction C_V and $B-V$ index as a function of $T_{\rm eff}$ for main sequence stars. From Flower (1996).

M_V from $ubvy\beta$ Strömgren photometry only

In Paper VIII, for HD 109762, whose parallax was not measured by Hipparcos, we estimated its absolute magnitude from the Strömgren photometry only. We used the calibration derived by North et al. (1997) from a sample of stars of types A and Am observed by Hipparcos:

$$M_V = 12.6 - 3.7\,\beta - 8.3\,(\delta c_1)_0 + 6.5\,(\delta m_1)_0 + 7.2\,10^{-6}\,(v_e \sin i)^2.$$

I.6.3 Effective temperature from $B-V$ color index

When Strömgren photometry was not available, we used the empirical calibration proposed by Flower (1996) that gives $T_{\rm eff}$ as a function of $B-V$ (see Table I.5). The reddening correction $E(B-V)$ due to interstellar absorption was estimated from the galactic charts of Lucke (1978) (see Fig. I.4).

For example, for HD 7119, we estimated $T_{\rm eff} \approx 7500$ K, on the basis of a de-reddened colour index $B-V = 0.28$ (Carquillat et al., 2002).

I.6.4 Stellar radius

The stellar radii can be estimated from $L/L_\odot$ and $T_{\rm eff}$ using Stefan's law, assuming that the stars radiate as black bodies, as calibrated by (Schmidt-Kaler, 1982):

$$\log R/R_\odot = -0.2 M_{\rm bol} - 2\log T_{\rm eff} + 8.47 \qquad \text{(I.20)}$$

As $M_{bol} = -2.5\,\log L/L_\odot + 4.75$ (Eq. I.13), we have:

$$\log R/R_\odot = 0.5\log L/L_\odot - 2\log T_{\rm eff} + 7.52 \qquad \text{(I.21)}$$

I.6.5 Masses and ages

The lack of knowledge of the orbital inclination i forbids a direct determination of the component masses from the mass function $f(m)$ derived from the spectroscopic orbits (see Sect. I.4.4). To estimate the stellar masses, we used Schaller et al. (1992)'s theoretical HR diagram with evolution tracks, and the isochrones given by Meynet et al. (1993) (see Fig. I.5). To position the stars in this diagram, we determined their effective temperature $T_{\rm eff}$ and intrinsic luminosity $L/L_\odot$ using the method described in Sect. I.6.1. Most of the Am stars we studied lay in the main-sequence domain and showed different degrees of evolution.

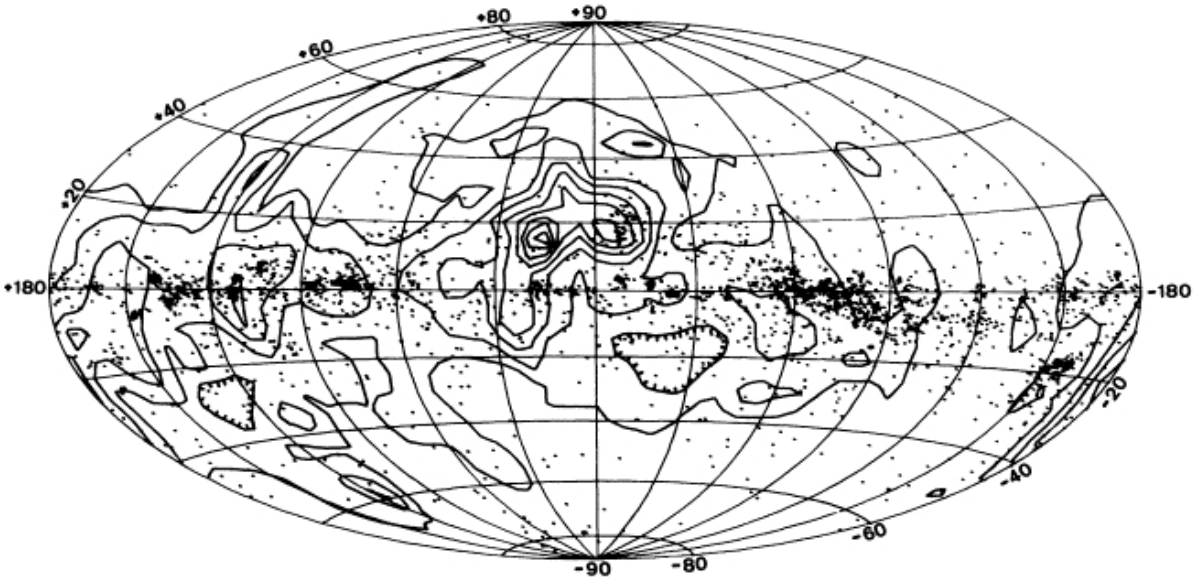

Fig. 3a. Aitoff equal area projection of the mean $E(B-V)$ per kiloparsec for OB stars within 2 kpc of the Sun. The center of the diagram is toward the Galactic center with longitude increasing to the left. Longitude lines are drawn every 30° and the parallels of latitude are drawn every 20°. The contour interval is 0.2 mag/kpc and the outermost contour is the lowest level. Contours surrounding depressed regions are indicated by tick marks

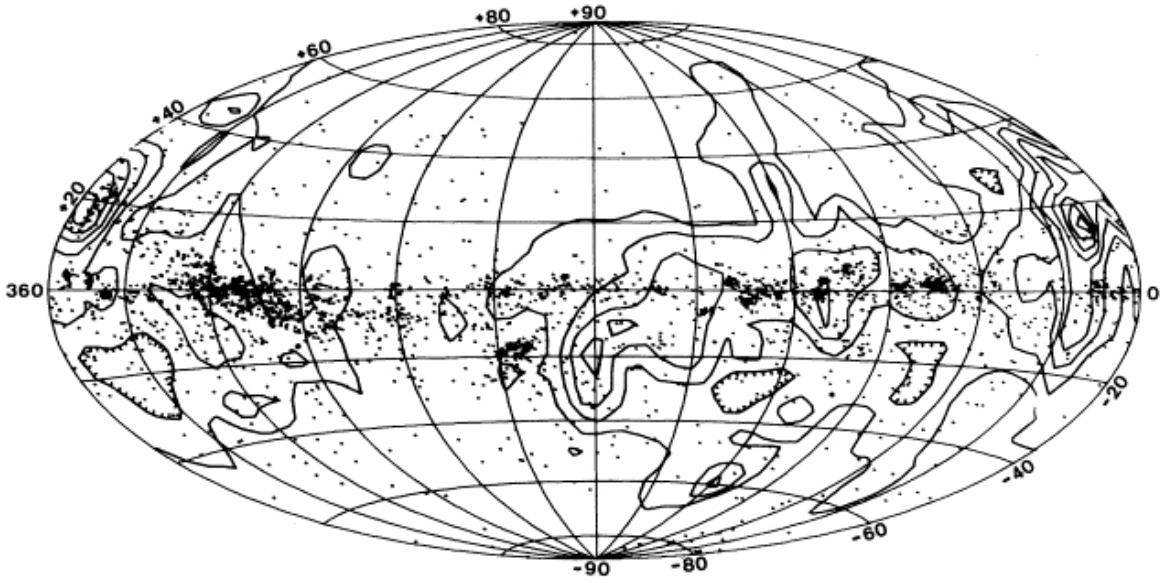

Fig. 3b. The same as Figure 3a except that the center of the diagram is toward the Galactic anticenter

Figure I.4: Galactic charts of reddening correction $E(B-V)$ due to interstellar absorption. From Lucke (1978).

For example in PaperII, for HD 7119, we determined $L/L_\odot$ from photometric measurements and Hipparcos parallax (Sect. I.6.2) and T_{eff} from its color index (Sect. I.6.3). Taking into account the uncertainties on these values, the two stars were plotted on the same isochrone with the constraint of a mass ratio equal to $K_2/K_1 = 1.10$, as observed. The corresponding mass values are $\mathfrak{M}_1 = 2.2 \pm 0.3\mathrm{M}_\odot$ and $\mathfrak{M}_2 = 2.0 \pm 0.3\mathrm{M}_\odot$, with an age of about 8. 10^8 years (Carquillat et al., 2001).

I.6.6 Masses and separations of the secondaries of *SB1*'s

When only one component was detected, it is not possible to position the secondary in the HR diagram. However, the absence of detection gives some indications that can be used for estimating the mass and separation of those secondaries.

From the values computed for $f(m)$ and $a_1 \sin i$ obtained when computing the spectroscopic binaries orbits, and assuming that the masses M_1 of the primaries are equal to the theoretical values, we can obtain, for a given value of the orbital inclination i, the values of M_2, the mass of the secondary, and a, the true mean separation of the components. To do so, we use the following formulae (see Sect. I.4.4 and Annexe B):

$$f(m) = M_1 \times \sin^3 i \times \mu^3 \,/\, (1+\mu)^2, \tag{I.22}$$

where $\mu = M_2/M_1$ is the mass-ratio in the system, and

$$a = a_1 + a_2 = (a_1 \sin i) \times (1 + 1/\mu)/\sin i. \tag{I.23}$$

The minimum values for μ, M_2 and a correspond to $\sin i = 1$ (i.e., $i = 90°$). As for the maxima of M_2 and μ, they can estimated taking into account the absence of CORAVEL correlation dips from the secondary spectroscopic components, that implies roughly $\Delta m_V \geq 2.0$, i.e., via the mass–luminosity relation, $\mu \leq 0.6$ (see Carquillat et al. (2004)). We then deduce minimum and maximum values of a and μ An example of this determination is given in Table I.6 of PaperVI).

As pointed out by Carquillat et al (1982), the separations obtained from Eq. I.23 have a small dependence on the value chosen for i (e.g., see line 15 of Table I.6). If a_0 is the separation corresponding $i = 90°$, and a the true separation, the ratio a/a_0 may be approximated by the function $(\sin i)^{-1/4}$, which is also an upper estimate of a/a_0. Hence, when i decreases from 90° to 20° (the most probable range for SBs, with a corresponding probability of 94%), a increases by less than 30% of its initial value, a_0.

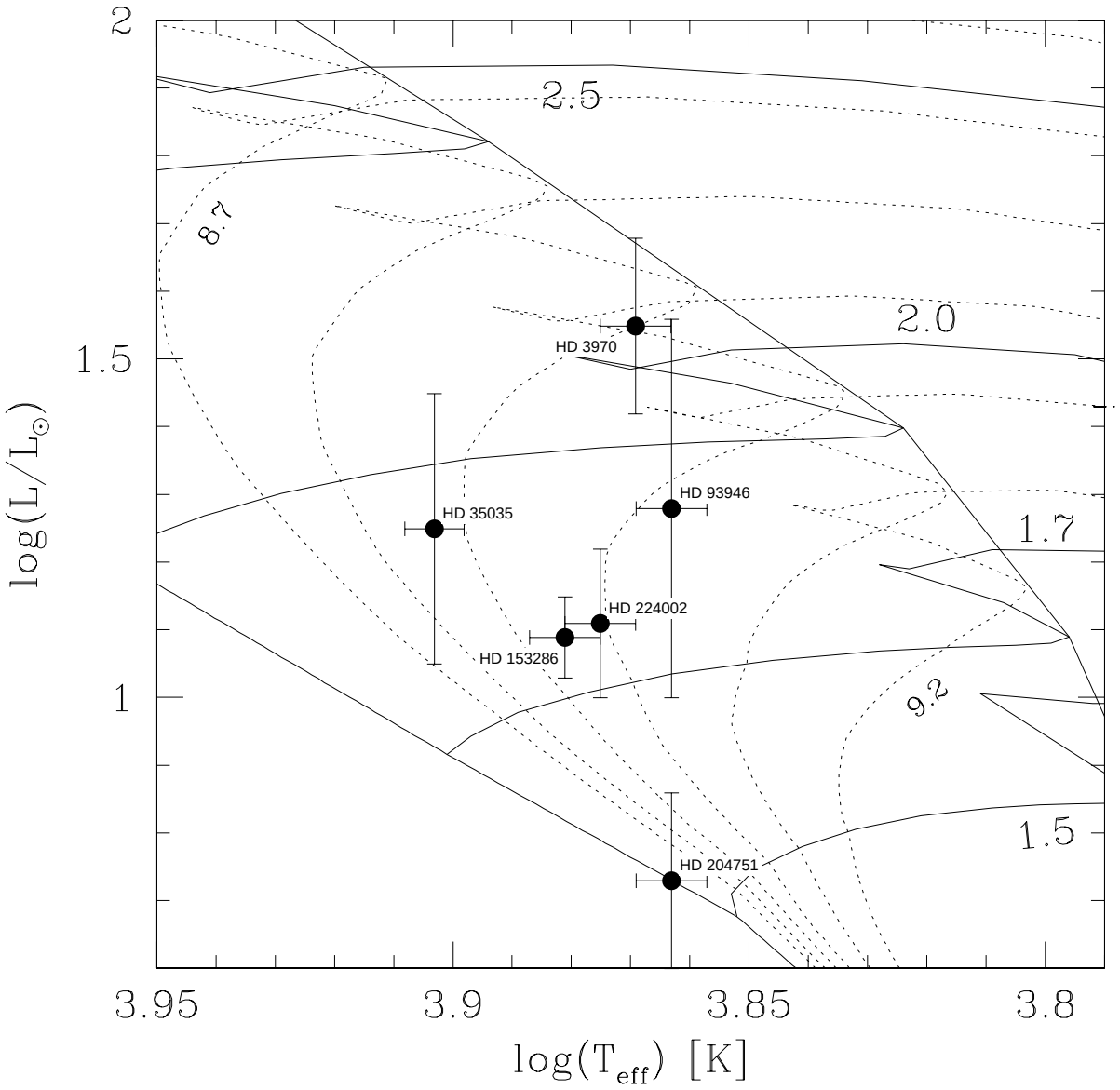

Figure I.5: Strömgren photometry has allowed us to position the primary components of the Am SB1 studied in PaperVII, in the theoretical evolutionary HR diagram computed by Schaller et al. (1992) for $Z = 0.02$, with the isochrones (dotted lines) given by Meynet et al. (1993), for log age[years] varying from 8.7 to 9.2 by steps of 0.1. The solid lines correspond to the evolution tracks for mass values of 1.5, 1.7, 2.0 and 2.5 $M_{\odot}$. The ages found were then compared with $t_{\rm sync}$ and $t_{\rm circ}$ (see Table I.7). From Prieur et al. (2006b).

I.7 Tidal effects

Tidal interaction is an important factor in changing the orbit of a close detached binary. Each star raises tides on the other that deviate from an instantaneous equipotential shape. This result in misalignment of the tides with respect to the line joining the centers of the two stars, which produces a torque component in the gravitational attraction of the stars. Via this spin-orbit coupling, angular momentum is exchanged between the orbit and the rotation of each star. At the same time, energy is dissipated in the tides, which diminishes the total energy of orbit and rotation. In a detached close binary, tidal evolution will continually change the orbital and rotational system parameters. Ultimately either an equilibrium state will be reached asymptotically, or the two stars will spiral in towards each other at an increasing rate, leading to a collision (see Zahn (1977); Hut (1981)).

In the case of detached binaries, an equilibrium state is characterized by:

- coplanarity (the equatorial planes of the two stars coincide with the orbital planes),
- circularity (of the orbit),
- corotation (the rotation periods of the two stars equal the revolution period).

Such an equilibrium state is stable (resp. unstable) if more (resp. less) than 3/4 of the total angular momentum is in the form of orbital momentum, as shown by Hut (1980) (see Annexe B).

The observations show that short orbital period detached systems are generally in an equilibrium state: the orbits are circular and the equatorial rotation of each companion is synchronized with the orbital motion (see Sect. I.7.1). Conversely, long period systems may still be in the evolution stage towards this final state. The orbital parameters will then asymptotically reach their equilibrium values, with different time scales. Theoretical studies have shown that the rotation of each component quickly synchronizes with the instantaneous orbital angular velocity at periastron, and could reach an intermediary state is called **"pseudo-synchronism"** before the orbit is fully circularized (Zahn, 1977; Hut, 1981; Claret & Cunha, 1997) (see Fig. I.6 and Hut (1981)). Pseudo-synchronization is caused by the fact that tidal interaction is strongest around periastron in elliptical orbits.

Synchronization (or pseudo-synchronization) is a powerful process for slowing the axial rotation of a star. This is therefore very important for Am stars, since it seems established that such a slow rotation is required to form Am-type stars through the diffusion of chemical elements (Michaud al., 1983).

I.7.1 Rotation-revolution synchronism test

A star belonging to a binary system is **synchronized** when its spin-axis rotation period is equal to its orbital period.

Synchronization test (circular orbits)

Kitamura & Kondo (1978) proposed a simple test to check whether synchronization has been reached by the components of a detached binary system. This test assumes that synchronism is verified and then estimates the value of the component radius corresponding to the observed rotation velocity and orbital period.

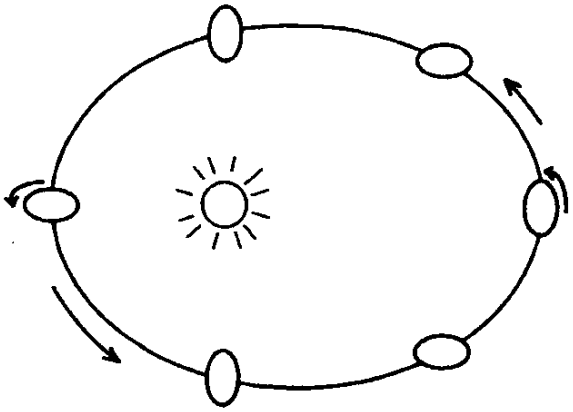

Figure I.6: Pseudo-synchronism: example of Mercury. Its (sidereal) rotation period is equal to 2/3 of its orbital period (2:3 resonance). Through a permanent asymmetry in its shape (exaggerated here), Mercury is locked in a state of pseudo-synchronization of orbit and rotation around perihelion. From Hut (1981).

Let $R_{\rm sync}$, the expected value of the radius of a stellar component obtained when assuming that (i) synchronism has been reached, and (ii) that the orbit and the equator of the star are coplanar. In that case the spin-axis angular rotation velocity Ω_s is equal to the mean orbital motion n:

$$\frac{\Omega_s}{n} = \frac{v_e/R_{\rm sync}}{50.6/P} = 1 \tag{I.24}$$

where v_e is the tangential equatorial velocity in km.s^{-1}, P is the orbital period in days, and $R_{\rm sync}$ is the star radius in solar radii ($R_\odot$).

We have then have the relation:

$$R_{\rm sync} = \frac{v_e\, P}{50.6} \tag{I.25}$$

The Kitamura and Kondo's test (hereafter KK-test). consists of comparing the estimated radius $R_\star$ of each component ($\star = 1$ or 2 for the primary, or secondary component, respectively) with $R_{\rm sync}$. The KK-test is positive when their values are similar: synchronism is likely to be verified by the corresponding component.

In fact, v_e cannot be determined from our spectroscopic observations. Only the projected equatorial velocity $v_e \sin i$ is an observational datum, that can be derived from the analysis of the CORAVEL correlation dips (see Benz & Mayor 1981, 1984). We thus preferred using the following relation derived from Eq. I.24:

$$R_{\rm sync} = \frac{v_e \sin i\ P}{50.6 \sin i} \tag{I.26}$$

As $\sin i \leq 1$, this relation implies a constraint on $R_\star$ the radius of the star:

$$R_\star \geq R_{\rm sync,min} \qquad \text{with} \quad R_{\rm sync,\,min} = v_{e\star} \sin i \times P/50.6 \tag{I.27}$$

which is a necessary condition for synchronism. Indeed, given P and $v_{e\star} \sin i$, a stellar component whose radius $R_\star$ is such that $R_\star < R_{\rm sync}$, has an angular rotation $\Omega = v_{e\star} \sin i / R_\star$ which is too large for synchronism (i.e., it rotates too quickly).

Another formulation is based on the rotation velocity only, assuming the stellar radius $R_\star$ is known. From Eq. I.26, we have:

$$v_{\rm sync} = \frac{50.6\, R_\star}{P} \tag{I.28}$$

As $\sin i < 1$, the observed projected velocity $v_e \sin i$ must be smaller than $v_{\rm sync}$:

$$v_e \sin i < v_{\rm sync} \tag{I.29}$$

This inequality constitutes another test for synchronism, since it is a necessary condition for synchronism.

Pseudo-synchronization test (elliptical orbits)

For non circular orbits, the *pseudo-synchronism test* involves a larger rotational velocity than for the equilibrium state: $\Omega_{ps} > \Omega_s$ in Eq. I.24. According to (Hut (1981), eq. 43), in the case of small elliptical orbits (i.e. $e \ll 1$) pseudo-synchronization is reached when the rotational velocity of each component is equal to:

$$\frac{\Omega_{ps}}{n} \approx 1 + 6\, e^2 + \tfrac{3}{8}\, e^4 + \tfrac{223}{8}\, e^6 \tag{I.30}$$

Hence, Eq. I.24 becomes:

$$\frac{v_{e\star}/R_{\rm psync}}{50.6/P} = 1 + 6\, e^2 + \tfrac{3}{8}\, e^4 + \tfrac{223}{8}\, e^6$$

where $R_{\rm psync}$ is the expected value of component radius in the case of pseudo-synchronization. We then have:

$$R_{\rm psync} = \frac{v_e \sin i\; P}{50.6 \sin i}\,(1 + 6\, e^2 + \tfrac{3}{8}\, e^4 + \tfrac{223}{8}\, e^6)$$

or when introducing the *pseudo-synchronization period* $P_{\rm psync}$:

$$R_{\rm psync} = \frac{v_e \sin i\; P_{\rm psync}}{50.6 \sin i} \qquad \text{with} \quad P_{\rm psync} = (1 + 6\, e^2 + \tfrac{3}{8}\, e^4 + \tfrac{223}{8}\, e^6)\, P$$

In the case of pseudo-synchronization, we then derive a condition similar to (I.27):

$$R_\star \geq R_{\rm psync,min} \qquad \text{with} \quad R_{\rm psync,\,min} = v_{e\star} \sin i \times P_{\rm psync}/50.6 \tag{I.31}$$

Since $P_{\rm psync} > P_{\rm sync}$ we have: $R_{\rm psync,min} > R_{\rm sync,min}$: the condition of pseudo-synchronization (I.31) seems more restrictive than the synchronization condition (I.27). In fact, assuming that the component radius remains the same, pseudo-synchronization of non-circular orbit occurs with a larger rotational velocity $v_{e\star}$ than synchronization of the circular orbit with the same semi-major axis a. In the tidal evolution process starting with a non-circular orbit and a large rotational velocity, (pseudo)-synchronization may thus reached before synchronization (i.e. before circularization). This is the case of HD 127263 and HD 138406 in Table I.6, and HD 204251 in Table I.7. But there is also the case of HD 19342 and HD 102925 (Table I.6) where circularisation has occurred before synchronization.

Note that the term of *pseudo-synchronization period* that we used for $P_{\rm psync}$ is somewhat misleading, because one should expect that a shorter period than P be involved in the case of eccentric orbits since tidal effects are maximum close to the periastron. Indeed, the osculating mean motion $n_{\rm peri}$ at the periastron is larger than n, the mean motion of a circular orbit of period P. More precisely (Hut (1981), eq. 44):

$$n_{\rm peri} = \frac{(1+e)^2}{(1-e^2)^{3/2}}\, n \tag{I.32}$$

To illustrate its dominance in the case of highly eccentric orbits, n_p can be used in the pseudo-synchronization condition (Hut (1981), eq. 45):

$$\frac{\Omega_{ps}}{n_{\rm peri}} = \frac{1+\frac{15}{2}e^2+\frac{45}{8}e^4+\frac{5}{16}e^6}{(1+3e^2+\frac{3}{8}e^4)(1+e)^2} \tag{I.33}$$

Example of application: binaries of PaperVII

We applied this test to the primary component of the seven systems studied in Prieur et al. (2006b). The primary radii were assumed to be equal to the theoretical values obtained with the Stefan law or, when not available (e.g. for HD 151746), we assumed the typical value $R \approx 2$ R$_\odot$ (see Table I.7, line 15). We thus obtained the equatorial velocity value for synchronism $v_{\rm sync}$, quoted in of Table I.7. This value could then be compared with the measured value of $v_e \sin i$ (line 6) and the result of the test is given in line 22. We see that the synchronism state has probably been reached for the two short-period circularised systems HD 93946 and HD 151746. This could be expected since the major axes are small for those two objects, which leads to strong tidal interaction. The same occurs for HD 204751 in terms of pseudo-synchronism. It is again not very surprising because, at periastron passage of this very eccentric orbit, the distance of the components is only 12 R$_\odot$.

I.7.2 Theory on synchronization and circularization of the orbits

To account for tidal effects occurring among early type stars, Zahn (1975, 1977) proposed that the main dissipative mechanism was **radiative damping** acting on the *"dynamical tide"* (whereas in late-type stars with a large convective zone, the *"static tide"* plays a major role, see Annexe B). He has studied in detail the theoretical aspects of the dissipative phenomena occurring in tidal interaction between early-type close binaries that finally lead to orbital circularization and synchronization between spin and orbital period. The "Spectroscopic Binary group" have had many fruitful discussions about tidal interaction with J.-P. Zahn who worked for many years in the same institute, in Toulouse We present here some results of his theory that can be confronted to our observations. More details can be found in Annexe B.

In Annexe B, we discussed the alternative solution of meridional circulation proposed by Tassoul (1987); Tassoul & Tassoul (1992) that we mentioned in Carquillat et al. (2004), but it was shown that those authors used wrong boundary conditions (Rieutord & Zahn, 1997).

Synchronization and circularization characteristic times

For stars with an outer radiative zone, like Am stars, Zahn (1975, 1977) proposed that the main dissipative mechanism was radiative damping acting on the *"dynamical tide"*, and

showed that the circularization timescale, $t_{\rm circ}$ (defined such that $1/t_{\rm circ} = -\dot{e}/e$), was a steep function of the fractional radius R/a:

$$\frac{1}{t_{\rm circ}} = \frac{21}{2}\left(\frac{GM}{R^3}\right)^{1/2} q\,(1+q)^{11/6}\,E_2\,\left(\frac{R}{a}\right)^{21/2} \tag{I.34}$$

where E_2 is related with the dynamic tidal contribution to the total perturbed potential.

The tidal constant E_2 is dependent on the stellar structure and on the mass of the star:

- For a given mass, it is a strongly decreasing function of the convective core size. When the star evolves off the main sequence, its core shrinks and E_2 decreases very quickly. It was shown that E_2 can change in several decades during stellar evolution for a given mass (Claret & Cunha, 1997).
- For nearly homogeneous models of stars near the ZAMS, with masses of 1.6 to 5 $M_\odot$, $\log E_2$ changes from -8.5 to -6.8 (Zahn, 1975; Claret & Cunha, 1997).

The strong dependence of E_2 on the internal stellar structure, which is unfortunately badly known, induces large uncertainties on $t_{\rm circ}$.

With the same theoretical description of radiative dissipation induced by tidal effects, Zahn (1975) also predicted values for $t_{\rm sync}$, the characteristic synchronization time of binary systems:

$$\frac{1}{t_{\rm sync}} = 5\times 2^{5/3}\times\left(\frac{GM}{R^3}\right)^{1/2} q^2\,(1+q)^{5/6}\,E_2\,\frac{MR^2}{I}\,\left(\frac{R}{a}\right)^{17/2} \tag{I.35}$$

where I is the momentum of inertia of the star.

In Carquillat et al. (2004) and Prieur et al. (2006b), we computed $t_{\rm circ}$ and $t_{\rm sync}$ by performing a parabolic interpolation of the tabulated E_2 values computed by Zahn (1975), which are in very good agreement with more recent computations by Claret & Cunha (1997). This was done with the program `tsync_tcirc.c` (see Sect. A.2) that I wrote for this purpose.

I.7.3 Comparison with theoretical characteristic times

Binaries studied in PaperVI

In Carquillat et al. (2004) we computed $t_{\rm circ}$ and $t_{\rm sync}$ for 10 binary systems, with the program `tsync_tirc.c` (see Sect. A.2). that interpolates the tabulated E_2 and MR^2/I of Zahn (1975). Except for HD 126031, for which $q = 0.75$ was known, we assumed $q = 0.5$ for all systems.

Circularization The results found in Carquillat et al. (2004) are reported in Table II.10. Unexpectedly, for every object, the characteristic circularization time $t_{\rm circ}$ we computed is larger (for HD 199360), or much larger (for the other systems) than the estimated age of the system. Hence the circular orbits of HD 19342, 102925, 126031, 155714, 195692 and 199360 *cannot be explained by tidal effects acting on the Am stars during their life in the main sequence*, in the context of Zahn's theory.

There are more circularized systems than what is expected from models with radiative dissipation of dynamical tides. However, let us recall that Eq. I.34 is valid for homogeneous

systems, made of two stars possessing a radiative envelope. As seen in Sect. II.5.8, the systems *SB1* studied in PaperVI are not homogeneous, and the unseen companions are likely to be convective late-type stars, with masses less than 1.4 $M_\odot$. For stars having a convective envelope, dissipation by turbulent viscosity is the dominant process. According to Zahn (1989), the circularization of orbits takes place in the very beginning of the Hayashi phase of pre-main sequence phase, for late-type binaries. There is little further decrease of the eccentricity on the main sequence. Hence the convective dissipation acting on the cool companion may circularize the orbit of a non-homogeneous binary system. Zahn & Bouchet showed that the theoretical cut-off period, which separates the circular from the eccentric systems is $P \sim 8$ days for convective stars with masses ranging from 0.5 to 1.25 $M_\odot$. This would provide a natural explanation for the presence of circular orbits for the shortest period systems of our sample, namely HD 126031, 155714 and 199360. The case of HD 19342 and 102925 with periods longer than 42 days and 16 days, respectively, is more puzzling: those systems may have formed as circular, indeed.

Conclusion: the radiative dissipation of dynamical tides as presented by Zahn (1975) seems not efficient enough to circularize the binary systems we have studied in PaperVI. Circularization of the orbit may have occurred during the pre-main sequence stage, with a greater efficiency by convective dissipation of tidal effects acting on the cool companion, and some systems may have formed with circular orbits.

Synchronization When comparing the results of Carquillat et al. (2004) with the predictions of Zahn's radiative theory for $t_{\rm sync}$, we found:

- All systems for which KK-test is negative have $t_{\rm sync} \gg t_{\rm age}$, where $t_{\rm age}$ is the age of the star (Line 23 of Table II.10);
- For HD 199360, $t_{\rm sync} \ll t_{\rm age}$ and indeed this system is very likely to be synchronized (since KK-test is positive and the period is very short, $P = 1.99$ d);
- The agreement with Zahn's theory is marginal with $\log t_{\rm sync} \sim \log t_{\rm age}$ for HD 126031 (synchronized) and HD 155714 (very likely to be synchronized with a positive KK-test and a very short period).
- A clear disagreement is found for the systems HD 127263, 138406 and 195692 which have a positive KK-test and $t_{\rm sync} > t_{\rm age} \times 10^2$.

Hence the tidal effects seem more efficient for synchronizing binaries than what is expected from Zahn's theory of radiative dissipation. A possible explanation could be that synchronization by tidal effects starts from the upper layers of the star and then proceeds inwards to the center (J.-P. Zahn, 2003, private communication). As observational data (rotation velocity) concern the surface of the star, there is a possible bias of considering as synchronized stars objects for which synchronism state is not fully reached on the whole star. A theoretical problem would then be to derive the characteristic time $t_{\rm start}$ when the process starts in the surface and the typical duration $\Delta t_{\rm mig}$ of this migration process, from the surface to the center. For HD 127263, 138406 and 195692, this time would be very large with $t_{\rm start} \leq 10^{-2}\, t_{\rm sync}$ and $\Delta t_{\rm mig} \sim t_{\rm sync}$.

Conclusion: Observations of PaperVI suggest that synchronization of the radiative primaries occurred much earlier than indicated by the characteristic times. This may be explained by the

Table I.6: Physical and tidal parameters derived from the study of the primary components of the seven new binaries studied in PaperVI. For the reddened objects, the magnitudes corrected for interstellar absorption are indicated in brackets (lines 3 and 4). For the eclipsing binary HD 126031, we assumed $i = 83°$. From Carquillat et al. (2004).

HD	19342	19910	36360	102925	126031	127263	138406	155714	195692	199360
HIP	14653	–	25995	57813	70287	70814	75764	84230	101300	103335
V	8.00 (7.59)	9.34 (9.19)	7.17	7.24 (7.14)	7.54	8.14	6.91 (6.74)	7.06	6.51	7.85 (7.73)
$B-V$	0.47 (0.33)	0.30 (0.25)	0.28	0.18 (0.15)	0.34	0.24	0.13 (0.07)	0.38	0.26	0.31 (0.27)
$v_e \sin i$ (km/s)	9.9 ±1.0	14.1 ±1.0	20.0 ±1.0	8.0 ±1.0	24.4 ±2.4	11.0 ±1.0	6.6 ±1.0	17.4 ±1.0	9.6 ±1.0	13.5 ±1.0
π (mas)	5.52 ±1.11	–	7.29 ±1.08	8.78 ±0.64	7.38 ±0.92	7.14 ±0.74	3.55 ±0.54	11.06 ±1.21	12.33 ±0.70	6.78 ±0.90
d (pc)	181^{+46}_{-30}	–	137^{+24}_{-18}	114^{+9}_{-8}	135^{+20}_{-15}	140^{+16}_{-13}	282^{+50}_{-38}	90^{+12}_{-9}	81^{+5}_{-4}	147^{+23}_{-17}
M_v	1.30 ±0.51	–	1.48 ±0.32	1.86 ±0.16	2.14 ±0.3	2.41 ±0.23	-0.51 ±0.36	2.28 ±0.24	1.96 ±0.13	1.89 ±0.29
$\log L/L_\odot$	1.37 ±0.22	–	1.30 ±0.14	1.14 ±0.08	1.03 ±0.15	0.92 ±0.10	2.09 ±0.16	0.98 ±0.11	1.10 ±0.06	1.13 ±0.13
$T_{\rm eff}$ (K)	7100 ±70	7800 ±70	7700 ±70	8100 ±100	7370 ±80	7900 ±70	8700 ±150	7000 ±80	7500 ±80	7800 ±80
$\log g$[cgs]	3.6	4.4	4.0	–	4.1	4.1	–	4.0	4.1	4.2
$[Fe/H]$	+0.67	+0.29	+0.55	–	+0.64	+0.93	–	+0.34	+0.30	+0.75
$R_1/R_\odot$	3.2 ±0.8	∼2	2.5 ±0.4	1.9 ±0.2	2.1 ±0.3	1.5 ±0.2	4.9 ±1.0	2.1 ±0.3	2.1 ±0.2	2.0 ±0.4
$M_1/M_\odot$	2.00 ±0.20	∼2.0	1.95 ±0.10	1.85 ±0.05	1.70 ±0.10	1.70 ±0.05	∼ 3	1.65 ±0.10	1.80 ±0.05	1.80 ±0.10
$M_{2\,\rm min}/M_\odot$	0.9	1.1	0.7	0.6	–	0.4	0.3	0.06	0.3	0.1
$M_{2\,\rm max}/M_\odot$	1.2	1.2	1.2	1.1	–	1.0	1.8	1.0	1.1	1.1
$a_{\rm min}/R_\odot$	73.1	38.2	209	36.5	14.5	31.8	54.8	11.2	28.8	8.3
$a_{\rm max}/R_\odot$	75.6	38.4	222	39.0	–	34.5	61.9	13.0	29.8	9.5
$\overline{a}$	74.4	38.3	216	37.8	14.5	33.2	58.4	12.1	29.3	8.9
$R/\overline{a}$	0.04	0.05	0.01	0.05	0.13	0.05	0.08	0.17	0.07	0.22
$i_{\rm min}$ (deg.)	53	75	39	36	–	31	13	5	53	7
$R_{\rm sync,min}/R_\odot$	8.3 ±0.8	4.3 ±0.3	79.6 ±4.0	2.6 ±0.3	1.8 ±0.2	1.9 ±0.2	2.6 ±0.4	1.15 ±0.07	2.1 ±0.2	0.53 ±0.04
Synchronized?	no	no	no	no	yes	∼likely	likely	likely	likely	likely
Circularized?	yes	no	no	yes	yes	no	no	yes	yes	yes
log age[yr]	$9.00^{+0.10}_{-0.08}$	–	$8.94^{+0.02}_{-0.03}$	$8.77^{+0.06}_{-0.12}$	$9.00^{+0.03}_{-0.10}$	∼8 ±0.7	∼8.7	$9.13^{+0.03}_{-0.02}$	$9.00^{+0.02}_{-0.05}$	$8.90^{+0.03}_{-0.14}$
$\log t_{\rm circ}$[yr]	17.6	16.3	23.4	16.7	12.3	17.2	14.1	11.4	15.4	9.9
$\log t_{\rm sync}$[yr]	14.1	12.9	18.7	13.3	9.6	13.7	11.1	9.1	12.2	7.8
P (days)	42.6	15.4	216.5	16.4	3.8	14.2	25.9	3.3	11.3	2.0

theory: synchronization of the whole star is a progressive process starting from the surface, and observations only detect the rotational velocity of the surface (see Annexe B).

Binaries studied in PaperVII

The values of $t_{\rm circ}$ and $t_{\rm sync}$ computed for the objects of Prieur et al. (2006b) are given in Table I.7 When a system has a non-circular orbit, we also give in this table (in the same line and column, but separated with a slash) the value obtained with the minimum separation $a(1-e)$ corresponding to the periastron passage, where the tidal effects are the strongest and the most efficient. For a system with a large eccentricity, like HD 204751 with $e = 0.87$, the minimum separation is much smaller than the mean separation (a) and the corresponding values of $t_{\rm sync}$ and $t_{\rm circ}$ are also much smaller. Note that those theoretical values are only rough estimates, since they are based on a simplified modelisation of the internal structure of those stars which is poorly known.

We estimated the ages for primary stars of the systems displayed in Fig I.5 by using the isochrones of Meynet et al. (1993) plotted in this figure as dashed lines. Those values are reported in Table I.7 (line 24).

Circularization We found a fair agreement between the ages of the stars and the theoretical values of $t_{\rm circ}$:

Table I.7: Physical and tidal parameters derived from the study of nine new binaries of PaperVII. The subscripts 1 and 2 refer to the primary and secondary components, respectively. From Prieur et al. (2006b).

HD	3970	35035	93946	151746	153286	204751	224002
HIP	3331	25160	53081	81757	82864	—	117856
m_V	7.20	7.56	8.65	6.82	7.03	7.93	7.99
$B-V$	0.34	0.31	0.28	0.22	0.31	0.33	0.31
E_{B-V}	0.04	0.08	0.00	0.00	0.00	0.03	0.06
$v_e \sin i$ (km.s^{-1})	29.1 ± 2.9	22.1 ± 2.2	25.3 ± 1.3	13.1 ± 2.6	7.3 ± 0.2	27.3 ± 2.7	38.8 ± 3.9
π (mas)	5.40 ± 0.81	5.33 ± 1.24	3.61 ± 1.15	8.26 ± 0.59	9.43 ± 0.60	12.0 ± 4.1	6.47 ± 0.86
d (pc)	185^{+33}_{-24}	188^{+56}_{-36}	277^{+130}_{-67}	121^{+9}_{-8}	106^{+7}_{-6}	83^{+44}_{-21}	155^{+23}_{-19}
$M_{V,1}$	0.83 ± 0.33	1.6 ± 0.5	1.52 ± 0.69	2.0 ± 0.2	1.98 ± 0.14	3.31 ± 0.74	1.94 ± 0.28
$T_{\rm eff}$ (K)	7400 ± 100	8000 ± 100	(7300 ± 100)	—	7500 ± 100	7300 ± 100	(7500 ± 100)
$\log g$ (cgs)	3.7	4.1	—	—	4.0	4.0	—
[Fe/H]	0.68	0.43	—	—	0.71	0.86	—
$\log(L/\mathrm{L}_\odot)$	1.55 ± 0.13	1.25 ± 0.20	1.28 ± 0.28	—	1.09 ± 0.06	$0.73^{+0.13}_{-0}$	1.11 ± 0.11
M_1 ($\mathrm{M}_\odot$)	2.2 ± 0.2	1.9 ± 0.2	1.9 ± 0.3	(~ 2)	1.80 ± 0.05	~ 1.6	1.8 ± 0.1
R_1 ($\mathrm{R}_\odot$)	3.6 ± 0.6	2.2 ± 0.6	2.7 ± 0.9	(~ 2)	2.0 ± 0.2	~ 1.6	2.1 ± 0.3
$M_{2,\,\rm min}$ ($\mathrm{M}_\odot$)	0.5	1.3	0.6	(~ 0.5)	0.7	~ 0.3	0.8
a ($\mathrm{R}_\odot$)	71.5 ± 4.0	647 ± 20	14.3 ± 1.0	(17.5 ± 1.2)	1386 ± 85	89.5 ± 4.5	44.5 ± 2.5
$a(1-e)$ ($\mathrm{R}_\odot$)	35 ± 2.0	250 ± 8	14.2 ± 1.0	—	863 ± 54	11.6 ± 0.6	39.6 ± 2.2
P (days)	40	1025	3.6	4.8	3458	60	20
$P_{\rm ps}$ (days)	16.62	238.14	—	—	1872.04	2.57	18.47
$v_{\rm sync}$ (km.s^{-1})	11.0	0.5	38.4	(21)	0.05	31.5	5.8
Synchronised?	no	no	likely	likely	no	likely	no
Circularised?	no	no	yes	yes	no	no	no
log age (yr)	$8.90^{+0.1}_{-0.1}$	$8.87^{+0.1}_{-0.1}$	$9.00^{+0.04}_{-0.10}$	—	$8.95^{+0.05}_{-0.05}$	< 8.95	$9.00^{+0.01}_{-0.05}$
log $t_{\rm sync}$ (yr)	13/10.6	23/20	8.4	(10)	26/25	17/10.0	14/13
log $t_{\rm circ}$ (yr)	17/13	29/25	10.7	(13)	33/31	22/12.5	17/16

- the cases of non-circular orbits correspond to values of $t_{\rm circ}$ much larger than the estimated ages.

- But the circularised systems have ages much smaller than the values computed for $t_{\rm circ}$ with Zahn's model (e.g., HD 93946 and HD 151746).

As in PaperVI, we have found in PaperVII circularized systems with $t_{\rm circ}$ much larger than their ages.

As already discussed in Carquillat et al. (2004), possible origins of this discrepancy for an SB1 binary system are:

- the unseen companions have a small mass and thus must have a convective envelope. Tidal interaction is much more efficient in this case and the cool companion alone can have circularised the mutual orbit (this circularisation has probably occurred in the Hayashi phase of the pre-main sequence).

- the binary system may have formed as circular.

Synchronization We found a rather good agreement between the ages of the stars and the theoretical values of $t_{\rm sync}$:

– the estimated age of HD 93946 is larger than $t_{\rm sync}$, and indeed the synchronisation test is positive;

– the cases when this test is negative correspond to values of $t_{\rm sync}$ much larger than the estimated ages.

– for HD 204751, the agreement is marginal with the value of $t_{\rm sync}$ obtained with the minimum separation $a(1-e)$.

Observations of PaperVII are in good agreement with the expectations of Zahn's theory concerning synchronization.

Another conclusion would be that there is a good agreement between the physical parameters deduced from our observations, Zahn's model and Meynet et al. isochrones.

I.7.4 Synchronisation and circularisation critical fractional radii

Zahn (1977) predicted a strong dependency of the strength of tidal effects with the *fractional radius* $r = R/a$, defined as the ratio of the star radius with the semi-major axis of the orbit. For stars with a convective core and a radiative envelope, $t_{\rm circ} \propto (R/a)^{-21/2}$i (Eq. I.34) and $t_{\rm sync} \propto (R/a)^{-17/2}$ (Eq. I.35). Hence the determination of the smallest component separations, or *critical fractional radii* $r_{\rm sync}$ and $r_{\rm circ}$, at which synchronism or orbit circularisation become mostly observed, is a valuable test for theoretical models.

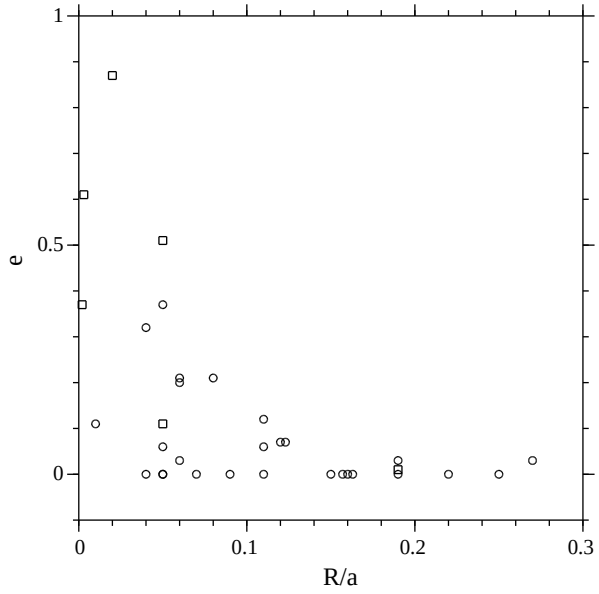

Figure I.7: Circularisation of the 33 binary systems we studied from Paper I to Paper VII. From Prieur et al. (2006b).

Curve e versus R/a

Giuricin et al. (1984a) showed on a sample of 200 early-type binaries (O, B, A-type) that the transition between eccentric and circular, or quasi-circular (i.e., $e < 0.05$) orbits was rather sharp and occurred at about $(R/a)_c \sim 0.24$, which agreed well with Zahn's theory.

Following those authors, we computed in Paper VI the fractional radius for each object of our sample by using for a the mean value $\overline{a}$ of $a_{\rm min}$ and $a_{\rm max}$ (Line 17 of Table I.6) and for the 8 short-period systems studied in Carquillat et al. (2003b). The resulting plot (Fig II.20) suggested that the critical value of the fractional radius is $(R/a)_c \sim 0.15$. This was smaller than that proposed by Giuricin et al., that was in full agreement with Zahn's model.

In Paper VII, we built a new plot (Fig. I.7) with the 33 stars studied in the series of our papers devoted to Am spectroscopic binary systems (see Papers I to VI in the bibliography). We report in Table I.8 the ellipticity and synchronisation parameters obtained by using all the relevant data contained in those papers. Fig. I.7 confirms what we found in Paper VI and clearly shows that all stars with $r \geq 0.15$ are orbiting on circular orbits.

Curve $\log(v \sin i/v_{\rm sync})$ versus R/a

Using Table I.8, we built in Paper VII the two curves of Fig. I.8a and I.8b in order to determine the critical fractional radius for synchronization and pseudo-synchronization.

In the diagram $\log(v_e \sin i/v_{\rm sync})$ versus r of Fig. I.8a, the synchronism test of the inequality $v_e \sin i \leq v_{\rm sync}$ (I.29) corresponds to imposing a threshold with the dotted line. This would lead to $r_{\rm sync} \approx 0.1$. We could also apply a stricter criterion involving the ratio $v_e/v_{\rm sync}$, with the unprojected equatorial velocity v_e. If we assume that the inclination has a uniform random distribution, the most probable value of $\sin i$ is 0.5, which corresponds to $i = 60°$ (dashed line). In Fig. I.8a, the test $v_e < v_{\rm sync}$ would lead to $r_{\rm sync} \approx 0.20$.

For the non-circular orbits, that are concerned with pseudo-synchronism we have plotted

Table I.8: Tidal effects on Am-type binary systems: ellipticity and synchronisation parameters obtained in our series of papers, Paper I to Paper VI. In col. 4: $\mathbf{v} = v_e \sin i$. Those data are used in Figs. I.7 and I.8.

Name	R/a	e	$\log(v_e \sin i)/v_{\rm sync}$	$R/[a(1-e)]$	Reference
HD 341	0.157	0.00	−0.40	0.16	Paper V
HD 3970	0.05	0.51	0.42	0.10	Paper VII
HD 7119 (prim)	0.27	0.03	−0.43	0.28	Paper III
HD 7119 (sec)	0.19	0.03	−0.50	0.20	Paper III
HD 19342	0.04	0.00	0.42	0.04	Paper VI
HD 19910	0.05	0.06	0.33	0.06	Paper VI
HD 35035	0.003	0.61	1.65	0.01	Paper VII
HD 36360	0.01	0.11	1.50	0.01	Paper VI
HD 55822	0.11	0.12	−0.01	0.13	Paper V
HD 61250	0.19	0.00	−0.23	0.19	Paper V
HD 67317	0.11	0.00	−0.19	0.11	Paper V
HD 81976	0.11	0.06	−0.18	0.12	Paper II
HD 93946	0.19	0.01	−0.18	0.19	Paper VII
HD 93991	0.25	0.00	−0.32	0.25	Paper V
HD 98880 (prim)	0.09	0.00	−0.05	0.09	Paper II
HD 98880 (sec)	0.05	0.00	0.13	0.05	Paper II
HD 100054B	0.06	0.03	−0.17	0.06	Paper IV
HD 102925	0.05	0.00	0.13	0.05	Paper VI
HD 125273 (prim)	0.12	0.07	−0.29	0.13	Paper I
HD 125273 (sec)	0.123	0.07	−0.31	0.13	Paper I
HD 126031	0.15	0.00	−0.06	0.14	Paper VI
HD 127263	0.04	0.32	0.10	0.07	Paper VI
HD 138406	0.08	0.21	−0.27	0.08	Paper VI
HD 153286	0.002	0.37	2.16	0.02	Paper VII
HD 155714	0.16	0.00	−0.27	0.17	Paper VI
HD 162950	0.06	0.20	−0.08	0.08	Paper V
HD 187258	0.05	0.37	−0.06	0.09	Paper IV
HD 195692	0.07	0.00	0.01	0.07	Paper VI
HD 199360	0.22	0.00	−0.57	0.22	Paper VI
HD 204751	0.02	0.87	−0.06	0.14	Paper VII
HD 224002	0.05	0.11	0.83	0.05	Paper VII
HD 224890	0.06	0.21	0.02	0.08	Paper V
HD 225137	0.163	0.00	−0.25	0.16	Paper V

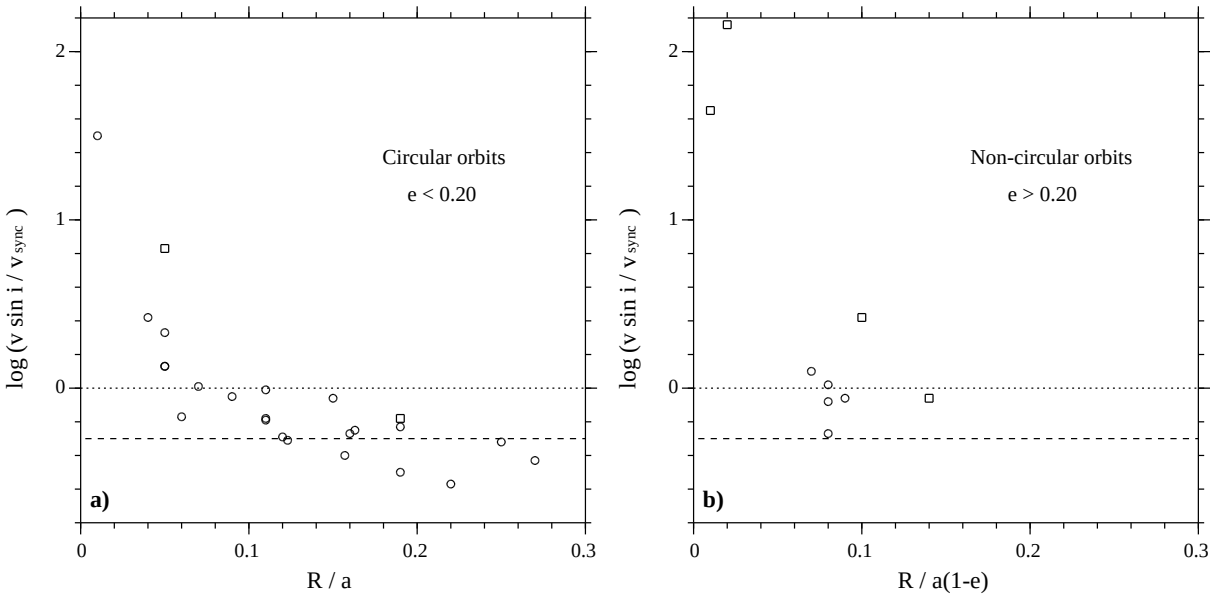

Figure I.8: Synchronisation of the binary systems belonging to the sample of PaperVII (squares), and to the whole list of Am stars studied from Paper I to Paper VI (circles). The dotted and dashed lines correspond to the synchronisation thresholds for $i = 0$ and $i = 60°$, respectively. From Prieur et al. (2006b).

$\log(v_e \sin i/v_{\rm sync})$ versus $R/[a(1-e)]$ (see Fig. I.8b), since the minimum separation $a(1-e)$ is more relevant in this case. Indeed tidal interaction is the strongest in the portion of the orbit close to the periastron passage. From this plot it seems that the critical fractional radius, expressed as $R/[a(1-e)]$, is larger than 0.15, but the number of points is unfortunately too small to enable us to be more precise.

Discussion

Zahn (1977) computed the limiting separations *"for which the corresponding characteristic times are equal to one quarter of the main sequence life span"*, for circularisation and synchronism. For a population of relatively evolved primaries (i.e. stars that have already spent one fourth of their lifetime on the main sequence), those values are thus equal to the critical radii that can be deduced from the observations.

Compared to the sample studied by Giuricin, our sample is limited to Am-type stars, which facilitates theoretical studies since it has a much more limited range of physical parameters (temperature, radius, mass). From table 2 of Zahn (1977) we obtain $r_{\rm sync} \approx 0.14$ and $r_{\rm circ} \approx 0.20$, for binary systems with $M_1 = 2$ M$_\odot$ and $\mu = 1$. If we assume a smaller mass ratio, $\mu = 0.5$, which is generally more likely for single-lined spectroscopic binaries, those values become somewhat larger: $r_{\rm sync} \approx 0.17$ and $r_{\rm circ} \approx 0.24$.

With our sample of Am stars we find $r_{\rm sync} \approx 0.20$ which is very close to the predicted value. Concerning the circularisation, our determination of $r_{\rm circ} \approx 0.15$ is smaller than Zahn's expectations. Let us note however that Zahn assumed that the two stars forming the system had a radiative envelope, which is generally not the case for our systems. Indeed most of the objects studied in this series of papers are SB1 and the mass estimates of the unseen secondary stars are small (see e.g. Table I.7, line 16). Hence those stars must have convective envelopes. As mentioned in Sect. I.7.3, tidal effects acting on the companions are more effective in this

case and may have led to the circularisation of the mutual orbits.

Zahn (1977) recognized that his theoretical predictions were rather imprecise, since they relied on many assumptions on the internal stellar structure, with very few observational constraints. He said that observations leading to the determination of the limiting separations, would be very helpful to revise the values of the tidal coefficients E_2, and precise the internal stellar structure. With those new values of $r_{\rm sync}$ and $r_{\rm circ}$, for Am-stars, we hope that this study will contribute to refining theoretical models.

Chapter II

Detailed study of our sample

II.1 Paper II: HD 81976 (*SB2*) and HD 98880 (*SB2*)

In Carquillat et al. (2001), we presented the results of the observations of two Am stars of eighth magnitude, the double-lined spectroscopic binaries HD 81976 and HD 98880, carried out with the CORAVEL instrument at the Observatoire de Haute-Provence in order to determine their orbital elements.

The first system, HD 81976, is formed by two quasi-identical stars, and the Hipparcos data (M_V, B-V) are consistent with late A stars in effective temperature; it is likely that the components rotate synchronised with the orbital motion. A third body may be present in this system since (i) the orbit has a significant eccentricity despite its short period and (ii) the systemic velocity V_0 shows a possible drift.

For the second system, HD 98880, we obtained $\Delta m_B = 1.25$ and we proposed a simple model based upon Strömgren photometric indices and the HR theoretical diagram of Schaller et al (1992) in addition to orbital parameters and Hipparcos data: $T_{\rm eff} = 7000$ K, $\log_{10} g = 4.0$, $M_1 = 1.9$ $M_\odot$, $M_2 = 1.6$ $M_\odot$, $\log_{10}(\text{age}) = 9.12$. The components do not rotate synchronously contrary to HD 81976.
Both binaries appear to be detached systems without possibility of eclipses.

The first of these two stars, HD 81976, was reported as Am in a paper by Bidelman (1988), in his "Miscellaneous spectroscopic notes", whereas the second, HD 98880, was included in the "Third catalogue of Am stars with known spectral types" (Hauck, 1986), which was the main source used for constructing our sample. Note that the Am type was attributed to HD 98880 by Abt (1984) during his spectroscopic investigation of a sample of possible peculiar stars which had peculiar indices in Strömgren photometry (Olsen 1980). Concerning their binarity, only HD 81976 had already been reported in the past as having a double lined spectrum (Adam 1915) from observations carried out at Mount Wilson, but to our knowledge, no spectroscopic orbit had ever been obtained.

II.1.1 HD 81976

The correlation dips measured with CORAVEL are quite similar for both components, which indicates that the two stars must have a similar type (Am in that case). This is supported by the value of the mass ratio $r = K_1/K_2 = 0.97$, very close to unity. Assuming that these stars

Table II.1: Orbital elements and standard errors for the systems HD 81976 and HD 98880. In 2nd line, T_0 is the periastron passage for HD 81976, and the ascending node passage for HD 98880. From Carquillat et al. (2001).

Element	HD 81976	Std error	HD 98880	Std error
P (days)	5.655750	0.000050	14.20783	0.00018
T_0 (HJD)	2449785.941	0.045	2448682.883	0.015
ω (degrees)	341.4	3.0		
e	0.061	0.003	0 (fixed)	
K_1 (km.s^{-1})	61.68	0.26	42.47	0.17
K_2 (km.s^{-1})	63.84	0.28	49.16	0.33
V_0 (km.s^{-1})	19.85	0.14	2.40	0.11
$a_1 \sin i$ (Gm)	4.788	0.020	8.298	0.033
$a_2 \sin i$ (Gm)	4.956	0.022	9.604	0.064
$M_1 \sin^3 i$ (M$_\odot$)	0.5875	0.0057	0.6091	0.0088
$M_2 \sin^3 i$ (M$_\odot$)	0.5676	0.0054	0.5262	0.0056
σ_1 (O-C) (km.s^{-1})	1.0		0.55	
σ_2 (O-C) (km.s^{-1})	1.2		1.7	

have a mass of the order of 2 M$_\odot$, the value obtained for $M_1 \sin^3 i = 0.5875$ M$_\odot$ would lead to $i = 42°$, which implies a quasi-certain impossibility of eclipse occurrence. With the same assumption, we would have $a = a_1 + a_2 = 14.66$ Gm$= 21$ R$_\odot$, and the system would appear as detached.

Comparison with the Hipparcos measurements

For HD 81976 = HIP 46588, the Hipparcos catalogue (ESA 1997) gives: $V = 8.17$, $\pi = 5,65 \pm 1.18$ mas, $B - V = 0.285$, $V - I = 0.32$.

From the value for the trigonometric parallax, the distance of this system is about 180 pc, and the absolute V magnitude can be estimated at 1.93±0.46, assuming negligible interstellar absorption. If we assume both component have the same luminosity, we obtain $M_V = 2.68 \pm 0.46$ for each component. This value is compatible with Am-type stars as shown by North et al. (1997), who obtained absolute V magnitues in the range +0.3 and +2.8 for a sample of 96 Am stars observed with the Hipparcos satellite.

Note also that the color indices as measured by Hipparcos are consistent with a late A-type star, about A7-A8 (Schmidt-Kaler, 1982). Such a spectral type should correspond to the strength of hydrogen lines and the effective temperature of the star (Bidelman does not give any detail for his classification but only the result: "Am"). This is also consistent with the dA7 classification given in the Mount Wilson catalogue (Wilson 1953), since such a classification was done at a time when the Am stars were not yet known as a family of its own.

Rotation-revolution synchronism

Since the orbital period is rather short, a synchronism can be expected between the axial rotation and the orbital revolution of the components. The test proposed by Kitamura & Kondo (1978) consists of calculating the radii that the two stars would have if synchronism

was effective. If the values found for these radii are compatible with those expected for stars of similar spectral type, one can deduce that the hypothesis of synchronism is plausible. Actually, the equatorial velocity for synchronism is $V_s = 50.6(R/\mathrm{R}_\odot)/P$.

In our case, V_s can be estimated from $v.\sin i$ as deduced from the profile of the correlation dips (method described in Benz & Mayor 1981), which is 14.5 ± 0.5 km s^{-1}. Assuming $i = 42°$ and the coplanarity between the equatorial and the orbital planes, one finds $V_s = 21.8$ km s^{-1} and hence $R = 2.4$ R$_\odot$. This value is quite compatible with those deduced from the study of similar systems showing eclipses (Kitamura & Kondo 1978). We can then conclude that the hypothesis of synchronism is relevant for HD 81976.

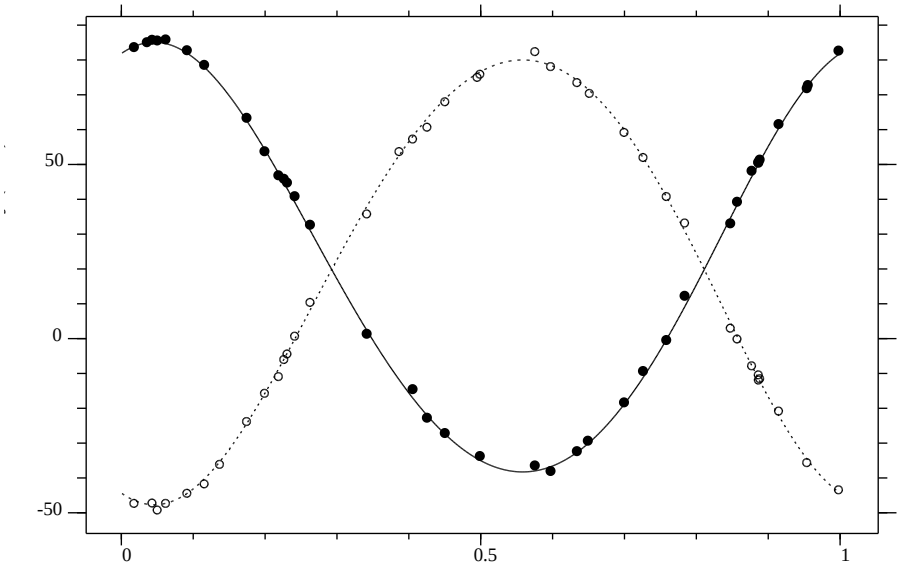

Figure II.1: Radial velocity curves for HD 81976. Filled circles: main component, open circles: secondary component. The origin for phases corresponds to the periastron passage. From Carquillat et al. (2001).

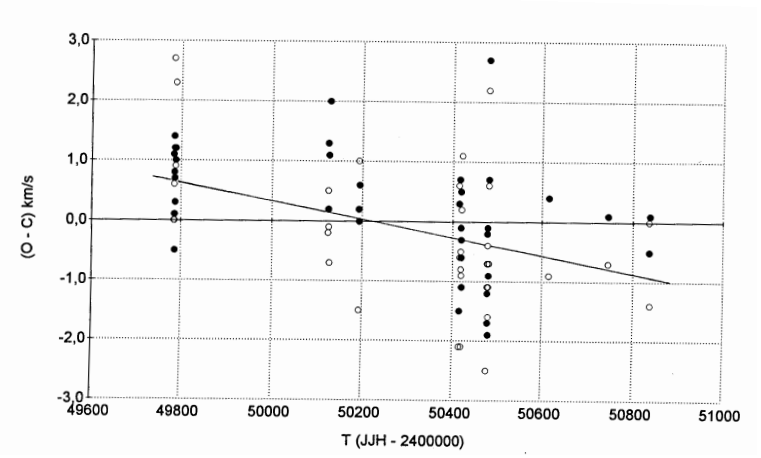

Figure II.2: Variation of the residuals (O-C) versus time for HD 81976. Filled circles: primary component, open circles: secondary component. The straight line with a negative slope corresponds to the least square fit. From Carquillat et al. (2001).

Hypothesis of a third body

In Sect. 2, we noticed that the eccentricity of the orbit of HD 81976 was not zero and that the other system studied here has a period nearly 2.5 times larger with a circular orbit. The existence of a non-circular orbit for a system with a period as short as 5.6 days is surprising. Actually, the study of a sample of Am stars belonging to the Hyades and Praesepe clusters by Debernardi et al. (2000) shows that orbits are quasi circular for $P < 10$ days, and the authors note that this is in agreement with the theoretical work of Zahn & Bouchet (1989).

On the other hand, when plotting the residuals (O-C) of Table 1 versus time (Fig. II.2), one notes they seem to decrease with time, which shows a possible drift of the velocity V_0 of the system's gravity center.

These two points lead us to suggest the presence of a third body in this system. We have already formulated such an hypothesis for the Am-type system HD 66068/9 (Carquillat et al. 1994), which also showed a V_0 drift and exhibited an abnormally high eccentricity for a period close to 8 days.

II.1.2 HD 98880

For this binary, the mass ratio of 0.86 is an indication that the two components have a similar type, but contrary to the previous case, the depths of the correlation dips are significantly different, which implies that their luminosities are also different. Actually, the magnitude difference of the two components can be inferred from the value of the ratio of the integrated aeras of the dips (Lucke & Mayor, 1980). For HD 98880, we obtain $\Delta m_B = 1.25 \pm 0.1$ mag.

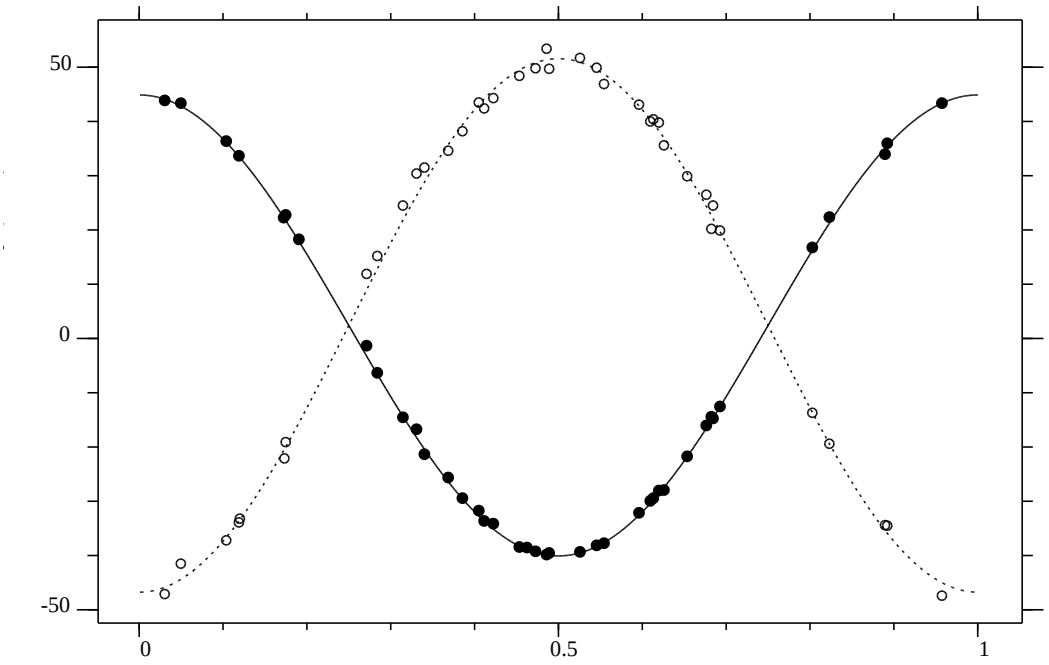

Figure II.3: Radial velocity curves for HD 98880. Filled circles: main component, open circles: secondary component. The origin for phases corresponds to the ascending node passage. From Carquillat et al. (2001).

Physical parameters and evolution state of the system

The Hipparcos parallax, $\pi = 4.25 \pm 0.91$ mas (i.e. $d = 235$ pc), combined with the apparent magnitude $V = 8.06$ leads to a global absolute magnitude of $M_V = 1.20 \pm 0.46$ for the system, if we neglect the interstellar absorption. If we assume that the effective temperatures of the two components are similar ($T_1 \approx T_2$), $\Delta m_V \approx \Delta m_B$, and if we use the value of $\Delta m_B = 1.25$ mag found previously, we obtain the absolute V magnitudes of both components: $M_{V1} = 1.5 \pm 0.5$ and $M_{V2} = 2.75 \pm 0.5$.

For HD 98880, Olsen (1983) gives the following Strömgren photometry indices $V = 8.063$, $b - y = 0.228$, $m_1 = 0.243$, $c_1 = 0.642$ (see Sect. I.5); the β index was not given by Olsen. The calibration by Crawford (1979) leads to $\beta = 2.72$ and $\delta m_1 = -0.066$ (blanketing parameter). These data allows us to estimate the effective temperature and the metallicity. The effective temperature, as well as the surface gravity, can be obtained with the theoretical grids computed by Moon & Dworetsky (1985) (see Sect. I.5).

In this case we find: $T \approx 7000$ K and $\log_{10} g \approx 4.0$. This value for T seems both compatible with the classification made by Abt (1984): A4-F3-F5 respectively for the K line, the Balmer lines and the metallic lines, and with the color index $B - V = 0.39$ reported in the Hipparcos catalogue (ESA, 1997). As for the metallicity, it can be estimated from the relation δm_1 versus [Fe/H] established by Crawford (1975). In this case, [Fe/H] $\approx$ 0.8 dex, which is a good signature of Am character.

On the other hand, if we refer to the theoretical HR diagram computed by Schaller et al. (1992) for solar metallicity stars (see fig. 4 of Carquillat et al. (2001)), the masses of the two components would be about 1.9 $M_\odot$ and 1.6 $M_\odot$, whose ratio is close to that of the RV curve amplitudes. To locate each component in this diagram, we applied a correction of -0.1 mag to the absolute magnitude, (i.e., bolometric correction for $T = 7000$ K) to derive $M_{\rm bol}$ and the luminosity L.

We can then propose the following (rough) model: the system HD 98880 is about 1.3×10^9 years old and constituted by two Am stars with effective temperature close to 7000 K; the primary (1.9 $M_\odot$) would be already a rather evolved main sequence star whereas the secondary (1.6 $M_\odot$) would be only about 1 mag above the zero-age main sequence. The corresponding theoretical radii would be 3.3 $R_\odot$ for the primary and 1.9 $R_\odot$ for the companion.

System dimensions, rotation-revolution synchronism

The value of 1.9 $M_\odot$ found for the mass of the primary would imply $i = 43°$, $a = 26.16$ Gm$= 37.6$ $R_\odot$. Hence, like HD 81976, HD 98880 is a detached system without the possibility of eclipses.

The values of $v. \sin i$ deduced from the correlation dip profiles are 10.6 ± 0.2 km/s for the primary and 9.2 ± 0.7 km/s for the secondary. We applied the Kiramura & Kondo test with these values and $i = 43°$. Assuming the coplanarity between the orbital and equatorial planes, the rotation-revolution synchronism would require radii of respectively 4.35 $R_\odot$ and 3.8 $R_\odot$ for the primary and secondary. These values are significantly larger than those (3.3 $R_\odot$ and 1.9 $R_\odot$) corresponding to the model described above. We conclude that, unlike HD 81976, the HD 98880 system has not yet reached the synchronism state, which is not surprising in view of its much longer orbital period.

II.2 Paper III: HD 7119 (*SB2* and triple system)

In Carquillat et al. (2002), we presented our study of HD 7119 from radial velocity observations made in 1992-1998 with the CORAVEL instrument at OHP. Known as an Am/δ Del metallic-line star, HD 7119 was included in our spectroscopic survey of Am-type stars whose purpose was to determine the frequency of binaries in this stellar family.

This object was found to be a double-lined spectroscopic binary with a variable value of V_0, the systematic velocity of the center of gravity of the pair. The variation of this parameter was interpreted in terms of orbital motion of an unseen third body with a much longer period. The orbital elements were derived for both the short and the long period orbits. These orbits can be considered as well determined since these observations were performed on a regular basis over the 1992-1998 period, covering more than 320 orbital cycles for the short-period (P=6.76 days) and 1.3 cycle for the long-period orbit (P$\sim$1700 days).

As deduced from the ratio of the correlation dip areas, the magnitude difference of the components of the short-period system is 0.7 mag. Combined with the Hipparcos data, this value lead to visual absolute magnitudes of 0.5 and 1.2 for the primary and secondary components respectively. Such magnitudes are consistent with evolved δ Del-type stars.

The third body could be a cool dwarf star with a minimum mass of 0.5 $M_{\odot}$, located at $\sim$0.016" from the main system. Consequently, this component it is different from the visual companion detected by Couteau with a separation of 3.35". If this latter visual component was confirmed to be a physical component, (not an optical one), HD 7119 would be a quadruple system.

II.2.1 Previous work

In the "Third catalogue of Am stars with known spectral types" (Hauck, 1986), Hauck selected Bertaud (1970)'s classification for HD 7119, i.e., A5 for the CaII K-line, and F2 for the metallic lines (nothing was mentioned about the hydrogen lines). HD 7119 was first reported as Am by Bidelman (1964) from objective-prism observations, and then re-classified as δ Del by A.P. and C.R. Cowley (1965), using Morgan's classification spectrograph. In a more recent paper, Bossi et al. (1983) reported a private communication where M. Jaschek confirmed Cowley's δ Del classification. More recently still, a new classification was established with the Marly spectrograph at OHP (IIaO plates with a dispersion of 80 Å.mm^{-1}) by Grenier et al. (1999), who gives: Am (A4 A8 F4). This last classification is close to Bertaud's. However, Grenier et al. note that the absolute magnitude of HD 7119 derived from the Hipparcos parallax leads to a much too large luminosity compared to the proposed spectral type. This apparent discrepancy vanishes when considering the δ Del type previously attributed to this object.

Bossi et al. have detected a possible photometric variability of HD 7119 in the visible domain, which may be due to pulsations. For these authors, evolved stars with metallic lines of δ Del type could also be pulsating variables, whereas this seems to be out of the question for dwarf stars of Am-type.

In Carquillat et al. (2002), we revealed the (to our knowledge, previously unknown) double-lined spectroscopic binary nature of HD 7119. Previous spectroscopic observations, also performed at OHP (Fehrenbach et al., 1997, Grenier et al., 1999), did not reveal the binary nature of this object. This lack of detection is probably the consequence of an insuffi-

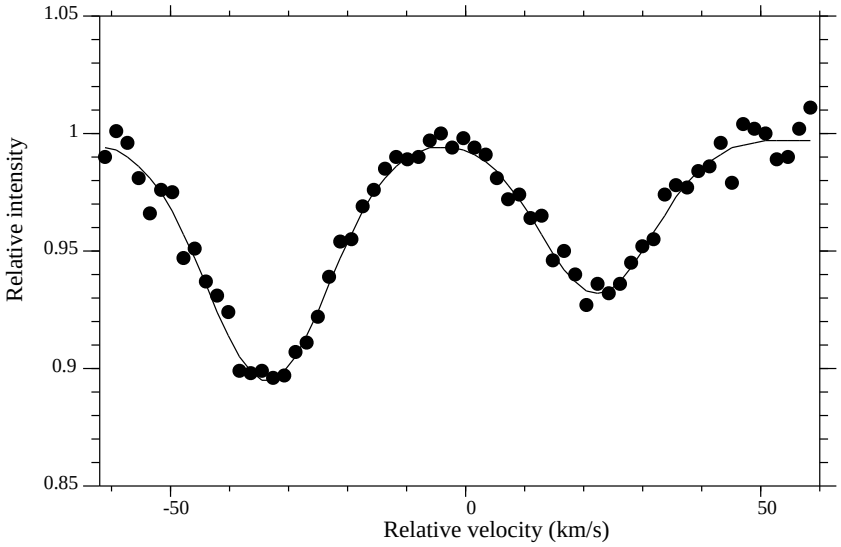

Figure II.4: Typical CORAVEL cross-correlation dip obtained for HD 7119. From Carquillat et al. (2002).

cient spectroscopic dispersion (80 Å/mm in both cases, which limits the resolution at ∼110 km/s). We find that the short-period system, with a period close to seven days, exhibits a variation of the velocity V_0 of its center of gravity with a period of 4.7 years. As HD 7119 is also known as a visual binary (Cou 147 AB, Couteau, 1978) we investigate whether the third "spectroscopic" body corresponds to the visual component detected by Couteau at Nice Observatory.

II.2.2 Observations and derivation of orbital elements

Sixty radial velocity (RV) measurements were performed with CORAVEL and were used for the determination of the orbital elements of the system. These observations (Table 1 of citeAm-PaperIII) were obtained over six years (November 1992 – October 1998) which correspond to 320 orbital cycles. Fig. II.4 shows an example of the correlation dips observed for the primary and secondary components of HD 7119. Five measurements had to be discarded because the correlation dips were blended. Indeed, given the width of these dips, the RV separation of two components had to be larger than ∼20 km/s to allow reliable measurements. The mean internal error is 0.7 km.s^{-1} for the primary RV and 0.9 km.s^{-1} for the secondary RV.

The orbital elements were first computed with my least-square program `BS1.for`. During a first test on the primary RV, it appeared that most residuals $(O-C)_{01}$ were too large, and not randomly distributed (Fig. II.5). Their standard deviation was $\sigma(O-C)_{01} = 1.7$ km.s^{-1}, which was more than twice the mean error of the RV measurements. The presence of a perturbing third body, with a much larger period was thus very likely.

For reducing those data, I wrote a new program (`BS3.for`) to simultaneously fit the orbit of the two visible components and that of the invisible third component. To obtain the initial values of the orbital parameters for the long-period system, we proceeded with the same method as for HD 83270-1 (Ginestet et al., 1991). We split the 60 RV measurements into 12 small "observation groups" (separated by blank lines in Table II.2) for which the variation

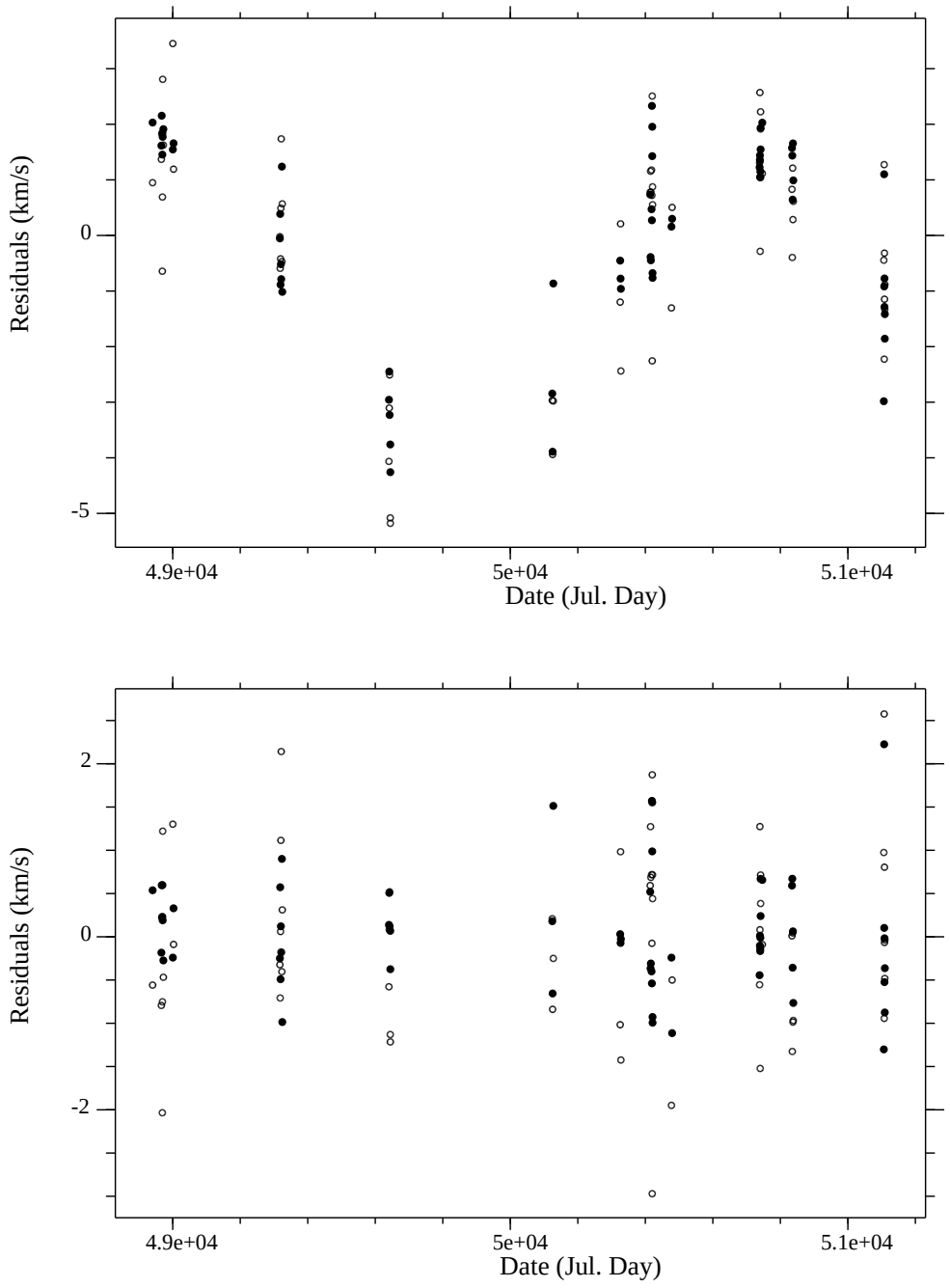

Figure II.5: HD 7119: residuals obtained when assuming two components only (left) and three components (right). From Carquillat et al. (2002).

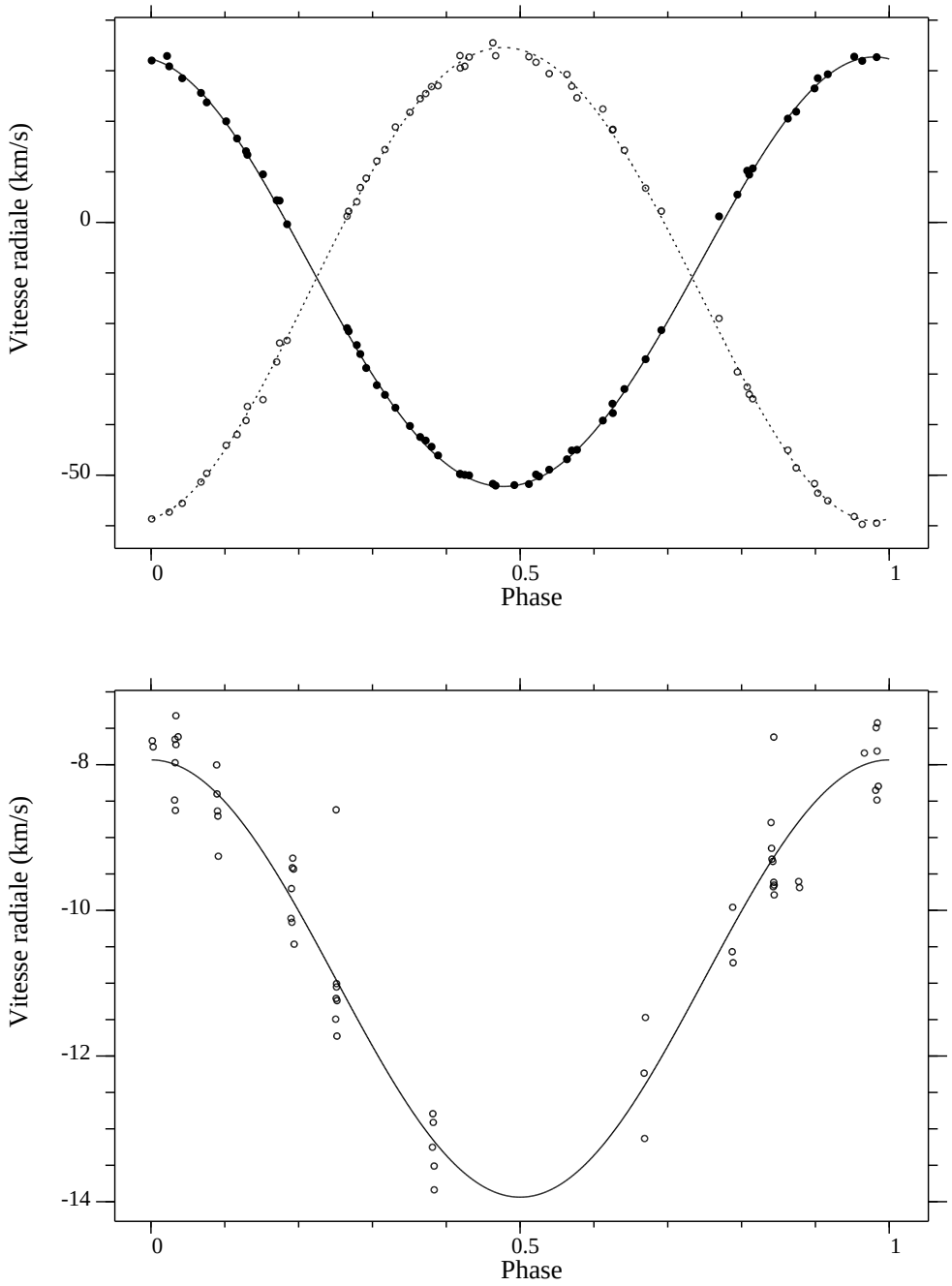

Figure II.6: HD 7119. Left: radial velocity curves of the primary (filled circles) and secondary (open circles) components of the short-period system. Right: radial velocity curve of the center of gravity of the short period system. Those orbits were calculated with `BS3.for`. From Carquillat et al. (2002).

Table II.2: Orbital elements of HD 7119. Orbit 1: final elements for the short-period system. Orbit 2: elements corresponding to the orbital motion of the center of gravity of the short-period system relative to the center of gravity of the triple system (Carquillat et al., 2002).

Elements		Orbit 1		Orbit 2	
P	days	6.761504	$\pm$0.000027	1687.	$\pm$26
$T_0^{(*)}$	JD2400000+	48945.35	$\pm$0.09	50684.4	$\pm$12.
ω	degrees	7.7	$\pm$5.0		
e		0.028	$\pm$0.003	0.	$\pm$0.04
K_1	km·s^{-1}	42.48	$\pm$0.13	3.00	$\pm$0.15
K_2	km·s^{-1}	46.81	$\pm$0.19		
V_0	km·s^{-1}	Variable		-10.94	$\pm$0.11
$a_1 \sin i$	Gm	3.945	$\pm$0.012	69.61	$\pm$3.64
$a_2 \sin i$	Gm	4.350	$\pm$0.018		
$M_1 \sin^3 i$	M$_\odot$	0.262	$\pm$0.002		
$M_2 \sin^3 i$	M$_\odot$	0.237	$\pm$0.002		
f(m)	M$_\odot$			0.0047	$\pm$0.0008
$\sigma(O-C)_1$	km·s^{-1}	0.68			
$\sigma(O-C)_2$	km·s^{-1}	1.04			

$^{(*)}$ T_0 : periastron passage for orbit 1; ascending node passage for orbit 2.

of the velocity V_0 of the center of gravity of the short-period system could be neglected. The variation versus time of the residuals obtained in these groups could be interpreted as a Keplerian motion due to the presence of a third body. We obtained a first estimation of the elements of the long-period orbit by applying the least-square program `BS1.for` to these residuals.

These values were then used as initial values by the least-square program `BS3.for` which simultaneously fitted the two orbits. For that computation, weights of 1.0 and 0.5 were respectively used for the primary and secondary RV measurements. The residuals obtained in that case (Fig. II.5) are very close to the mean standard deviation of the measurement errors for both components and do not exhibit any long-term variation. The two orbits are displayed in Fig. II.6 and the corresponding elements with their errors are given in Table II.2.

The eccentricity of the two visible components is very small and the orbit is nearly circular, which is not surprising, given the short period of 6.76 days. This small value for the eccentricity is nevertheless significant with regards to its error value. The presence of a third body may have contributed to the small eccentricity in a system already circularized Mazeh (1990).

The orbit of the third body was first assumed to be circular, on the basis of the distribution of the residuals. When adding two more parameters (eccentricity and omega for the long-period orbit) to the model, the residuals remained at the same level and the eccentricity derived was very small, equal to zero within the errors.

II.2.3 Physical parameters of the short-period system

The ratio of the correlation dip areas given by CORAVEL for the primary and secondary components allows an evaluation of the magnitude difference (Lucke & Mayor, 1980). For

HD 7119, this ratio is 1.93, which leads to $\Delta m_V = 0.715$, if we assume that the two stars have similar temperatures.

The mass luminosity relation for main sequence stars with $M_{\rm bol} < 7.5$, as given by Schmidt-Kaler (1982), is: $logM/\mathrm{M}_\odot = 0.46 - 0.10M_{\rm bol}$, i.e., in the case of a binary system: $logM_1/M_2 = 0.10\Delta M_{\rm bol}$. For HD 7119, let us assume that the effective temperatures of both components are similar and thus $\Delta M_V \approx \Delta M_{\rm bol}$. The mass ratio is directly derived from orbital data with $M_1/M_2 = K_2/K_1$. From Table II.2 we obtain $M_1/M_2 = 1.102 \pm 0.003$ and $\Delta M_V = 0.42 \pm 0.03$ mag., which is smaller than the value derived from the correlation dips. This is an indication that the two stars are not at the same evolution stage. In particular, the primary is more luminous than a dwarf star with a similar mass.

In the Hipparcos catalogue (ESA , 1997), we find the following values: $V = 7.57$, $B - V = 0.34$, $\pi = 3.38 \pm 0.93$ mas. HD 7119 would then be at a distance $d = 300$ (+110, -70) pc. Its global absolute magnitude would be $M_V = 0.035 \pm 0.60$, assuming an interstellar absorption of 0.18 mag. Lucke (1978). If we neglect the contribution of the invisible third body, this would lead to: $M_{V1} = 0.50 \pm 0.60$ and $M_{V2} = 1.20 \pm 0.60$ for the absolute magnitudes of the primary and the secondary, respectively. If both stars are hot late stars with metallic lines, which is very likely when considering the global index $B - V$, these values correspond to the magnitudes of giant stars (Schmidt-Kaler, 1982). The two visible components are then two δ Del stars.

Obviously, the lack of knowledge of the orbital inclination i forbids a direct determination of the component masses. To estimate these values, we can use Schaller et al. (1992)'s theoretical HR diagram with evolution tracks, and the isochrones given by Meynet et al (1993), as in Carquillat et al. (2001) for the system HD 98880. For HD 7119, we estimated $\mathrm{T_{eff}} \approx 7500$ K, on the basis of a de-reddened colour index $B - V$=0.28, and the luminosity of each component by applying a bolometric correction of -0.1, to the absolute magnitudes previously found. Taking into account the uncertainties on these values, the two stars were plotted on the same isochrone with the constraint of a mass ratio equal to $K_2/K_1 = 1.10$, as observed. The corresponding mass values are $M_1 = 2.2 \pm 0.3\mathrm{M}_\odot$ and $M_2 = 2.0 \pm 0.3\mathrm{M}_\odot$, with an age of $\sim$8. 10^8 years.

The radii can be estimated using the well-known relation $\log R/R_\odot = 0.5 \log L/L_\odot - 2 \log T + 7.54$ with $\log L = 1.9 - 0.4M_{bol}$. This leads to $R_1 = 4.6^{+1.4}_{-1.1} R_\odot$ and $R_2 = 3.3^{+1.1}_{-0.8} R_\odot$. If we are dealing with late Am-type stars, as proposed in this section, these radii are compatible with those of evolved stars (Schmidt-Kaler, 1982).

The value of $M_1 \sin^3 i$ found in Table II.2 then leads to $i = 29.5 \pm 2.0°$, and to a separation of the components of $a = a_1 + a_2 = 17.0 \pm 1.0$ Gm, i.e., 24.0 $\pm 1.5 R_\odot$. Given the estimated radii of 3–5 $\mathrm{R}_\odot$, the system appears detached.

II.2.4 Rotation-revolution synchronism

When considering the short period of the main couple, one may expect that their rotation is synchronized with their orbital motion. In order to check this hypothesis, we applied the Kitamura & Kondo (1978) test on each component. This test assumes that synchronism indeed is verified and then estimates the value of the component radius corresponding to the observed rotation velocity and orbital period (i.e., $R/R_\odot = V_e \times P/50.6$, where V_e is the equatorial rotation velocity in km.s^{-1} and P the orbital period in days). When the values found for each component are compatible with typical radii of stars with similar spectral

types, it is likely that there is indeed synchronism. Let us note that this test assumes that the orbital and equatorial planes of both stars are co-planar. This assumption is needed since the rotation velocity is only measured via the projected equatorial velocity $v_e \sin i$.

As shown by Benz & Mayor (1981, 1984), the projected equatorial velocity can be derived from the analysis of the CORAVEL correlation dips. For HD 7119, the values of $v_e \sin i$ for the primary and secondary are respectively 12.8 ± 0.2 km.s^{-1} and 7.8 ± 0.4 km.s^{-1}. With the assumptions already mentioned (synchronism and co-planarity) these values lead to radii of 3.5 $R_\odot$ and 2.1 $R_\odot$ for the primary and secondary respectively. These values are smaller than the estimated values from the physical parameters (cf. Sect. II.2.3), but they are still in reasonable agreement, given the rather large uncertainties. For instance a small deviation from coplanarity with an inclination of the rotation axes of $i = 22°$ (instead of $i = 29°$ for the orbital axes) would lead to $R_1 = 4.5\ R_\odot$ and $R_2 = 2.8\ R_\odot$, in very good agreement with the theoretical values. We thus conclude that synchronism is plausible for both components.

II.2.5 Hypotheses on the third body

Let $f(m) = (M_1 + M_2) \sin^3 i\ g(\mu)$ be the mass function of the long-period orbit (orbit 2 of Table II.2), with $\mu = M_3/(M_1 + M_2)$, $g(\mu) = \mu^3/(1+\mu)^2$, where M_3 is the mass of the third body.

With the values found in Sect. II.2.3, the total mass of the short-period system is $M_1 + M_2 = 4.2$ M$_\odot$. As the mass function is $f(m) = 0.0047$ M$_\odot$ (Table II.2), the mass ratio is $\mu \geq 0.11$, i.e., $M_3 \geq 0.47$ M$_\odot$. This boundary value (assuming $i = 90°$ for orbit 2) corresponds to the mass of a cool dwarf with a spectrum close to M2 (Schmidt-Kaler, 1982). As an alternative, if we assume that the orbital plane of the short-period couple and that of the third body are co-planar ($i \sim 30°$), we obtain: $\mu = 0.24$ and $M_3 = 1.0$ M$_\odot$. In that case, the third body could be a dwarf star of solar type, and would also be invisible because of a too large brightness difference ($\Delta m_V \sim 5$ mag.).

Using the value $a_1 \sin i = 69.61$ Gm for the long-period orbit (Table II.2), the separation a' of the third body may thus be approximated by: $a' \approx a_1 \sin i(1 + 1/\mu)/\sin i$. For $i = 90°$ and $i = 30°$, we obtain $a' = 702$ Gm (4.7 AU) and $a' = 724$ Gm (4.8 AU) respectively. At the expected distance of 300 pc, this corresponds to an angular separation of 0.016".

In the introduction, we mentioned that HD 7119 was known as a visual binary (Cou 147), since Couteau's discovery in 1967 with the 50 cm refractor of Nice Observatory (Couteau 1968). The visual companion was recently confirmed by a new observation in 1992 by Thorel (1996). Although the magnitude difference of ~ 5 mag. reported by Thorel is close to that of the third "spectroscopic" body that we found, the separation of 3.35" of the visual companion is considerably larger than the estimation we have just done (0.015"). Note that the visual companion could also be an optical one, since the position parameters (θ, ρ) did not significantly change between the two observations of 1967 and 1992. On the other hand, if the visual companion really was a physical companion, HD 7119 would be a quadruple system.

II.3 Paper IV: HD 100054 B (*SB1* and triple system) and HD 187258 (*SB1*)

In Ginestet et al. (2003) we reported the results of our study of HD 100054 B and HD 187258 from observations made with CORAVEL instruments at Haute-Provence and Cambridge Observatories (in collaboration with R. Griffin). Known as Am/Fm metallic-line stars, both objects were included in our spectroscopic survey of Am-type stars whose purpose was to determine the frequency and properties of binaries in this stellar family.

HD 100054 B was found to be a single-lined spectroscopic binary with a variable value of V_0, the systemic velocity of the centre of gravity of the pair. The variation of this parameter is interpreted in terms of orbital motion of an unseen third body with a much longer period. The orbital elements were derived for both the short- and the long-period orbits.

HD187258 was found to be a single-lined spectroscopic binary from which we computed an orbit.

Physical parameters wer derived for the primary components of both systems

II.3.1 Previous work

HD 100054 B is the faint component of the wide visual binary ADS 8191 AB. This pair is constituted by two A-type stars of visual magnitudes $V = 7.31$ and $V = 8.34$, with a separation near 12" (ESA , 1997). HD 100054 A (HIP 56202) is classified as A5 in the SIMBAD data base; we did not find any correlation dip with CORAVEL for that object.

Olsen (1980) first suspected the chemically-peculiar nature of HD 100054 B: on the basis of its Strömgren photometric indices, he estimated its spectral classification as Ap. Some years later, Bidelman (1988) recognized the star as Am on the basis of spectroscopic observations performed with a slit-spectrograph at Lick Observatory. According to the $B - V$ value of 0.095 quoted in the Hipparcos Catalogue (ESA , 1997), HD 100054 B would be an early-type Am star.

Although that star was reported a long time ago as *SB* (Young 1942), no previous spectroscopic orbit has been determined, to our knowledge, for this object. Our observations (Sect. II.3.2) show that HD 100054 B is a single-lined *SB* (i.e, *SB1*), belonging to a triple spectroscopic system with a short-period orbit ($P \approx 13$ days) and a long-period one ($P \approx 2.4$ years).

Classified as F2 in the Henry Draper Catalogue, HD 187258 ($V = 7.59$) was recognized by Bidelman (1951) as a metallic-line star of type Fm. More precisely, the types for the K-line and the metallic lines are F0 and F5 III, respectively. Those classifications agree with the values of the colour index $B - V$ measured for this star: 0.32 from Mendoza, Gómez & González (1978), and 0.36 ($\pm$0.01) from Hipparcos (ESA , 1997). Apparently, no information about the *RV* of this star was known before the survey, related to the Hipparcos mission, carried out at OHP by S. Grenier and her team. For HD 187258, Grenier et al. (1999) quote an RV of -45.3 ± 3.2 km s^{-1}. That value was obtained from three independent observations, but there is no mention of any indication of *RV* variability. Our observations clearly establish that HD 187258 is a *SB1* with a period close to 26 days (Sect. II.3.2).

II.3.2 Observations and derivation of orbital elements

HD 100054 B

For HD 100054 B, 48 *RV* measurements were performed (39 at OHP and 9 at Cambridge), and for HD 187258, 40 *RV* were similarly obtained (26 at OHP and 14 at Cambridge). Those data are displayed in Tables 1 and 2 of Ginestet et al. (2003). They were obtained with CORAVEL-type instruments, i.e., spectrophotometers that make *RV* measurements by performing a cross-correlation of the stellar spectrum with a physical mask placed in the focal plane of the spectrograph. In the case of the OHP observations, Gaussian functions are fitted to the cross-correlation dips to derive radial velocities (Baranne, 1979); Cambridge traces are cross-correlated with functions derived from one that was empirically established from observations of practically non-rotating stars by convolving it with a broadening function to mimic stellar rotation. The OHP CORAVEL is mounted at the Cassegrain focus of the 1-m Swiss telescope, while the Cambridge one is at the coudé focus of the 91-cm telescope.

The observations later than JD 2451690 were obtained by R. Griffin at Cambridge and adjusted by a velocity offset of -0.8 km s^{-1} to make them consistent with the others, which were all performed at OHP by the Toulouse group. The r.m.s. uncertainties of the *RV*s were $\sigma_O = 0.64$ km s^{-1} for HD 100054 B and 0.55 km s^{-1} for HD 187258; the two instruments give errors very similar to one another.

We also added the 6 RV obtained by Young (1942), with a weight of 0.07 to account for the larger errors of his measurements. In this case also, a velocity offset (of $+4$ km s^{-1}) was required to make these data consistent with our measurements.

A first determination of the orbital elements of HD 100054 B revealed its character of a triple system, as can be easily seen in the residuals presented in Fig. II.7a. This system is constituted by a pair of stars in an orbit which has a period of about 13 days and a variable systemic velocity, V_0, that can be interpreted in terms of a perturbation from a third object. To carry out the orbital determination, we used the new program, `BS4.for`, that I developed to fit simultaneously the orbital parameters of the inner orbit and the outer (third-body) one. The first step was to obtain an estimation of the elements of the long-period orbit by applying the least-squares program `BS1.for` to the residuals from the fit of the short-period elliptical orbit to the observed radial velocities (Nadal et al., 1979, that I revised completely). The second step was to use the resulting values as the initial elements for the least-squares program `BS4.for` which simultaneously fits the two orbits. The final residuals obtained by this program (Fig. II.7b) have a standard deviation $\sigma_{(O-C)} = 0.61$ km s^{-1}, which is very close to the mean error of the *RV* measurements. The two orbits are displayed in Fig. II.8 and the corresponding elements with their errors are given in Table II.3. Another calculation was independently performed by R. Griffin with a analogous program and led to the same results.

HD 187258

The orbital elements of HD 187258 were derived with my program `BS1.for`. For that object, no evidence for the presence of a third component could be seen in the residuals (cf. Fig. 3 of Ginestet et al. (2003)). The orbital elements are given in Table II.3, and the corresponding radial velocity curve in Fig II.9.

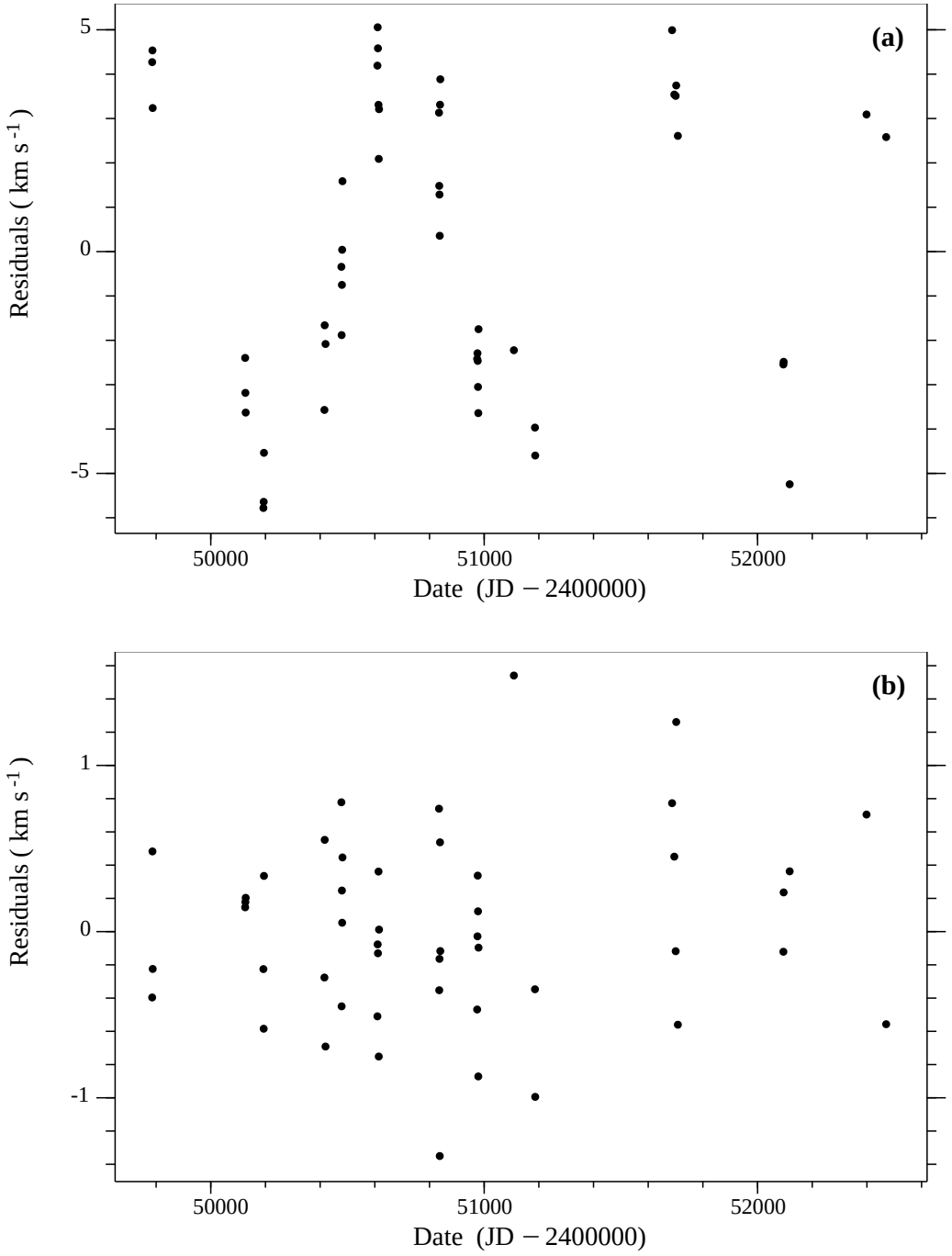

Figure II.7: HD 100054 B: RV residuals $(O - C)$ obtained for our measurements when assuming two components only (a), and three components (b). Notice the difference in the vertical scales. From Ginestet et al. (2003).

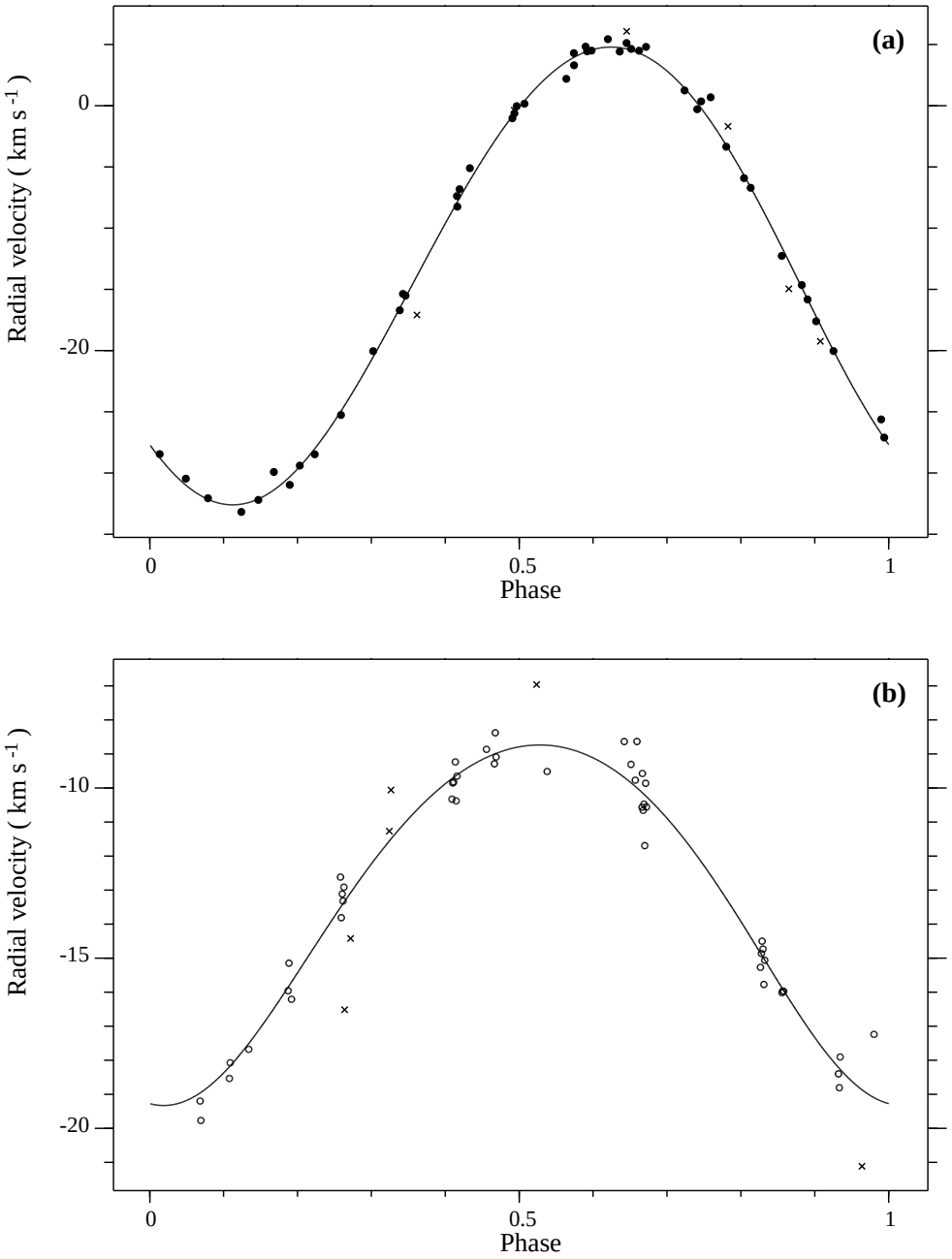

Figure II.8: HD 100054 B: RV curves computed with the orbital elements of Table II.3. (a): short period system (orbit 1); (b): motion of the centre of gravity of the inner system (orbit 2). Both orbits were fitted to the data simultaneously with my program `BS4.for`. The origin of the phases corresponds to the periastron passage. Circles correspond to our measurements and crosses to Young (1942)'s data. From Ginestet et al. (2003).

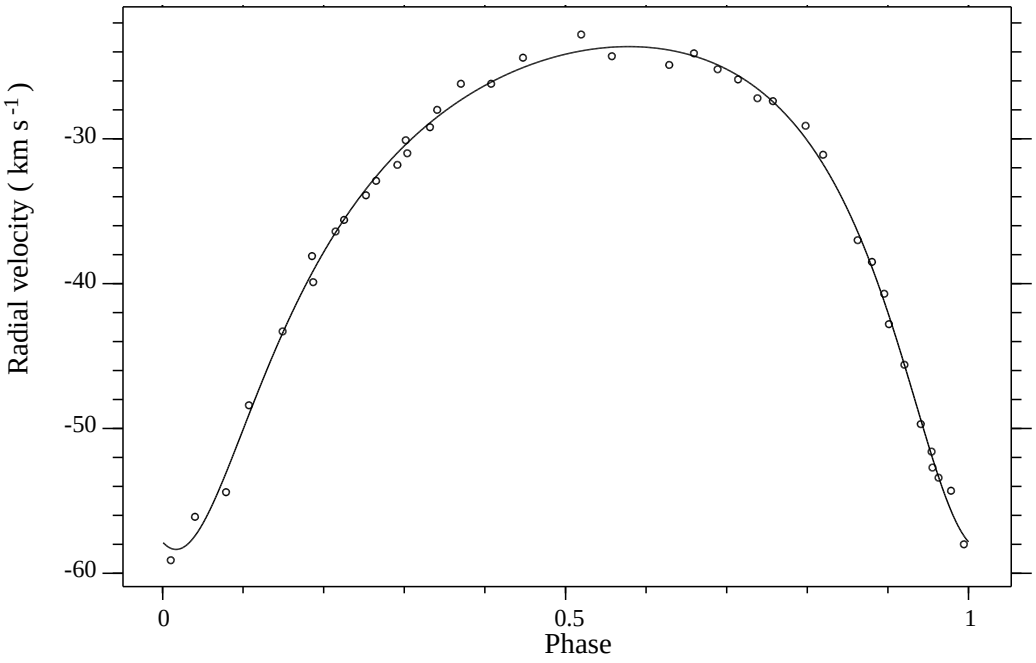

Figure II.9: HD 187258: RV curve computed with the orbital elements of Table II.3. The origin of the phases corresponds to the periastron passage. From Ginestet et al. (2003).

Table II.3: Orbital elements of HD 100054 B and HD 187258. For HD 100054 B, these elements were obtained with a simultaneous fit of two orbits. Orbit 1 refers to the short-period system, whereas orbit 2 refers to the orbital motion of the centre of gravity of the short-period system relative to the centre of gravity of the triple system. In Col. 3, T_0 is the periastron passage. From Ginestet et al. (2003).

Object	P days	T_0 (JD) 2400000+	ω deg.	e	K_1 km s^{-1}	V_0 km s^{-1}	$a_1 \sin i$ Gm	$f(m)$ M$_\odot$	$\sigma_{(O-C)}$ km s^{-1}
HD 100054 B	12.79430	49781.19	137.	0.028	18.69		3.29	0.0087	
(orbit 1)	$\pm$0.00008	$\pm$0.53	$\pm$15.	$\pm$0.008	$\pm$0.15		$\pm$0.03	$\pm$0.0002	
HD 100054 B	874.2	49377.	172.	0.097	5.30	$-$13.52	63.4	0.013	0.61
(orbit 2)	$\pm$1.6	$\pm$36.	$\pm$15.	$\pm$0.033	$\pm$0.17	$\pm$0.10	$\pm$2.4	$\pm$0.001	
HD 187258	25.8048	49628.91	165.9	0.370	17.36	$-$34.76	5.72	0.011	0.68
	$\pm$0.0012	$\pm$0.12	$\pm$1.6	$\pm$0.011	$\pm$0.20	$\pm$0.14	$\pm$0.09	$\pm$0.001	

II.3.3 Eccentricities of the inner and outer orbits of HD 100054 B

The eccentricities of both orbits of HD 100054 B are very small. That is not surprising for the inner system, given the period of 12.79 days: with such a short period, the orbits of binary systems are usually circular. Following Lucy & Sweeney (1971) and Bassett (1978), we performed an F-test to check whether these orbits could be considered as circular, taking the errors into account.

Let S_e and S_c be the weighted sum of squares of the residuals, corresponding to an elliptical or a circular orbit, respectively. Estimates of residual variance are given by $S_e/(N-M)$ and $S_c/(N-(M-2))$ in the two cases, where N is the number of measurements, and M is the number of fitted parameters when two elliptical orbits are fitted simultaneously (here $N = 54$ and $M = 11$). The efficacy of the two additional elements ($e\cos\omega$, $e\sin\omega$) in reducing S_c may be then measured by the ratio F of the variances:

$$F = \frac{(S_c - S_e)/2}{S_e/(N-M)} \tag{II.1}$$

If the hypothesis of circularity is correct, F is distributed as F_{ν_1,ν_2}, with $\nu_1 = 2$ and $\nu_2 = N - M = 43$ degrees of freedom.

When both orbits are elliptical, the weighted sum of squares is $S_e = 18.2$ km^2 s^{-2}. When imposing a constraint of circularity on the inner and then the outer orbit, which we will call orbits 1 and 2 respectively, we obtain $S_c(orbit1) = 23.6$ km^2 s^{-2} and $S_c(orbit2) = 22.0$ km^2 s^{-2}. We then have $F(orbit1) = 6.38$ and $F(orbit2) = 4.49$. Using the distribution of $F_{2,43}$, this corresponds to a level of significance of 0.4% and 1.7%, for orbits 1 and 2, respectively.

Hence this test indicates that the eccentricity of the short-period orbit of HD 100054 B is significant at the 0.4% level. The presence of a third body may well have contributed a small eccentricity to a system that is in principle already circularized (Mazeh 1990).

II.3.4 Physical parameters

For the two systems, we can use both Hipparcos data and Strömgren photometric indices for an estimation of the physical parameters (see Sect. I.5), although those data are more accurate for HD 187258 than for HD 100054 B.

Indeed, for HD 100054 B, the Hipparcos Catalogue (ESA , 1997) gives $\pi = 8.52 \pm 5.27$ mas (relative error 62%), and the Strömgren indices $V = 8.24$, $b-y = 0.048$, $m_1 = 0.232$, $c_1 = 1.009$ (Olsen 1983) do not include β photometry. For HD 187258, the Hipparcos parallax, $\pi = 7.68 \pm 0.90$ mas is more accurate (relative error 12%), and the Strömgren photometry (Jordi et al. 1996) includes β photometry: $V = 7.59$, $b-y = 0.218$, $m_1 = 0.170$, $c_1 = 0.717$, $\beta = 2.721$. Hence the quoted parallaxes would imply similar distances around 120–130 pc for the two systems.

To obtain a better estimate of the distance of HD 100054 B, we could also refer to HD 100054 A. The two stars almost certainly form a physical system for two reasons:

- on statistical grounds alone, one would not expect to find two stars so bright so close together very often.
- they have similar RVs. Young (1942) gives a value of -15.5 km s^{-1} for HD 100054 A, which is very close to $V_0 = -13.5$ km s^{-1} that we measured for HD 100054 B.

Table II.4: Physical parameters of HD 100054 B and HD 187258 primary components according to their colours in the Strömgren photometry. From Ginestet et al. (2003).

Object	M_V (mag.)	$T_{\rm eff}$ (K)	$\log g$ (cgs)	[Fe/H] (dex)	$\log(L/{\rm L}_\odot)$	M ($M_\odot$)	R ($R_\odot$)
HD 100054 B	1.7	8500	4.2	0.50	1.3	2.0	2.1
HD 187258	1.95	7000	3.75	0.13	1.15	1.8	2.7

For HD 100054 A, Hipparcos found $\pi = 3.87 \pm 1.95$ mas (relative error 50%), which corresponds to a distance of ∼260 pc. The mean value for the distance of that system is therefore $d \approx 200$ pc, with still a large uncertainty. That estimate is in agreement with the visual absolute magnitude $M_V = 1.7$ of HD 100054 B deduced from Strömgren photometry.

The physical parameters of the primary components that we obtained from these data are given in Table II.4. For HD 187258, the value of M_V in Col. 2 corresponds to the mean of the values derived from Hipparcos and Strömgren photometry. For HD 100054 B, the value given by Hipparcos was too inaccurate; M_V was thus computed from Strömgren photometry only.

We derived the other parameters of the table from Crawford (1975, 1979)'s calibrations and the grids of Moon & Dworetsky (1985). For HD 100054 B, the value of β is indirectly deduced from the close correlation (Crawford 1979) between that parameter and the $(b-y)$ index, i.e., $\beta = 2.90$ (value also obtained when using Moon's (1985) UVBYBETA program). For these investigations, we neglect the contributions of the unseen components and the interstellar extinction. Indeed, using the ubvy photometry, Moon's (1985) UVBYBETA program shows that there is no reddening for HD 100054 B, and only $E(b-y) = 0.005$ for HD 187258.

Finally, we report in Fig. II.10 the position of the single observed component of each of the systems in the theoretical HR diagram from Schaller et al. (1992), with the isochrones given by Meynet, Mermilliod & Maeder (1993). We shall adopt what follows:

- the primary of the spectroscopic triple system HD 100054 B is a little-evolved early Am star with a theoretical mass near 2 $M_\odot$ and some 500 million years old (log (age) ≈ 8.7).

- the primary of the spectroscopic binary HD 187258 is an Am/Fm star that is already evolved above the MS. Its mass is about 1.8 $M_\odot$ and its age ∼1300 million years (log (age) ≈ 9.1). Notice that its low metallicity, $[Fe/H] = 0.13$ dex, could indicate it is a marginal Am star.

II.3.5 Rotation–revolution synchronism

Synchronization is a mechanism involved in the slowing of the rotation required to form Am stars under the diffusion process. We therefore applied the synchronism test of Kitamura & Kondo (1978) to the primary components of the two systems.

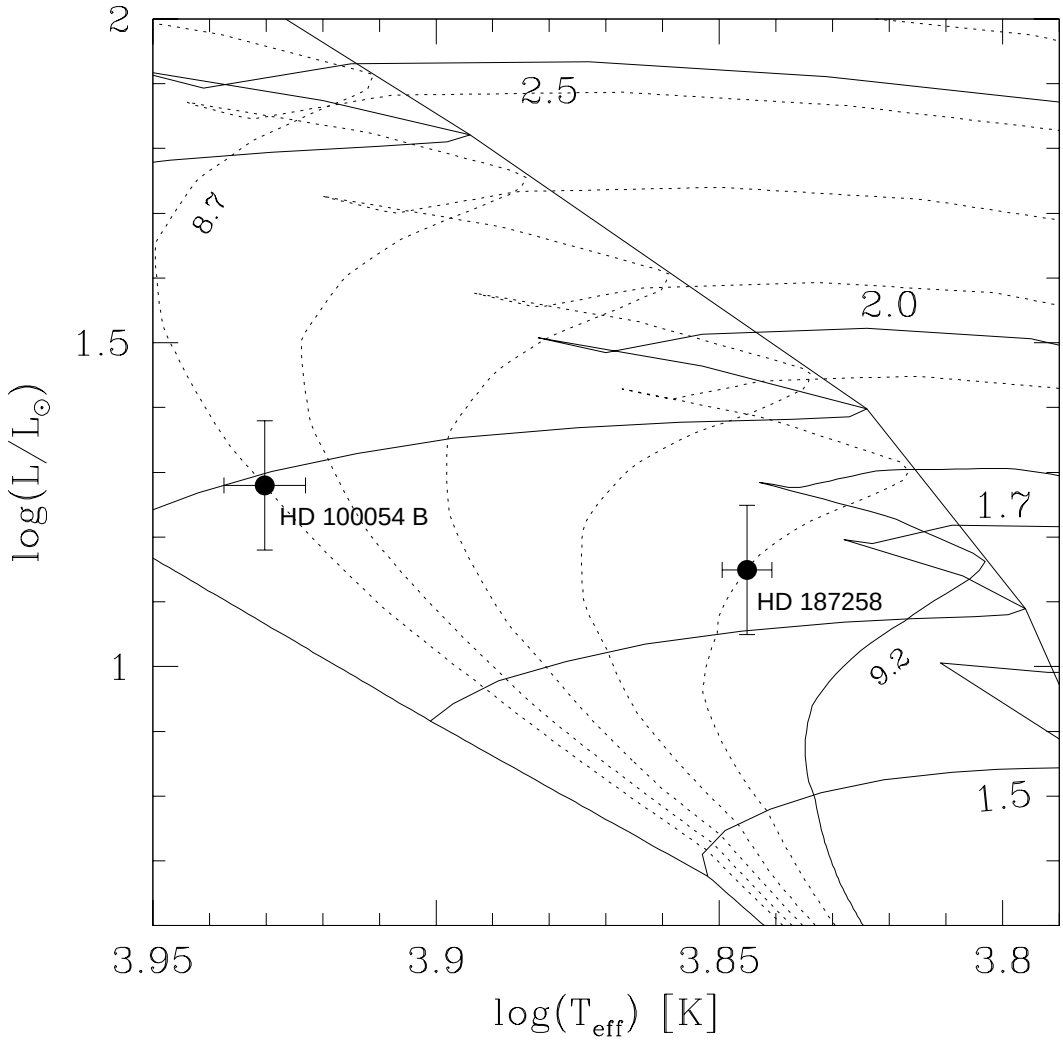

Figure II.10: Location of the primary components of HD 100054 B and HD 187258 in the theoretical evolutionary HR diagram computed by Schaller et al. (1992), with the isochrones given by Meynet et al. (1993). From Ginestet et al. (2003).

This test consists of calculating the radius R of the star in the hypothesis of synchronism between axial rotation and orbital revolution, assuming that the equatorial plane of the star and the orbital plane are coplanar. That leads to $R/R_\odot = V_e \times P/50.6$, where V_e is the tangential, equatorial, rotation velocity in km s^{-1} and P is the orbital period in days. When the value of R is consistent with the value derived from theoretical predictions or other standard data, it is likely that there is indeed synchronism.

We have no direct knowledge of V_e but only of the projected rotation velocity, $V_e \sin i$, that can be derived from the analysis of the CORAVEL correlation dips, as shown by Benz & Mayor (1981, 1984). For the two systems concerned, the values of $V_e \sin i$ are 5.6 ± 1.0 km s^{-1} and 11.4 ± 1.0 km s^{-1} for HD 100054 B and HD 187258, respectively.

Case of HR 100054 B (inner orbit).

Let R_s be the radius of synchronism. The inequality $V_e \geq V_e \sin i$ implies $R_s \geq 1.4 R_\odot$, and if we assume $30° < i < 90°$ (the most probable range for *SB*s, taking into account that the probability that $i < 30°$ is only $1 - \cos i = 0.13$) we have 2.8 R$_\odot$ $> R_s >$ 1.4 R$_\odot$ and we thus conclude that synchronism is plausible (see Table II.4).

Case of HD 187258.

HD 187258 has an elliptical orbit with a large eccentricity which rules out the possibility of a "true synchronism" (actually the inequality $V_e \geq V_e \sin i$ would imply $R_s \geq 5.8$ R$_\odot$ which is too large compared to the value found in Table II.4).

For elliptical orbits, Hut (1981) proposed instead a "pseudo-synchronism" near periastron, which may be marginally reached for HD 187258. Indeed Hut's process implies a pseudo-synchronous rotation period of 13.7 days (formulae 44 and 45 in his paper) and consequently $V_e \sin i \leq 10$ km s^{-1}, which is close to the value of 11.4 ± 1.0 km s^{-1} estimated from the correlation dips (see above).

II.3.6 Nature and separation of the unseen companions

Let

$$f(m) = M_1 \sin^3 i \; \mu^3/(1+\mu)^2 \tag{II.2}$$

be the mass function of a spectroscopic binary, where $\mu = M_2/M_1$ is the mass ratio, and let

$$a = a_1 + a_2 = a_1 \sin i \; (1 + 1/\mu)/\sin i \tag{II.3}$$

be the mean separation of components. In these two equations, the known (measured) quantities are $f(m)$ and $a_1 \sin i$, deduced from the orbit. In the following, we shall attribute to M_1 its theoretical value, in order to constraint the values of μ, M_2, and a. Let us also recall that we have shown (Carquillat et al. 1982) that a good estimation of a can be obtained even if the orbital inclination i is unknown. Let us now consider the equations (II.2) and (II.3) in the case of our two systems.

HD 100054 B (short-period system)

The orbital data lead to $f(m) = 0.0087$ M$_\odot$ and $a_1 \sin i = 3.29$ Gm (Table II.3). Assuming a mass of the primary of $M_1 = 2$ M$_\odot$ (Table II.4), we obtain $\mu \geq 0.18$ (from Eq. II.2) and therefore $M_2 \geq 0.4$ M$_\odot$. The non-detection of the secondary component implies that it is at least 2 magnitudes fainter than the primary, and the same is true for the third body. Given the adopted value of $M_{V_1} = 1.7$ (Table II.4), we then have $M_{V_2} > 3.7$, and the secondary is likely to be a dwarf star in the spectral range F6–M2 (Schmidt-Kaler, 1982).

The smallest separation of the components, obtained with the highest inclination, $i = 90°$, and corresponding to a M2V secondary companion, is (from Eq. II.3): $a = 21.6$ Gm ≈ 31 R$_\odot$. For a F6V secondary companion, its mass would be ~ 1.5 M$_\odot$, and the mass ratio would be $\mu = 0.75$. In that case, Eq. (II.2) leads to $\sin i = 0.316$ ($i \approx 18°$), and consequently (from Eq. II.3) $a = 24.3$ Gm ≈ 35 R$_\odot$ (i.e., 0.8 mas at a distance of 200 pc).

HD 100054 B (outer orbit)

The orbital data are $f'(m) = 0.013$ M$_\odot$, $a'_1 \sin i' = 63.4$ Gm (Table II.3). Equation (II.2) becomes:

$$f'(m) = (M_1 + M_2) \sin^3 i' \; {\mu'}^3/(1+\mu')^2 \qquad \text{(II.4)}$$

with $\mu' = M_3/(M_1 + M_2)$, where M_3 is the mass of the third body. We now consider the two following boundary cases, which takes into account the total mass of the short-period pair:

- $M_1 + M_2 = 2.4$ M$_\odot$ (M2V secondary), that implies from Eq. II.4 that $\mu' \geq 0.20$, and thus $M_3 \geq 0.48$ M$_\odot$.
- $M_1 + M_2 = 3.5$ M$_\odot$ (F6V secondary), that implies $\mu' \geq 0.17$, and thus $M_3 \geq 0.60$ M$_\odot$.

Our conclusion is that the third body could have a minimum mass of about 0.5 solar mass, i.e., the mass of a star of type M0V. The distance of this third component to the centre of gravity of the close pair can be estimated at 380 Gm = 2.5 AU for a mass ratio of $\mu = 0.20$, and 436 Gm = 2.9 AU for a mass ratio of $\mu = 0.17$, assuming $i = 90°$, i.e., a value of about 2.7 AU that leads, at some 200 pc, to an angular separation of 0.014 arcsecond.

HD 187258

The orbital data are $f(m) = 0.0112$ M$_\odot$, $a_1 \sin i = 5.72$ Gm (Table II.3), and the assumed mass of the primary is 1.8 M$_\odot$ (Table II.4). Then, Eq. II.2 implies: $\mu \geq 0.21$, and therefore $M_2 \geq 0.4$ M$_\odot$. Another constraint, as for HD 100054 B, is $\Delta m > 2$ mag. because the secondary remains unseen. Given $M_{V_1} = 1.95$ (Table II.4), the absolute magnitude of the companion would be $M_{V_2} \geq 4$ mag., which corresponds to a main-sequence star of spectral type F8V, or later, with a mass $M_2 \leq 1.2$ M$_\odot$ (Schmidt-Kaler, 1982). Therefore, the companion is most likely a dwarf star whose type can be G, K or early M. As stated above, we can obtain an valuable estimate of component separation, assuming an arbitrary value for i. Here, taking $i = 90°$ to simplify, we found (from Eq. II.3): $a = 33.1$ Gm$= 47$ R$_\odot$. Thus, HD 187258 appears as a well detached system.

II.4 Paper V: study of eight short period spectroscopic binaries (*SB1*)

In Carquillat et al. (2003b), we presented the results of a radial-velocity study of eight Am stars (HD 341, 55822, 61250, 67317, 93991, 162950, 224890, and 225137) observed at Observatoire de Haute-Provence with the CORAVEL instrument. This paper was devoted to the radial velocity study of eight single-lined (SB1) short-period ($P \leq 10$ days) spectroscopic binaries, namely HD 341, 55822, 61250, 67317, 93991, 162950, 224890, and 225137. We found that those systems were single-line spectroscopic binaries whose orbital elements are determined for the first time.

II.4.1 Observations and derivation of orbital elements

To our knowledge, among these eight stars, only HD 225137 was previously detected as having a variable radial velocity (Grenier et al. 1999). Our observations were performed during the period 1992–1999 with the CORAVEL instrument at OHP. For HD 224890, we also added three measurements made by Benz & Mayor in 1980–1982 during the first determinations of $v_e \sin i$ values for the Am stars with CORAVEL.

Forty to seventy observations for each object have been carried out. These data were kindly reduced and input into the Geneva RV data base (Udry, Mayor & Queloz 1999) by S. Udry. For each star, the mean internal standard error strongly depends upon its rotational velocity $v_e \sin i$. That error varies from about 0.5 km s^{-1} for $v_e \sin i \approx 10$ km s^{-1} to about 1.1 km s^{-1} for $v_e \sin i \approx 25$ km s^{-1}. As an illustration, we give two examples of correlation dips, for HD 93991 ($v_e \sin i = 26$ km s^{-1}), and for HD 162950 ($v_e \sin i = 9$ km s^{-1}), in Fig. II.11. For all systems, the secondary dip from the spectroscopic companion could not be detected.

The orbital elements of the eight stars (Table II.5) were subsequently calculated by applying the least-squares program BS1 (Nadal et al, 1979, revised by JLP) to the observed RVs. Those RVs, and the corresponding $(O - C)$ residuals are given in Tables 2 to 9 of Carquillat et al. (2003b), and the computed radial-velocity curves in Fig. II.12 and Fig. II.13. For each of those SBs, the standard deviation of the residuals, $\sigma_{(O-C)}$ is consistent with the RVs mean error, which indicates the absence of detectable spectroscopic third bodies in those systems. Note that HD 61250, HD 67317, and HD 93991 have a circular orbit according to Lucy & Sweeney's (1971) statistical test. Hence, all the orbits of the binaries of our sample with $P < 5$ days are circularized.

II.4.2 Notes for individual systems

In these notes, we shall report the classifications mentioned in Hauck's catalogue. For an Am star, let us recall that there are three spectral classifications k, h and ml, according to the spectral features that are used: K line of Ca II (k), Balmer lines (h), and metallic lines (ml).

HD 341. The Am star is the B component of the visual triple system STT 4256 = CCDM 00081+3123. Strömgren photometry is available. Classified A3(k) F0(h) F2(ml).

HD 55822. That star belongs to the system ADS 5922 AB = CCDM 07154+1904 AB. $\Delta m_{\rm Hip} = 3.2$, Sep. 2.2". Strömgren photometry is available. Classification: A2(k) F2(h) F5(ml).

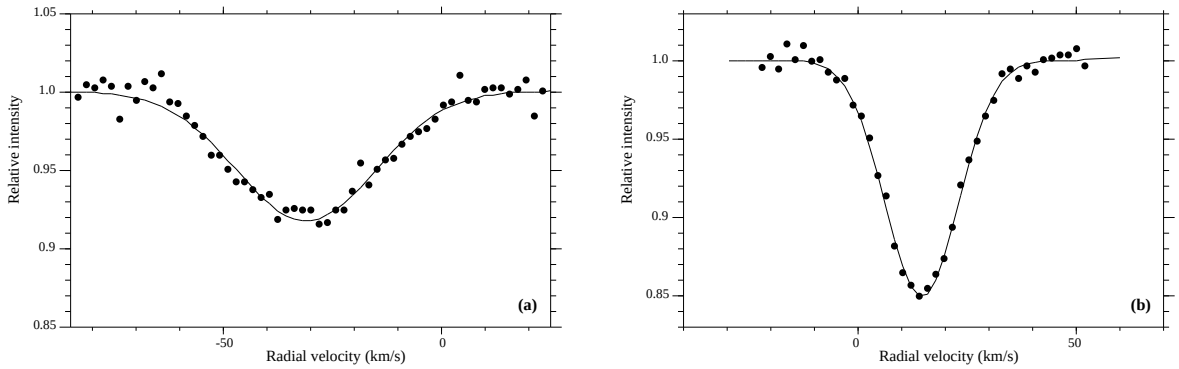

Figure II.11: Examples of correlation dip obtained with CORAVEL: (a) HD 93991 and (b) HD 162950. From Carquillat et al. (2003b).

Table II.5: Orbital elements. In Col. 3, T_0 is the epoch of periastron passage, except for HD 61250, HD 67317, HD 93991 and HD 225137, for which T_0 corresponds to the ascending node passage. From Carquillat et al. (2003b).

Name	P	T_0 (JD)	ω	e	K_1	V_0	$a_1 \sin i$	$f(m)$	$\sigma_{(O-C)}$
	days	2400000+	deg.		km s^{-1}	km s^{-1}	Gm	M$_\odot$	km s^{-1}
HD341	6.24268	48941.63	299.1	0.010	32.46	-3.19	2.79	0.0221	0.46
	±0.00003	±0.32	±18.7	±0.003	±0.11	±0.08	±0.01	±0.0002	
HD55822	5.12294	48673.60	70.6	0.122	40.20	30.87	2.81	0.0338	0.84
	±0.00003	±0.03	±2.0	±0.004	±0.18	±0.12	±0.01	±0.0005	
HD61250	2.23024	48939.29	—	0.000	25.37	-5.43	0.78	0.00378	1.27
	±0.00002	±0.01	—	—	±0.27	±0.19	±0.01	±0.00012	
HD67317	4.43324	49321.05	—	0.000	33.23	6.37	2.03	0.0169	0.69
	±0.00003	±0.01	—	—	±0.16	±0.11	±0.01	±0.0002	
HD93991	3.20858	48675.01	—	0.000	16.46	-15.33	0.73	0.00149	1.01
	±0.00003	±0.01	—	—	±0.21	±0.14	±0.01	±0.00006	
HD162950	10.04288	49153.90	257.9	0.205	11.87	7.03	1.60	0.00164	0.35
	±0.00017	±0.05	±1.6	±0.006	±0.07	±0.05	±0.01	±0.00004	
HD224890	9.54640	48971.19	85.6	0.214	10.89	-8.02	1.40	0.00119	0.52
	±0.00011	±0.06	±2.3	±0.008	±0.09	±0.06	±0.01	±0.00004	
HD225137	4.33346	49326.559	—	0.000	56.42	0.94	3.36	0.0808	0.79
	±0.00002	±0.004	—	—	±0.19	±0.13	±0.01	±0.0008	

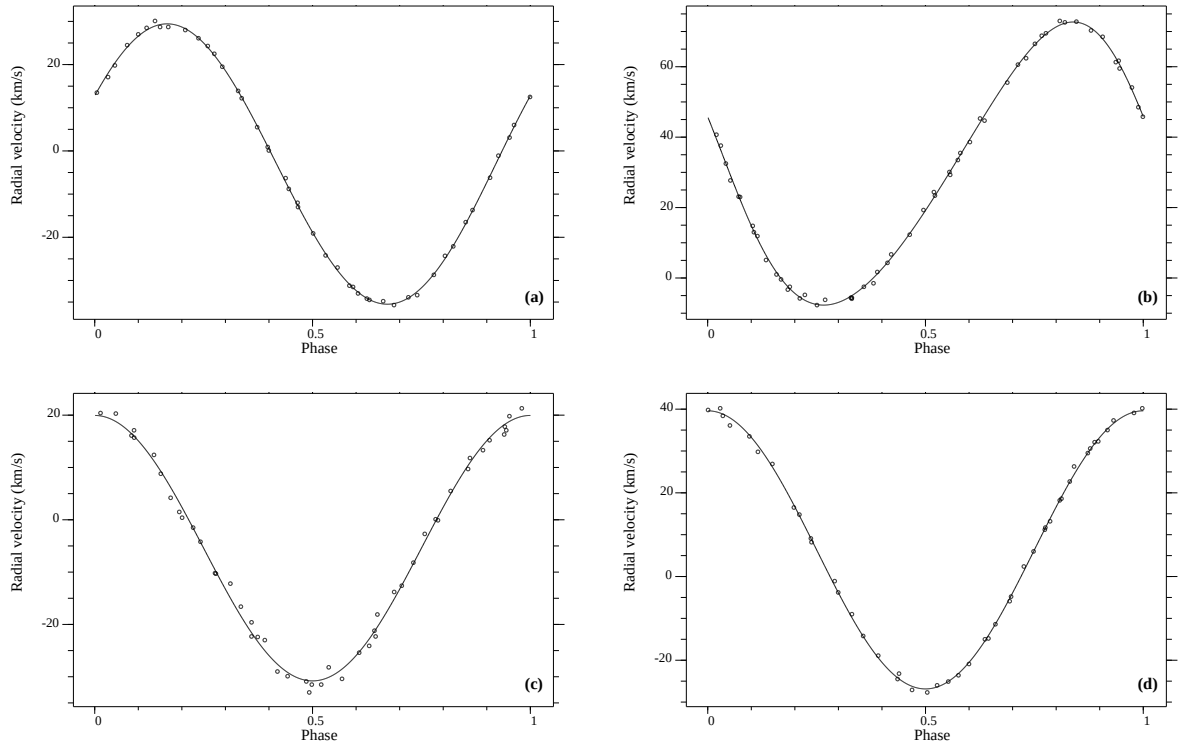

Figure II.12: RV curves computed with our orbital elements: (a) HD 341, (b) HD 55822, (c) HD 61250, and (d) HD 67317. For HD 61250 and HD 67317 (circular orbit) the ascending node is taken as the origin of the phases T_0. For the other systems, T_0 corresponds to the periastron passage. From Carquillat et al. (2003b).

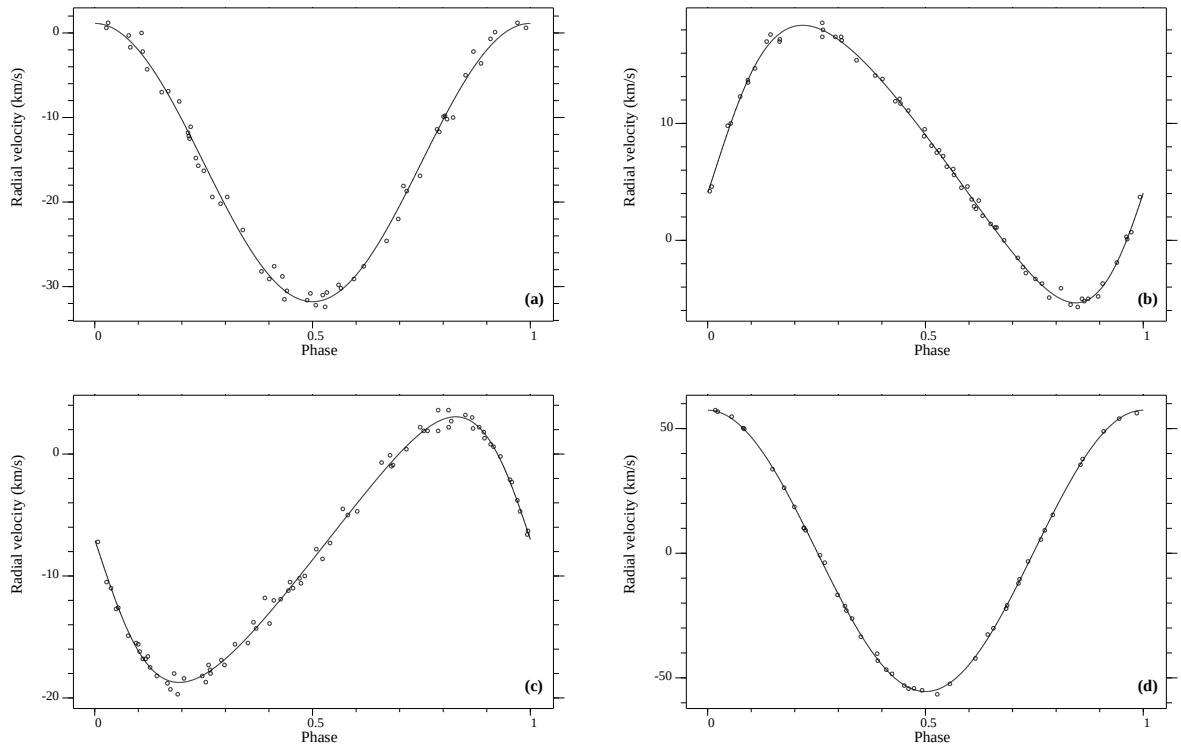

Figure II.13: RV curves computed with our orbital elements: (a) HD 93991, (b) HD 162950, (c) HD 224890, and (d) HD 225137. For HD 93991 and HD 225137 (circular orbit) the ascending node is taken as the origin of the phases T_0. For the other systems, T_0 corresponds to the periastron passage. From Carquillat et al. (2003b).

HD 61250. Visual double HEI 132 = WDS 07429+6517. $\Delta m_v = 1.4$, Sep. 0.5". Strömgren and H_β photometry are available. Classification: A3(k) F3(h) F5(ml).

HD 67317. The star is ADS 6620 AB = CCDM 08102+5548 AB. $\Delta m_{\rm Hip} = 3.1$, Sep. 1.4". Geneva photometry is available. Classification: A1(k) F1(h) F2(ml) (Hauck, 1986). A2(k) A5(h) F3(ml) (Grenier et al. 1999).

HD 93991. Strömgren and H_β photometry are available. Classification: A8(k) F2(h) F3(ml).

HD 162950. Bright component of the visual double system CCDM 17525+2712. Strömgren, H_β, and Geneva photometry are available. Classification: A3(k) F4(ml) (Hauck, 1986). A3(k) A7(h) F3(ml) (Grenier et al. 1999).

HD 224890. Geneva photometry is available. Classification: A1(k) F2(ml).

HD 225137. The star is HJ 1926 AD = CCDM 00039+5723 AD ($\Delta m_v = 6.0$). Geneva photometry is available. Classification: A3(k) F2(ml) (Hauck, 1986). A3(k) A7(h) F2(ml) (Grenier et al. 1999).

II.4.3 Physical parameters of the primaries

For all the systems studied here, we detected the radial velocity variations of the primary only. As seen in the previous section, six of those stars are also members of visual binary systems, with very faint companions: $\Delta m_v > 3$ for all systems, except for HD 61250. Hence we shall admit for all systems but HD 61250 that the photometric data (V, $B-V$, Strömgren indices, for example) practically concern only the primaries of the SB1s of our sample.

For HD 61250, photometric magnitudes of both components were obtained, in the Tycho system, by Fabricius & Makarov (2000). We deduce: $(B-V)_{1,\rm Tyc} = 0.27$ and $(B-V)_{2,\rm Tyc} = 0.60$ for the components A and B, respectively. Converted to Johnson's system, this leads to: $(B-V)_1 = 0.23$, $(B-V)_2 = 0.51$, and $\Delta m_V = 1.41$. Then, the primary of the visual system, the Am star, would have a temperature about 7600 K, and the visual secondary could be a cooler dwarf star ($\sim$ F8 V) with $T \approx 6200$ K (cf. calibrations of Schmidt-Kaler (1982); Flower (1996)).

Parallaxes of the eight stars are available in the Hipparcos catalogue (ESA , 1997). They are given in Line 6 of Table II.6, with their errors and the corresponding distances in Line 7. From those parallaxes, we estimated the absolute magnitudes (Line 8). Since all those stars are rather close to the Sun, we can neglect the interstellar absorption.

Except for the composite system HD 61250 (see above), when Strömgren indices were available (Hauck & Mermilliod, 1998), we deduced the parameters $T_{\rm eff}$ and $\log g$ (Lines 10-11) for the primary component, using the grids giving c versus β from Moon & Dworetsky (1985), When the β index was not available (case of HD 341 and HD 55822), we estimated its value from the straight correlation that exists between $b-y$ and β, as given by Crawford (1979). For the $[Fe/H]$ estimation (Line 12), we first computed $\delta\, m_1 = m_1({\rm standard}) - m_1({\rm observed})$, where $m_1({\rm standard})$ was deduced from $b-y$ or β using Crawford (1979)'s calibration. Then we used the $\delta\, m_1$ versus $[Fe/H]$ relation given by Crawford (1975).

For HD 67317, 162950, 224890 and 225137, Geneva photometry was available (Burki et al., 2003); we could use Kunzli et al. (1997)'s calibration for all those objects except for HD 67317, which appeared outside Kunzli's calibration grids. A possible explanation for this discrepancy could be a photometric perturbation from the secondary spectroscopic component. The effective temperature of HD 67317 given in Table II.6 was estimated from

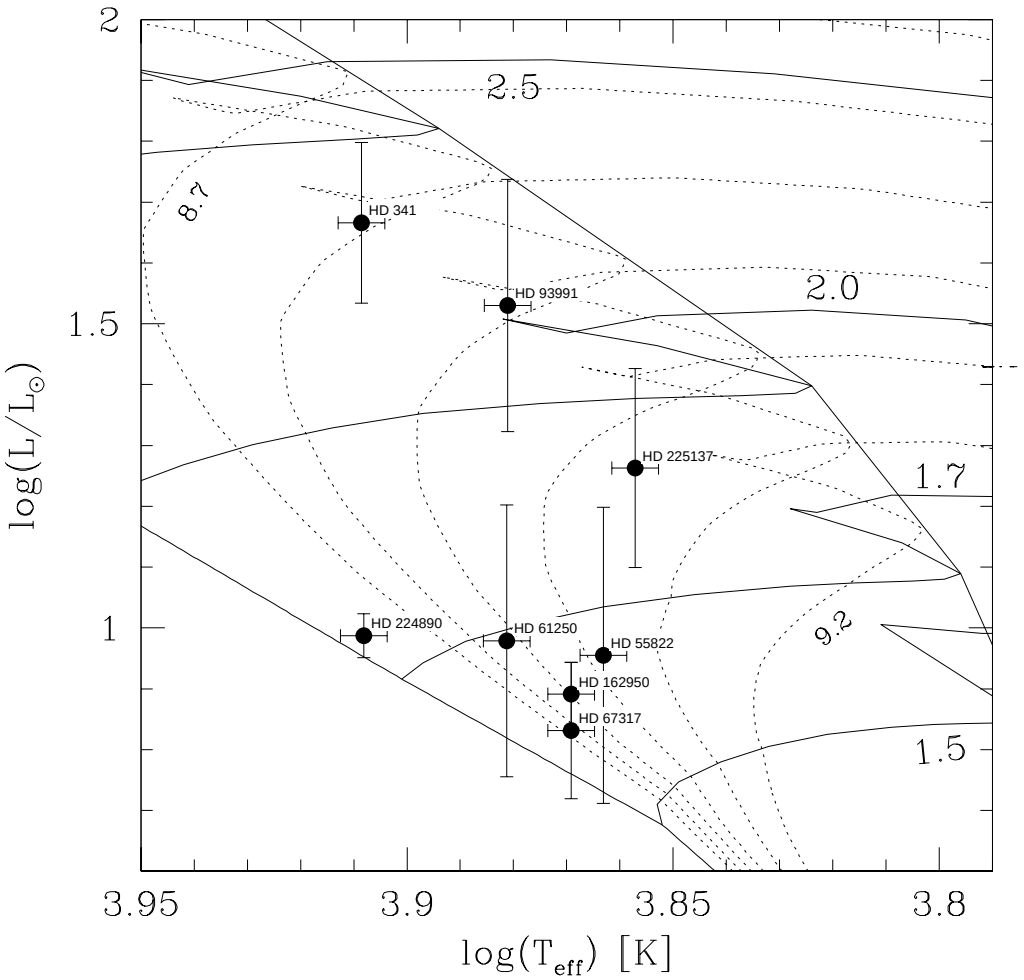

Figure II.14: Location of the primary components in the theoretical evolutionary HR diagram computed by Schaller et al. (1992), with the isochrones (dotted lines) given by Meynet et al. (1993), for log age[years] varying from 8.7 to 9.2 by steps of 0.1. The solid lines correspond to the evolution tracks for mass values of 1.5, 1.7, 2.0 and 2.5 $M_{\odot}$. From Carquillat et al. (2003b).

the $B-V$ index and the calibration table of Flower (1996). For HD 162950, since photometry was available both in Strömgren and Geneva systems, we give the mean values of those physical parameters in Table II.6.

Finally, we report in Fig. II.14 the positions of the eight primaries in the theoretical Hertzprung-Russel (HR) diagram from Schaller et al. (1992), completed with the isochrones computed by Meynet et al. (1993). The values of the absolute luminosity L come from those of M_v (Table II.6) via the bolometric corrections tabulated by (Schmidt-Kaler, 1982). The positions of the stars in this HR diagram lead to *theoretical* estimates of their masses M_1 and ages (Lines 14 and 17 of Table II.6), and give an idea of their evolutionary status. Five stars, namely HD 55822, 61250, 67317, 162950, and 224890, are little evolved bona fide dwarfs, while the three others are already evolved in the main sequence. In Table II.6, we also give the *theoretical* radius R_1 (Line 13), calculated from the L and $T_{\rm eff}$ values. Those estimates will be used for the study of synchronism (Sect. II.4.5).

II.4.4 Minimum masses and separations of the secondaries

Using the mass function derived from the orbits (Table II.5) and the theoretical value found for M_1, the mass of the primary (see above), we can estimate the minimum mass $M_{2\,\mathrm{min}}$ of the unseen spectroscopic companion. The mass function can be written as (see sect. I.4.4):

$$f(m) = M_1 \times \sin^3 i \times \mu^3 \,/\, (1+\mu)^2, \tag{II.5}$$

where $\mu = M_2/M_1$ is the mass-ratio in the system.

The value of i is unknown, and $M_{2\,\mathrm{min}}$ is obtained for $\sin i = 1$. Except for HD 225137, the corresponding masses are those of red dwarfs of type K or M (cf. Line 15 of Table II.6).

We can then estimate the mean separation a for each system from the values of $a_1 \sin i$ obtained in Table II.5:

$$a = a_1 + a_2 = (a_1 \sin i) \times (1 + 1/\mu) / \sin i, \tag{II.6}$$

As pointed out by Carquillat et al. (1982) in the case of SB1s, the separations we obtain have a small dependence on the value chosen for i. Let a_0 be the separation assuming $i = 90°$, and a the true separation. The ratio a/a_0 may be approximated by the function $(\sin i)^{-1/4}$. More precisely, this is an upper estimation. Hence, when i decreases from 90° to 20° (the most probable range for SBs, with a corresponding probability of 94%), a increases by less than 30% of its initial value, a_0. The separations we obtain (Line 16 of Table II.6) are a few tens of solar radii: hence, those systems are detached binaries.

II.4.5 Rotation-revolution synchronism

Synchronization of a binary system is a powerful process for slowing the axial rotation of a star. It seems established that such a slow rotation is required to form Am stars through the diffusion of chemical elements (Michaud al., 1983).

If we assume that the components rotate in synchronism with the orbital motion (corotation), and also that the equatorial plane of a star is equal to its orbital plane (coplanarity), we have the relation (see Sect. I.7.1):

$$R = \frac{v_e\, P}{50.6} = \frac{v_e \sin i\; P}{50.6 \sin i}$$

where v_e is the tangential equatorial velocity in km s^{-1}, P is the orbital period in days, and R is the star radius in solar radii. Indeed we only have access to the projected rotational velocity $v_e \sin i$, deduced from the CORAVEL correlation dips (Benz & Mayor, 1981), and given in Line 5 of Table II.6.

Notice that for the systems with a significant eccentricity ($e > 0.1$), like HD 55822, 162950, and 224890, we must take into account the pseudo-synchronous rotation period (see Hut (1981), formulae 44 and 45) instead of the orbital period. For those three stars, the pseudo-synchronous rotation periods are 4.70, 8.08, and 7.53 days, respectively.

For each binary, we computed the values of $\sin i_{\mathrm{sync}}$ from the preceding formula, i.e., $\sin i_{\mathrm{sync}} = P \times v_e \sin i/(50.6R)$, using the theoretical estimates for R given in Table II.6 (Line 19). One sees that for all systems, except for HD 224890, the values of $\sin i_{\mathrm{sync}}$ we obtained are plausible. Taking into account the uncertainties, the corresponding inclination

Table II.6: Estimated physical parameters from observational data and theoretical statements. A asterisk * was added when pseudo-synchronism was involved instead of genuine synchronism (case of non-circular orbits). From Carquillat et al. (2003b).

HD	341	55822	61250	67317	93991	162950	224890	225137
HIP	659	35086	37604	40006	53119	87486	128	303
V	7.27	8.53	8.23	7.56	8.09	7.29	6.50	8.13
$B-V$	0.21	0.30	0.23	0.27	0.29	0.29	0.18	0.32
$v_e \sin i$	11.7 ±1.0	21.0 ±1.0	25.2 ±1.0	12.6 ±1.0	26.2 ±1.0	8.8 ±1.0	11.9 ±1.0	19.1 ±1.0
π	4.90 ±0.76	6.08 ±1.68	6.05 ±1.60	11.03 ±1.46	3.85 ±0.91	11.65 ±0.70	15.20 ±0.63	5.15 ±0.98
d (pc)	$204\ ^{+38}_{-27}$	$164\ ^{+63}_{-35}$	$165\ ^{+60}_{-34}$	$91\ ^{+13}_{-11}$	$260\ ^{+80}_{-50}$	$86\ ^{+5}_{-5}$	$66\ ^{+3}_{-3}$	$194\ ^{+46}_{-31}$
M_v	0.72 ±0.33	2.45 ±0.61	2.40 ±0.56	2.77 ±0.28	1.02 ±0.52	2.62 ±0.13	2.41 ±0.09	1.69 ±0.41
$\log L/L_\odot$	1.67 ±0.13	0.96 ±0.24	0.98 ±0.22	0.83 ±0.11	1.53 ±0.21	0.89 ±0.05	0.99 ±0.04	1.26 ±0.16
$T_{\rm eff}$ (K)	8100 ±80	7300 ±75	7600 ±75	7400 ±75	7600 ±75	7400 ±75	8100 ±80	7200 ±75
$\log g$(cgs)	3.90	4.00	—	—	4.00	4.24	4.50	3.65
$[Fe/H]$	+0.60	+0.91	—	—	+0.76	+0.40	+0.22	+0.41
$R_1/R_\odot$	3.6 ±0.2	2.0±0.2	1.9±0.2	1.7±0.1	3.5±0.2	1.7±0.1	1.7±0.1	2.9±0.2
$M_1/M_\odot$	2.30 ±0.20	1.65 ±0.20	1.70 ±0.15	1.60 ±0.10	2.20 ±0.20	1.60 ±0.05	1.75 ±0.05	1.90 ±0.15
$M_{2\,\rm min}/M_\odot$	0.57	0.55	0.24	0.41	0.21	0.17	0.16	0.85
$a/R_\odot$	23 ±3	18 ±3	10 ±2	16 ±2	14 ±2	27 ±4	27 ±4	18 ±3
log age[yr]	$8.80\ ^{+0.03}_{-0.05}$	$9.00\ ^{+0.03}_{-0.4}$	$8.90\ ^{+0.07}_{-0.3}$	$8.75\ ^{+0.2}_{-0.15}$	$8.90\ ^{+0.05}_{-0.1}$	$8.90\ ^{+0.05}_{-0.1}$	∼8.6	$9.03\ ^{+0.04}_{-0.06}$
$\log t_{\rm sync}$[yr]	4.66	5.59	4.73	5.51	4.48	6.99	7.11	4.50
$\sin i_{\rm sync}$	0.40 ±.06	0.98 ±.14*	0.59 ±.09	0.65 ±.09	0.48 ±.05	0.83 ±.14*	1.04 ±0.15*	0.56 ±.07
$\mu_{\rm sync}$	0.78 ±0.20	0.34 ±0.08	0.26 ±0.06	0.43 ±0.10	0.21 ±0.04	0.13 ±0.03	0.094 ±0.016	0.97 ±0.22

values lie in the range 20°–90°. For HD 224890, we found an aberrant value of 1.04, that seems to indicate the absence of synchronism. It is also the youngest and the least evolved system of our sample and could have not yet reached its equilibrium state. Nevertheless the corresponding uncertainty is ±0.15, and we may consider that the marginal discrepancy is not definitive. For the other seven stars, we thus conclude that synchronism (or pseudo-synchronism for the eccentric orbits) is plausible.

Assuming that all systems are synchronized, we can derive the mass ratio $\mu_{\rm sync}$ from the mass function values $f(m)$ reported in Table II.5 (see sect. I.4.4 and Eq. II.5. The resulting values (Line 20 of Table II.6) have a wide range from ∼0.1 to $\mu_{\rm sync} = 0.97 \pm 0.22$ for HD 225137. This system has also the largest mass function in our sample (Col. 9 of Table II.5). Such a high value for the mass ratio would imply that the companion could be also an A-type star. Note that it cannot be an Am star since in that case, CORAVEL would have detected two correlation dips. If we take into account the uncertainties on the value of $\mu_{\rm sync}$, the mass ratio of HD 225137 could go down to ∼1.4 $M_\odot$ (lowest value at one sigma), which corresponds to a spectral type of ∼F5V (Schmidt-Kaler, 1982). The resulting magnitude difference would be $\Delta m_v \sim 1.8$, which could account for the non-detection of the secondary with CORAVEL. Further high resolution spectroscopic observations of HD 225137 are thus required to investigate this problem.

II.5 Paper VI: study of 10 new spectroscopic binaries, implications on tidal effects

In Carquillat et al. (2004) we presented the results of a radial velocity (RV) monitoring of ten Am stars, namely HD 19342, 19910, 36360, 102925, 126031, 127263, 138406, 155714, 195692 and 199360. We found that these systems were spectroscopic binaries whose orbital elements were determined for the first time. Both components could be measured for HD 126031, an eclipsing binary, whereas the other systems were detected as single-line binaries only. Physical parameters were inferred from this study for the primaries of all systems, and for the secondary of HD 126031. We observed a higher rate of synchronized/circularized systems than what is expected from the theoretical models of radiative dissipation of dynamical tides.

II.5.1 Introduction

Most of the observations were carried out with the CORAVEL instrument of the 1-m Swiss telescope at Haute-Provence Observatory (OHP) and that of the 91 cm telescope of Cambridge Observatory. All those stars were detected as single-lined spectroscopic binaries (SB1) with CORAVEL. We thus could determine for the first time (to our knowledge) their orbital elements. For the eclipsing binary HD 126031, complementary observations, obtained with the ELODIE spectrograph mounted on the 1.93 m telescope at OHP, allowed us to detect the secondary component.

Six stars of the present sample come from the *"Third catalogue of Am stars with known spectral types"* (Hauck (1986), hereafter HCK86), and four from the list of Bidelman (1988) (hereafter BID88) entitled *"Miscellaneous spectroscopic notes"*. Only for 5 objects was the variability of the radial velocity already mentioned in previous studies. In Section II.5.2, we present the RV observations and the orbital elements we computed. In Section II.5.3 we give some complementary bibliographical information for each system. In Section II.5.5 we derive some physical parameters deduced from available Strömgren photometry, Hipparcos parallaxes and theoretical evolutionary tracks. We then estimate the minimum masses and separations of the companions (Sect. II.5.6). We present an analysis of the Hipparcos light-curve of the eclipsing binary HD 126031 in Sect. II.5.7. In Sect. II.5.9, we compare our results with some theoretical predictions about the circularization of the orbits caused by tidal effects. Finally, using the projected rotational velocity $v_e \sin i$ derived from the correlation dips, we discuss the occurrence of rotation–revolution synchronism among those systems (Sect. II.5.10).

II.5.2 Observations and derivation of orbital elements

Our observations were performed in three-fold parts:

- J.-M. Carquillat and N. Ginestet first observed at OHP during the 1992–1998 period, with the CORAVEL instrument mounted on the 1-m Swiss telescope.
- In 2001–2002, E. Oblak and M. Kurpinska-Winiarska performed radial velocity measurements of HD 126031 on the 1.93-m at OHP, with the ELODIE spectrograph (Baranne et al., 1996).

- Finally in 2003, R.F. Griffin kindly made measurements with his own CORAVEL on the 91-cm telescope of Cambridge observatory.

For each star, between 30 and 50 RVs were obtained (Tables 1 to 10 of Carquillat et al. (2004)) with a mean internal standard error that depends upon the depth and the width of the correlation dip. The latter is strongly correlated with the projected equatorial rotational velocity $v_e \sin i$. The best precision was reached for HD 19342 (0.4 km.s^{-1}), the poorest for HD 195692 (1.3 km.s^{-1}), while eight stars have RVs errors in the range 0.4—0.8 km.s^{-1}. The RVs obtained at Cambridge were reduced to the RV data base system of Geneva Observatory (Udry, Mayor & Queloz 1999), via the application of appropriate offsets. For HD 155714 we added 4 RVs published by Nordström et al. (1997) derived from the cross-correlation of digitized spectra with optimized synthetic template spectra. Taking into account the errors, those RVs were weighted 0.55 (whereas we used 1.0 for the CORAVEL measures).

For HD 126031, the ELODIE RVs were weighted 2.0, to take into account their better quality than the CORAVEL data (weighted as 1.0). The small values of the internal errors given by ELODIE ($\sim$0.1 km.s^{-1}) would suggest larger values for the weights. Nevertheless, as the corresponding observations were concentrated in a short period of time, using larger weights for the ELODIE data degraded the accuracy of most parameters of the orbit (in particular P and T_0).

We calculated the spectroscopic orbital elements of the binaries (Tables II.7 and II.8) by applying the least-squares programs BS1 and BS2 (first created by Nadal et al. 1979 and revised by J.-L. Prieur) to the observed RVs. The $(O - C)$ residuals are given in Tables 1 to 10 of Carquillat et al. (2004), and the computed RV curves in Figs II.15 and II.16. In all cases, the standard deviation of the residuals, $\sigma_{(O-C)}$, is consistent with the RV mean error (and even smaller, in the case of 7 objects), which indicates the absence of detectable spectroscopic third components in those systems.

The application of Lucy & Sweeney's (1971) statistical test to the orbital elements showed that six systems have circular orbits: HD 19342, 102925, 126031, 155714, 195692, and 199360. The periods of HD 102925 ($P = 16.4$ days) and HD 19342 ($P = 42.6$ days) seem rather large for the orbit to be circularized by tidal effects. We shall discuss that topic in Sect. II.5.9.

II.5.3 Notes for individual systems

In this section, we report some information about the studied stars and, in particular, the source for the Am classification (HCK86, BID88 or Grenier et al. (1999), hereafter GRE99) with, when available, the classifications from Ca II K line (k), hydrogen lines (h) and metallic lines (m).

HD 19342. HCK86 gives A7(k) F0(m) according to Walther (1949) and A5(k) F2(m) according to Bertaud (1970). GRE99 give the classification A3(k) A7(h) F3(m), and note the variability of the RV.

HD 19910. HCK86 gives A2(k) F5(m) according to Drilling & Pesch (1973).

HD 36360. HCK86 gives A5(k) F2(m) according to Slettebak & Nassau (1959), but GRE99 classify the star as A3(k) A7(h) F3(m). Fehrenbach et al. (1987) first put in evidence a variable RV.

HD 102925. Classified as Am by BID88. First discovered as a variable RV star at Mount Wilson Observatory (Wilson & Joy 1950, Abt 1970).

HD 126031. This system is DV Boo (Kazarovets et al. 1999), and was discovered as an eclipsing binary of Algol type by Hipparcos. The period quoted in the Hipparcos catalogue (ESA , 1997) is 1.26 days, i.e., exactly the third of the period we found: a stroboscopic effect? (see Sect. II.5.7). Classified as Am by BID88 and A3(k) A7(h) F5(m) by GRE99.

HD 127263. An Am star according to BID88, but GRE99 give the classification A2p Sr, and report a variable RV.

HD 138406. Am according to BID88 (but could be a giant: see Sect. II.5.5). First reported as a variable RV star by Young (1942) from observations at David Dunlap Observatory.

HD 155714. Visual double ADS 10398 AB = CCDM 17130+0745 AB = STT 325 AB. $\Delta m_{\rm Hp}$=1.79; ρ=0.4 arcsec. HCK86 gives A9(k) F1(h) F4(m), according to Abt (1981).

HD 195692. Visual double ADS 13964 AB = CCDM 20320+2548 AB = STF 2695 AB. $\Delta m_{\rm Hp}$= 2.17; ρ=0.16 arcsec. Classified A4(k) F0(m) in HCK86, according to Bertaud (1970), and A2(k) F1(h) F0(m) by Abt & Morrell (1995).

HD 199360. HCK86 gives A7(k) F1(h) F5(m), according to Abt (1984), and GRE99 find A5(k) F0(h) F3(m).

Thus, our observations have shown that HD 155714 and HD 195692 are triple systems.

II.5.4 Reddening correction

Strömgren photometry was available for eight objects of our sample (Hauck & Mermilliod, 1998). In Table II.9, we present the corresponding β, $b-y$, m_1 and c_1 in Cols. 2, 3, 5 and 7. The color excess $E(b-y)$ produced by interstellar reddening (Col. 4) was computed with Crawford (1979)'s calibration of A-type stars (see Sect. I.5). The corresponding indices $(m_1)_0$ and $(c_1)_0$, corrected for reddening, are in Cols. 6 and 8. The index $(\delta m_1)_0 = (m_1)_{std} - (m_1)_0$, where $(m_1)_{std}$ is the standard m_1 corresponding to an A-type star with the same β as the object is given in Col. 9. We used Crawford (1979)'s calibration on the Hyades for determining $(m_1)_{std}$ from β. This index $(\delta m_1)_0$ will be used for the determination of [Fe/H], given in Table II.10 (see Sect. II.5.5).

For HD 155714, 195692, and 199360, the β indices have not been measured; the values indicated in brackets were obtained from the (β,$(b-y)_0$) relation given by Crawford (1979). We neglected the interstellar absorption for the nearest stars HD 155714 and HD 195692 (with $d < 100$ pc). For HD 199360 ($d = 147$ pc), we used Lucke (1978)'s extinction maps for correcting $b-y$, and then verified that the $E(b-y)$ derived from Crawford (1979), was compatible with Lucke's $E(B-V)$ value. Note that $E(b-y) = 0.73\,E(B-V)$ (Crawford, 1975).

Table II.9 shows that the reddening is negligible (i.e., $E(b-y) \leq 0.01$) for HD 36360, 126031, 127263, 155714 and 195692. For HD 19342, 19910 and 199360, we shall use the reddening-corrected values from this table in the following of this paper.

Strömgren photometry was not available for HD 102925 and 138406, which are distant of 114 and 282 pc, respectively (cf. Table II.10). The corresponding interstellar extinction values $E(B-V)$, estimated from Lucke (1978)'s galactic charts are 0.03 and 0.06, respectively.

Table II.7: Orbital elements of the SB1 systems studied in Carquillat et al. (2004). In Col. 3, T_0 is the epoch of periastron passage, except for systems with $e = 0$ (circular orbits). In that case T_0 corresponds to the ascending node passage.

Name	P	T_0 (JD)	ω	e	K_1	V_0	$a_1 \sin i$	$f(m)$	$\sigma_{(O-C)}$
	days	2400000+	deg.		km.s^{-1}	km.s^{-1}	Gm	M$_\odot$	km.s^{-1}
HD19342	42.6301	49323.630	—	0.0	26.80	6.16	15.71	0.0853	0.37
	±0.0027	±0.075	—	—	±0.10	±0.07	±0.06	±0.0009	
HD19910	15.41418	49325.46	67.2	0.059	45.77	11.64	9.68	0.1526	0.94
	±0.00022	±0.20	±4.8	±0.005	±0.23	±0.17	±0.05	±0.0024	
HD36360	216.54	49129.1	116.1	0.112	12.37	13.90	36.60	0.0417	0.47
	±0.12	±3.6	±6.2	±0.012	±0.17	±0.11	±0.59	±0.0020	
HD102925	16.43718	49798.439	—	0.0	26.62	-0.89	6.02	0.0322	0.64
	±0.00091	±0.046	—	—	±0.17	±0.12	±0.04	±0.0006	
HD127263	14.23834	50488.062	248.6	0.319	24.87	-14.07	4.62	0.01936	0.42
	±0.00014	±0.035	±0.8	±0.004	±0.11	±0.08	±0.03	±0.00034	
HD138406	25.8513	49792.55	9.8	0.213	10.75	-6.68	3.73	0.00311	0.36
	±0.0011	±0.19	±2.6	±0.010	±0.11	±0.08	±0.05	±0.00012	
HD155714	3.334772	49144.192	—	0.0	6.28	-43.63	0.288	0.000086	0.82
	±0.000055	±0.022	—	—	±0.18	±0.13	±0.008	±0.000007	
HD195692	11.292249	48138.102	—	0.0	39.92	-25.49	6.20	0.0746	0.88
	±0.000081	±0.014	—	—	±0.19	±0.14	±0.03	±0.0011	
HD199360	1.9986874	49640.743	—	0.0	11.74	4.90	0.323	0.000336	0.42
	±0.0000086	±0.005	—	—	±0.11	±0.07	±0.003	±0.000009	

Table II.8: Orbital elements of HD 126031, the only SB2 system of the sample studied in Carquillat et al. (2004). In Col. 3, T_0 is the epoch of the ascending node passage.

P	T_0 (JD)	ω	e	K_1	K_2	V_0	$a_1 \sin i$	$a_2 \sin i$	$M_1 \sin^3 i$	$M_2 \sin^3 i$	$\sigma_{1(O-C)}$	$\sigma_{2(O-C)}$
days	2400000+	deg.		km.s^{-1}	km.s^{-1}	km.s^{-1}	Gm	Gm	M$_\odot$	M$_\odot$	km.s^{-1}	km.s^{-1}
3.782624	50480.328	—	0.	82.23	110.10	-28.37	4.277	5.727	1.600	1.195	0.92	0.49
±0.000006	±0.003	—	—	±0.18	±0.26	±0.12	±0.009	±0.014	±0.011	±0.008		

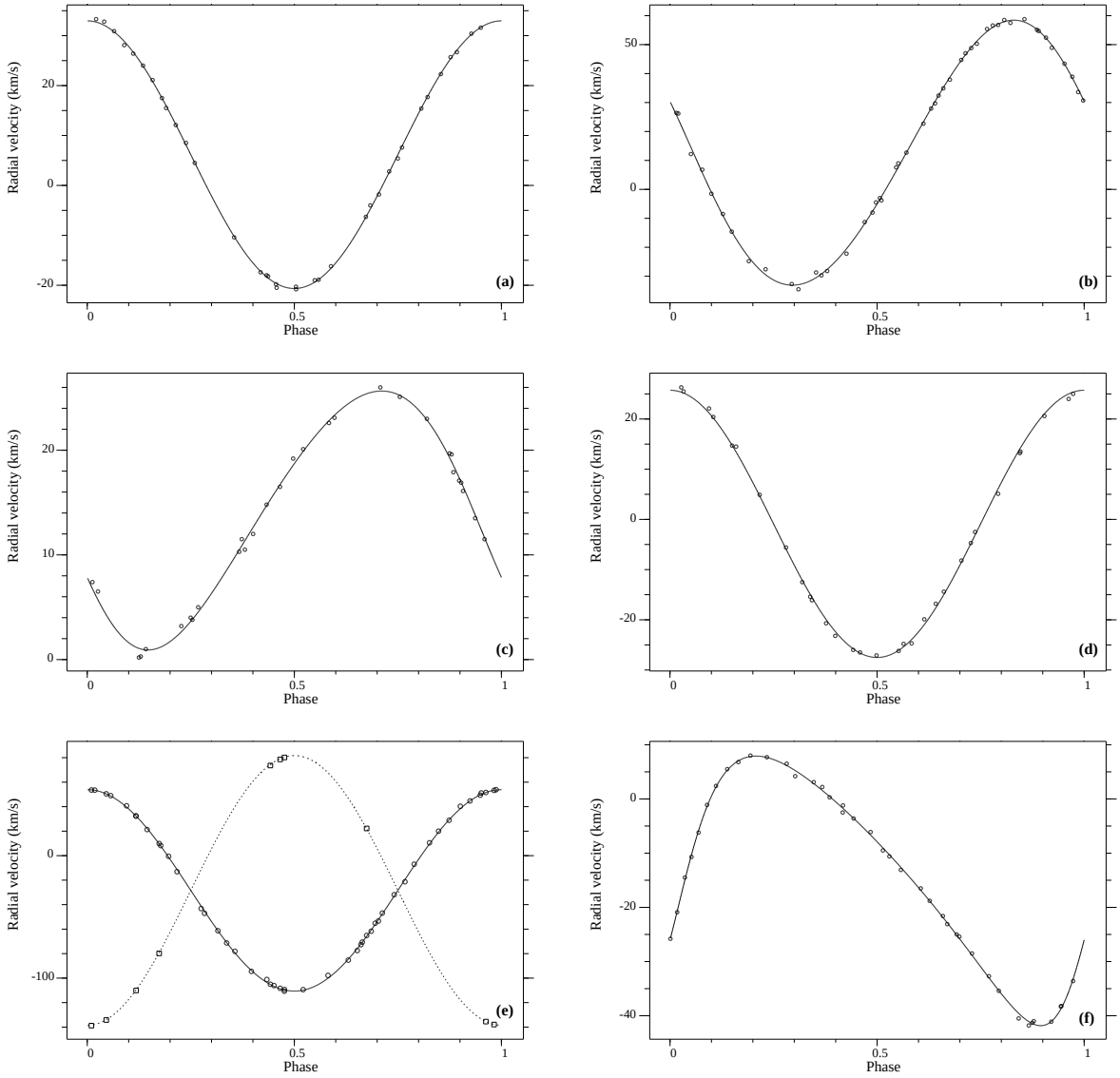

Figure II.15: RV curves computed with the orbital elements of Tables II.7 and II.8: (a) HD 19342, (b) HD 19910, (c) HD 36360, (d) HD 102925, (e) HD 126031, and (f) HD 127263. For HD 19342, HD 102925, and HD 126031 which have circular orbits, the ascending node is taken as the origin of the phases. For the other systems, the origin of the phases corresponds to the periastron passage.

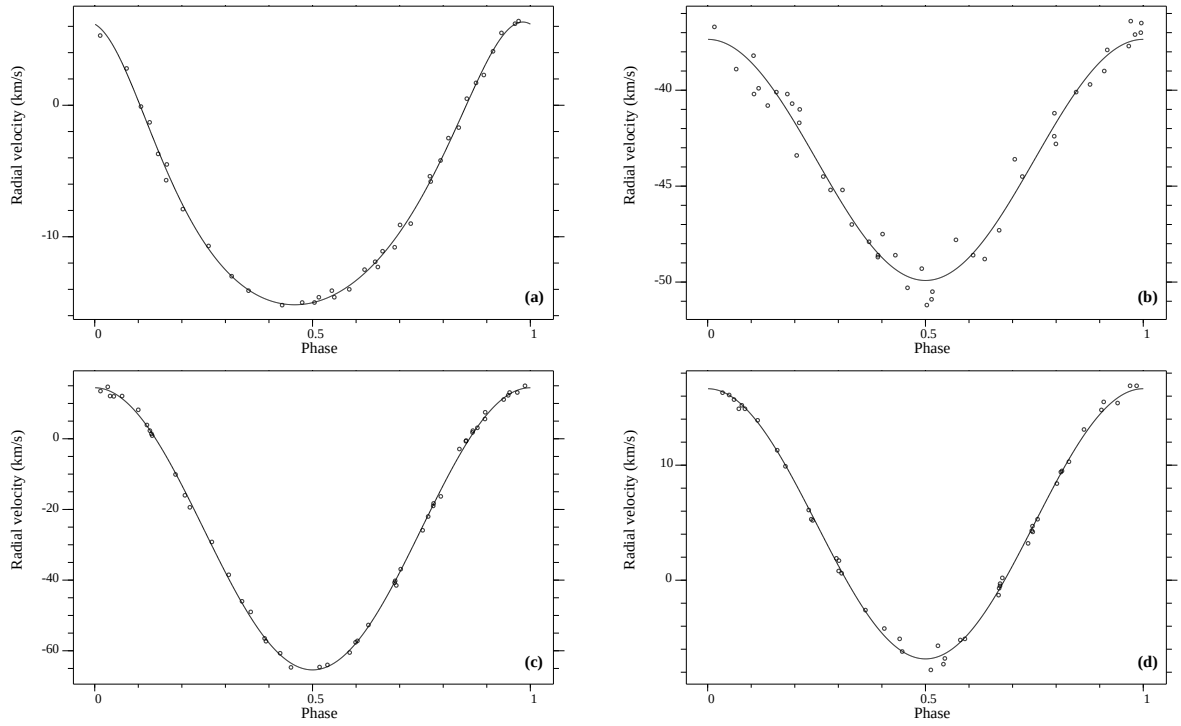

Figure II.16: RV curves computed with the orbital elements of Table II.7: (a) HD 138406, (b) HD 155714, (c) HD 195692 and (d) HD 199360. For HD 138406, the origin of the phases corresponds to the periastron passage. For the other systems, which have a circular orbit, the ascending node is taken as the origin of the phases.

II.5.5 Physical parameters of the primaries

To estimate some physical parameters of the primaries, which are presented in Table II.10, we have used Strömgren photometry and the Hipparcos parallaxes, when those data were available. We have assumed that the photometric contribution of the unseen spectroscopic companion was negligible for all systems, except for HD 126031 for which the secondary was detected. We shall discuss the possible influence of the undetected companion in Sect. II.5.8.

As in Paper V, we proceeded as follows:

1 – From Hipparcos parallaxes π (ESA , 1997), we obtained the distances and the visual absolute magnitudes of the systems (except for HD 19910 that was not observed by the satellite), and their errors (Lines 5 and 6).

2 – When Strömgren photometry was available (cf. Sect. II.5.4), we deduced the quantities $T_{\rm eff}$ and $\log g$ (Lines 8 and 9) using the $(c_1)_0$ versus β grids of Moon & Dworetsky (1985). For $\log g$ determination, we applied the correction for metallicity proposed by Dworetsky and Moon (1986) for Am stars. The parameter $[Fe/H]$ (Line 10) was estimated from the δm_1 versus $[Fe/H]$ Cayrel's correlation, as quoted in (Crawford, 1975): $[Fe/H] = 0.2 - 10\,\delta_{m1}(\beta)$. For HD 102925 and HD 138406, Strömgren $uvby, \beta$ photometry was not available: the effective temperature given in Line 8 is based upon the $B-V$ index and Flower (1996)'s calibrations.

3 – The quantities M_V and $T_{\rm eff}$ lead to an estimation of the theoretical radius of the stars (Line 11), using the radiation law: $\log(R/{\rm R}_\odot) = -0.2M_{\rm bol} - 2\log T_{\rm eff} + 8.47$ (Schmidt-

Table II.9: Strömgren photometry β, $(b-y)$, m_1, c_1 and derived data using Crawford (1979)'s calibration (see Sect. II.5.4). From Carquillat et al. (2004).

HD	β	$b-y$	$E(b-y)$	m_1	$(m_1)_0$	c_1	$(c_1)_0$	$(\delta m_1)_0$
19342	2.73	0.31	0.10	0.20	0.23	0.77	0.75	-0.05
19910	2.81	0.19	0.04	0.20	0.21	0.73	0.72	-0.01
36360	2.80	0.16	0.01	0.24	0.24	0.81	0.81	-0.04
126031	2.74	0.20	−0.01	0.23	0.23	0.66	0.67	-0.04
127263	2.83	0.14	−0.01	0.28	0.28	0.80	0.80	-0.07
155714	(2.72)	0.23	0.01	0.19	0.19	0.68	0.67	-0.01
195692	(2.78)	0.16	0.00	0.21	0.21	0.76	0.76	-0.01
199360	(2.81)	0.18	0.03	0.25	0.26	0.74	0.73	-0.06

Kaler, 1982). The bolometric corrections we used are those tabulated by Flower (1996) (Table I.5).

4 – Finally, we report in Fig. II.18 the positions of the stars in the theoretical Hertzsprung-Russell diagram, $\log(L/L_\odot)$ versus $\log T_{\rm eff}$, from Schaller et al (1992), completed with the isochrones computed by Meynet, Mermilliod & Maeder (1993). The positions of the stars in this diagram lead to theoretical estimates of their masses M_1 and ages (Lines 12 and 23 of Table II.10). Three stars are missing in the diagram: HD 19910, which was not observed by Hipparcos, HD 126031, whose two components are plotted in Fig. II.19, and HD 138406 which is not a *classical* Am star and falls beyond its boundaries. Indeed, with the data we have for that star, it could be a hot giant, even though metallic lines are certainly present, as noted by Young (1942) which reported the following comment *"Many very fine lines."* The other stars lie in the main-sequence domain and show different degrees of evolution, the least evolved being HD 127263. The case of the eclipsing binary HD 126031, for which the two components have been detected with ELODIE is dealt with in Sect. II.5.7.

II.5.6 Masses and separations of the secondaries

From the values computed for $f(m)$ and $a_1 \sin i$ (Table II.7), and assuming for the primaries the theoretical masses M_1 (Table II.10), we can obtain, for a given value of the orbital inclination i, the values of M_2, the mass of the secondary, and a, the true mean separation of the components. For that, we use the formulae:

$$f(m) = M_1 \times \sin^3 i \times \mu^3 \,/\, (1+\mu)^2, \tag{II.7}$$

where $\mu = M_2/M_1$ is the mass-ratio in the system, and

$$a = a_1 + a_2 = (a_1 \sin i) \times (1 + 1/\mu)/\sin i. \tag{II.8}$$

The minimum values for μ, M_2 and a correspond to $\sin i = 1$ (i.e., $i = 90°$). As for the maxima of those quantities, they can be approximated taking into account the absence

Table II.10: Physical and tidal parameters derived from the study of the primary components of the seven new binaries studied in PaperVI. For the reddened objects, the magnitudes corrected for interstellar absorption are indicated in brackets (lines 3 and 4). For the eclipsing binary HD 126031, we assumed $i = 83°$. From Carquillat et al. (2004).

HD	19342	19910	36360	102925	126031	127263	138406	155714	195692	199360
HIP	14653	–	25995	57813	70287	70814	75764	84230	101300	103335
V	8.00 (7.59)	9.34 (9.19)	7.17	7.24 (7.14)	7.54	8.14	6.91 (6.74)	7.06	6.51	7.85 (7.73)
$B-V$	0.47 (0.33)	0.30 (0.25)	0.28	0.18 (0.15)	0.34	0.24	0.13 (0.07)	0.38	0.26	0.31 (0.27)
$v_e \sin i$ (km/s)	9.9 ±1.0	14.1 ±1.0	20.0 ±1.0	8.0 ±1.0	24.4 ±2.4	11.0 ±1.0	6.6 ±1.0	17.4 ±1.0	9.6 ±1.0	13.5 ±1.0
π (mas)	5.52 ±1.11	–	7.29 ±1.08	8.78 ±0.64	7.38 ±0.92	7.14 ±0.74	3.55 ±0.54	11.06 ±1.21	12.33 ±0.70	6.78 ±0.90
d (pc)	181^{+46}_{-30}	–	137^{+24}_{-18}	114^{+9}_{-8}	135^{+20}_{-15}	140^{+16}_{-13}	282^{+50}_{-38}	90^{+12}_{-9}	81^{+5}_{-4}	147^{+23}_{-17}
M_v	1.30 ±0.51	–	1.48 ±0.32	1.86 ±0.16	2.14 ±0.3	2.41 ±0.23	-0.51 ±0.36	2.28 ±0.24	1.96 ±0.13	1.89 ±0.29
$\log L/\mathrm{L}_\odot$	1.37 ±0.22	–	1.30 ±0.14	1.14 ±0.08	1.03 ±0.15	0.92 ±0.10	2.09 ±0.16	0.98 ±0.11	1.10 ±0.06	1.13 ±0.13
$T_{\rm eff}$ (K)	7100 ±70	7800 ±70	7700 ±70	8100 ±100	7370 ±80	7900 ±70	8700 ±150	7000 ±80	7500 ±80	7800 ±80
$\log g$[cgs]	3.6	4.4	4.0	–	4.1	4.1	–	4.0	4.1	4.2
$[Fe/H]$	+0.67	+0.29	+0.55	–	+0.64	+0.93	–	+0.34	+0.30	+0.75
$R_1/\mathrm{R}_\odot$	3.2 ±0.8	∼2	2.5 ±0.4	1.9 ±0.2	2.1 ±0.3	1.5 ±0.2	4.9 ±1.0	2.1 ±0.3	2.1 ±0.2	2.0 ±0.4
$M_1/\mathrm{M}_\odot$	2.00 ±0.20	∼2.0	1.95 ±0.10	1.85 ±0.05	1.70 ±0.10	1.70 ±0.05	∼ 3	1.65 ±0.10	1.80 ±0.05	1.80 ±0.10
$M_{2\,\rm min}/\mathrm{M}_\odot$	0.9	1.1	0.7	0.6	–	0.4	0.3	0.06	0.3	0.1
$M_{2\,\rm max}/\mathrm{M}_\odot$	1.2	1.2	1.2	1.1	–	1.0	1.8	1.0	1.1	1.1
$a_{\rm min}/\mathrm{R}_\odot$	73.1	38.2	209	36.5	14.5	31.8	54.8	11.2	28.8	8.3
$a_{\rm max}/\mathrm{R}_\odot$	75.6	38.4	222	39.0	–	34.5	61.9	13.0	29.8	9.5
$\overline{a}$	74.4	38.3	216	37.8	14.5	33.2	58.4	12.1	29.3	8.9
$R/\overline{a}$	0.04	0.05	0.01	0.05	0.13	0.05	0.08	0.17	0.07	0.22
$i_{\rm min}$ (deg.)	53	75	39	36	–	31	13	5	53	7
$R_{\rm sync,min}/R_\odot$	8.3 ±0.8	4.3 ±0.3	79.6 ±4.0	2.6 ±0.3	1.8 ±0.2	1.9 ±0.2	2.6 ±0.4	1.15 ±0.07	2.1 ±0.2	0.53 ±0.04
Synchronized?	no	no	no	no	yes	∼likely	likely	likely	likely	likely
Circularized?	yes	no	no	yes	yes	no	no	yes	yes	yes
log age[yr]	$9.00^{+0.10}_{-0.08}$	–	$8.94^{+0.02}_{-0.03}$	$8.77^{+0.06}_{-0.12}$	$9.00^{+0.03}_{-0.10}$	∼8 ±0.7	∼8.7	$9.13^{+0.03}_{-0.02}$	$9.00^{+0.02}_{-0.05}$	$8.90^{+0.03}_{-0.14}$
$\log t_{\rm circ}$[yr]	17.6	16.3	23.4	16.7	12.3	17.2	14.1	11.4	15.4	9.9
$\log t_{\rm sync}$[yr]	14.1	12.9	18.7	13.3	9.6	13.7	11.1	9.1	12.2	7.8
P (days)	42.6	15.4	216.5	16.4	3.8	14.2	25.9	3.3	11.3	2.0

Table II.11: HD 126031: parameters determined by our study (Carquillat et al., 2004).

Parameter	Value	Error	Unit	Origin
i	82.7	0.3	°	light curve
$T_{\rm eff1}$	7370	80	K	Strömgren's photometry
$T_{\rm eff2}/T_{\rm eff1}$	0.87	0.01	—	light curve
R_1	1.94	0.03	$\mathrm{R}_\odot$	light curve & spectro.
R_2	1.39	0.04	$\mathrm{R}_\odot$	light curve & spectro.
a	14.49	0.01	$\mathrm{R}_\odot$	light curve & spectro.
M_1	1.64	0.02	$\mathrm{M}_\odot$	light curve & spectro.
M_2	1.23	0.02	$\mathrm{M}_\odot$	light curve & spectro.
Δm_V	1.41	0.15	mag.	light curve & spectro

of CORAVEL correlation dips from the secondary spectroscopic components, that implies roughly $\Delta m_V \geq 2.0$, i.e., via the mass–luminosity relation, $\mu \leq 0.6$.

Following that procedure, we give in Table II.10: (i) on one hand $M_{2\min}$ and $a_{\min}$, the minimum values that we found when $i = 90°$ for M_2 and a, respectively (Lines 13 and 15), (ii) on the other hand $M_{2\max}$ and $a_{\max}$, the maximum values of M_2 and a (Lines 14 and 16), obtained with the minimum value of i corresponding to $\mu = 0.6$ (Line 19).

For HD 19910, for which no theoretical value could be derived, we assumed $M_1 = 2\,\mathrm{M}_\odot$, a typical value for A-type stars. Notice that, as already pointed out by Carquillat et al. (1982), the separation we obtain with (II.8) has a very small dependence on the value of i, and we can conclude that all those binary systems are detached.

The two short-period systems HD 155714 and HD 199360 have very low mass functions (see sect. I.4.4), that permit a wide range of possibilities for i, the orbital inclination, and M_2, the mass of the companion. As an indication, the (very plausible) hypothesis of rotation–revolution synchronism (see Sect II.5.10) would imply $i = 33°$, $M_2 = 0.1\mathrm{M}_\odot$ for HD 155714 and $i = 14°$, $M_2 = 0.5\mathrm{M}_\odot$ for HD 199360. Such masses are those of red dwarf stars.

II.5.7 The eclipsing binary HD 126031

The light curve of HD 126031 provided by Hipparcos is plotted in phase in Fig. II.17, using the period of 3.78 days found with our spectroscopic observations. It clearly shows two eclipses with two peaked minima. The period quoted in the Hipparcos catalogue (1.26 days) is definitely false and must be due to a stroboscopic effect.

We performed an analysis of that curve using two programs: EBOP, from Popper & Etzel (1981) that fits the light curve only, and WD (version 1996), from Wilson & Devinney (1971) that performs a fit which also takes into account the radial velocity orbital parameters. Note that the results should be considered as preliminary, since the residuals are rather large and the light curve is under-sampled, especially around the minima.

The parameters found by WD and EBOP are in very good agreement; the mean values are displayed in Table II.11. The fitted solution and the residuals are plotted in Fig. II.17. The two solutions have an rms error smaller than 0.01 mag., and do not show any difference in that plot.

The two models WD and EBOP lead to $\Delta m_{Hp} = 1.38 \pm 0.08$, and $\Delta m_{Hp} = 1.28 \pm 0.08$, respectively. Given the closeness of the effective temperatures of the two components, $\Delta m_{Hp} \approx \Delta m_V$ (the corresponding differential correction is negligible: ∼0.02 mag.). Hence the analysis of the light curve leads to $\Delta m_V = 1.33 \pm 0.1$ We also obtained an independent estimate of $\Delta m_V \sim 1.57 \pm 0.2$ from the ELODIE correlation dips of the two components, using the relation $\Delta m_V = -2.5 \log[(S_1/S_2) \times (T_{\mathrm{eff2}}/T_{\mathrm{eff1}})]$, where S_1 (resp. S_2) is the surface of the correlation dip of component 1 (resp. 2) (Duquennoy, 1994, private communication). Hence we finally adopted the weighted mean value of the two determinations, from the light curve and ELODIE, i.e., $\Delta m_V = 1.41 \pm 0.15$.

From the knowledge of the ratio $T_{\mathrm{eff2}}/T_{\mathrm{eff1}}$ (Line 3 of Table II.11), the global $B - V$ index (Line 2 of Table II.10) and this determination of Δm_V, we computed the correction ΔT to be applied to T_{eff1} as determined by Strömgren photometry, due to the presence of the companion. This was done with an iterative process, which used Flower (1996)'s table of T_{eff} versus $B-V$ for main sequence stars. We obtained: $T_{\mathrm{eff1}} = 7370 \pm 80$ K, $T_{\mathrm{eff2}} = 6410 \pm 80$ K, $(B-V)_1 = 0.31 \pm 0.02$ and $(B-V)_2 = 0.47 \pm 0.02$.

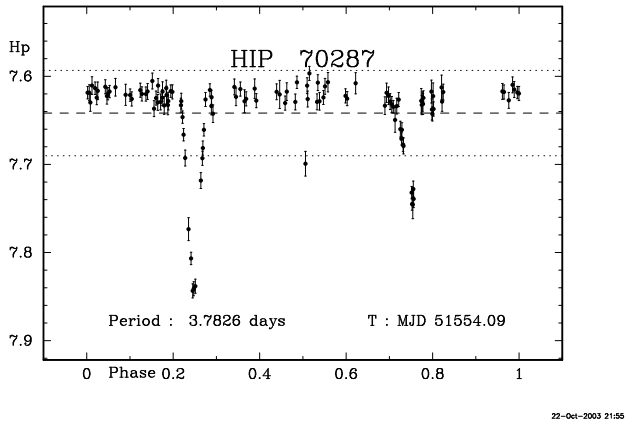

Figure II.17: Light curve of HD 126031 obtained by Hipparcos, rescaled to the spectroscopic period, with Min I = HJD 2447859.9071±0.0005 as the origin of phases. The fitted model with EBOP and WD are plotted in solid line and the residuals are given in the bottom with the 3-sigma level marked with dotted lines. From Carquillat et al. (2004).

From the global value $M_V = 1.88$, as determined with Hipparcos parallax, and $\Delta m_V = 1.41 \pm 0.15$, we obtain $M_{V1} = 2.14 \pm 0.3$ and $M_{V2} = 3.54 \pm 0.3$. When applying the bolometric corrections $BC_1 = 0.03$ and $BC_2 = -0.02$, corresponding to the component temperatures $T_{\rm eff1}$ and $T_{\rm eff2}$ (Flower, 1996), we find $\log(L_1/L_\odot) = 1.03 \pm 0.15$ and $\log(L_2/L_\odot) = 0.49 \pm 0.15$.

Both components of HD 126031 are plotted in Fig. II.19. Their location on this theoretical diagram is in good agreement with the mass determination from the light curve (Table II.11), and they are located on the same isochrone of $\sim 10^9$ years, within the error bars.

Hence all parameters that we found for the secondary (radius, temperature, mass and luminosity) are consistent and suggest a late F dwarf star (F6/7 V).

II.5.8 Influence of the undetected companions

As already mentioned, we assumed that the photometric contribution of the companion was negligible for the other systems which were detected as SB1 only. The absence of a secondary correlation dip in the VR data, implies a large magnitude difference between the two components (roughly $\Delta m_V \geq 2.0$) or a large spin velocity for the companion ($v_e \sin i > 40$ km.s^{-1}). As we shall see in Sect. II.5.10, tidal interaction between the two stars tend to reduce the spin velocity which makes the latter possibility rather unlikely. Another possibility for accounting for the absence of detection of the secondary could be that the companion is a hot star without metallic lines (e.g, A-type star). But the values of the mass function (see sect. I.4.4) that we found ($f(m) \leq 0.15$ M$_\odot$) for those objects implies that, statistically, the companion has a mass of $M_2 \leq 1.4$ M$_\odot$ (value obtained with $i = 60°$ and $M_1 = 2$ M$_\odot$), which corresponds to a star of F5-type or later. Note that the spectrum of such stars exhibits metallic lines which make those stars detectable by CORAVEL when $\Delta m_V < 2$. Hence the absence of detection suggests that the companions are not brighter than this limit.

In the case of a companion with $\Delta m_V \sim 2$, the locations of the primaries in the HR diagram of Fig II.18 would be slightly shifted to the bottom left (about -0.06 in $\log L$ and $+0.006$ in $\log T$), since their luminosities would be overestimated and their temperatures

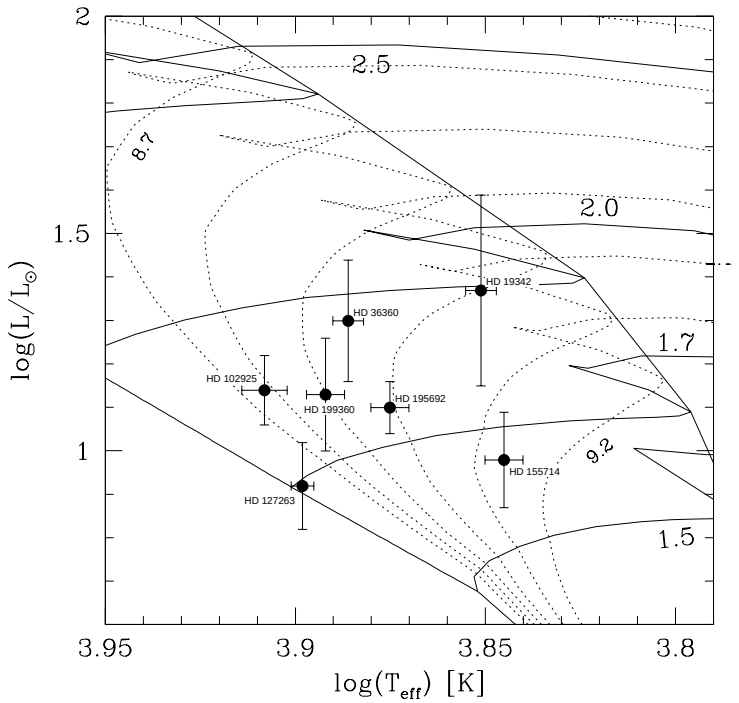

Figure II.18: Location of the primary components of the Am SB1 in the theoretical evolutionary HR diagram computed by Schaller et al. (1992) for $Z = 0.02$, with the isochrones (dotted lines) given by Meynet et al. (1993), for log age[years] varying from 8.7 to 9.2 by steps of 0.1. The solid lines correspond to the evolution tracks for mass values of 1.5, 1.7, 2.0 and 2.5 $M_{\odot}$. From Carquillat et al. (2004).

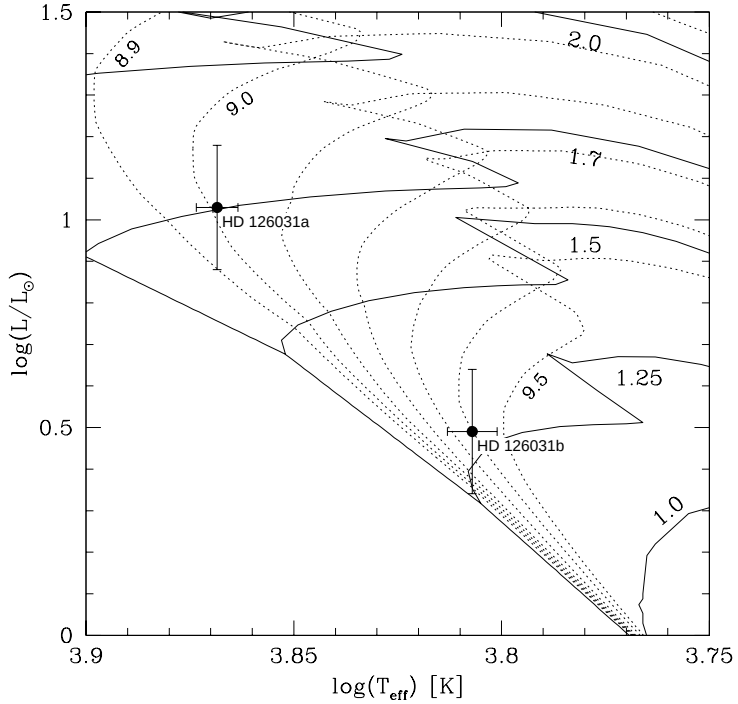

Figure II.19: Location of the two components of HD 126031 in the theoretical evolutionary HR diagram computed by Schaller et al. (1992) for $Z = 0.02$, with the isochrones (dotted lines) given by Meynet et al. (1993) (shifted version of Fig. II.18). From Carquillat et al. (2004).

underestimated.

II.5.9 Tidal effects: circularization of the orbits

Zahn's theory of dynamical tides

Dissipative phenomena occurring in tidal interaction between components of close binaries lead to orbital circularization and synchronization between spin and orbital period. For stars with an outer radiative zone, like Am stars, Zahn (1975, 1977) proposed that the main dissipative mechanism was radiative damping acting on the *"dynamical tide"*. In that case, Zahn showed that the circularization timescale, $t_{\rm circ}$ (defined such that $1/t_{\rm circ} = -\dot{e}/e$), is a steep function of the fractional radius R/a:

$$\frac{1}{t_{\rm circ}} = \frac{21}{2}\left(\frac{GM}{R^3}\right)^{1/2} q\,(1+q)^{11/6}\,E_2\,\left(\frac{R}{a}\right)^{21/2} \qquad \text{(II.9)}$$

where E_2 is related with the dynamic tidal contribution to the total perturbed potential. The tidal constant E_2 is dependent on the stellar structure and strongly varies with mass and time:

- For a given mass, it is a strongly decreasing function of the convective core size. Thus, when the star evolves off the main sequence, its core shrinks and E_2 decreases very quickly. E_2 can change in several decades during stellar evolution for a given mass (Claret & Cunha, 1997).
- For nearly homogeneous models of stars near the ZAMS, with masses of 1.6 to 5 $M_\odot$, $\log E_2$ changes from -8.5 to -6.8 (Zahn, 1975, and Claret & Cunha, 1997).

The strong dependence of E_2 on the internal stellar structure, which is unfortunately badly known, induces large uncertainties on $t_{\rm circ}$.

To compute $t_{\rm circ}$ for our systems (Line 24 of Table II.10) we performed a parabolic interpolation of the tabulated E_2 values computed by Zahn (1975), which are in very good agreement with more recent computations by Claret & Cunha (1997). Except for HD 126031, for which q was known, we assumed $q = 0.5$ for all systems (note that $t_{\rm circ}$ has a small dependence on q). In all cases, the characteristic circularization times we found are larger (for HD 199360), or much larger (for the other systems) than the ages of the stars. Hence the circular orbits of HD 19342, 102925, 126031, 155714, 195692 and 199360 cannot be explained by tidal effects acting on the Am stars during their life in the main sequence, in the context of Zahn's theory (see discussion in next section).

Curve of e versus R/a

In Eq. II.9 we have seen that Zahn's theory stressed the importance of the "fractional radius" parameter (R/a), and predicted that $t_{\rm circ} \propto (R/a)^{-21/2}$. Indeed, Giuricin et al. (1984a) showed on a sample of 200 early-type binaries (O, B, A-type) that the transition between eccentric and circular, or quasi-circular (i.e., $e < 0.05$) orbits was rather sharp and occurred at about $(R/a)_c \sim 0.24$, which agreed well with Zahn's theory.

Following those authors, we computed the fractional radius for each object of our sample (Line 18 of Table II.10), by using for a the mean value $\overline{a}$ of $a_{\rm min}$ and $a_{\rm max}$ (Line 17) and for

the 8 short-period systems of Carquillat et al (2003, Paper V). The resulting plot (Fig II.20) suggests that the critical value of the fractional radius is $(R/a)_c \sim 0.15$. This is smaller than that proposed by Giuricin et al., that was in full agreement with Zahn's model. Hence this plot illustrates also the discrepancy that we find with Zahn's predictions: there are more circularized systems than what is expected from models with radiative dissipation of dynamical tides.

However, let us recall that Eq. II.9 is valid for homogeneous systems, made of two stars possessing a radiative envelope. As seen in Sect. II.5.8, our systems are not homogeneous, and the unseen companions are likely to be convective late-type stars, with masses less than 1.4 $M_\odot$. For stars having a convective envelope, dissipation by turbulent viscosity is the dominant process. According to Zahn & Bouchet (1989), the circularization of orbits takes place in the very beginning of the Hayashi phase of pre-main sequence phase, for late-type binaries. There is little further decrease of the eccentricity on the main sequence. Hence the convective dissipation acting on the cool companion may circularize the orbit of a non-homogeneous binary system. Zahn & Bouchet showed that the theoretical cut-off period, which separates the circular from the eccentric systems is $P \sim 8$ days for convective stars with masses ranging from 0.5 to 1.25 $M_\odot$. This would provide a natural explanation for the presence of circular orbits for the shortest period systems of our sample, namely HD 126031, 155714 and 199360. The case of HD 19342 and 102925 with periods longer than 42 days and 16 days, respectively, is more puzzling: those systems may have formed as circular, indeed.

II.5.10 Tidal effects: rotation–revolution synchronism

In Paper V, we studied eight binaries with orbital period $P \leq 10$ days, and concluded that all those systems have probably reached the rotation–revolution synchronism state. In the present sample, as seven out of ten binaries had periods larger than 10 days, it was interesting to test the rotation–revolution synchronism for those objects.

Kitamura & Kondo's test

For that purpose, we used the KK-test that is described in Sect. I.7.1, which consists in comparing the radius R_1 of the primary with $R_{\rm sync}$, the expected value of the radius obtained when assuming that (i) synchronism has been reached, and (ii) that the orbit and the equator of the star are coplanar. The values of $R_{\rm sync,\,min}$ are given in Line 20 of Table II.10 Notice that for the eccentric orbits, namely for HD 36360, 127263 and 138406, we must take into account the pseudo-synchronous rotation period (see Hut 1981, formulae 44 and 45) instead of the orbital period, i.e., 201.5, 8.7 and 20.3 days, respectively.

Comparing those values to the theoretical values of the radii (Line 11 of Table II.10), we see that the last six stars of the list (HD 126031 to HD 199360) satisfy the inequality (I.27), taking into account the quoted errors: therefore they are likely to rotate in synchronism or pseudo-synchronism (in Line 21, we put "likely" synchronism for those objects). As expected, among the synchronized stars we find the systems with the shortest periods, namely HD 126031, 155714 and 199360 (for clarity, the orbital periods of Tables II.7 and II.8 are displayed in Line 26).

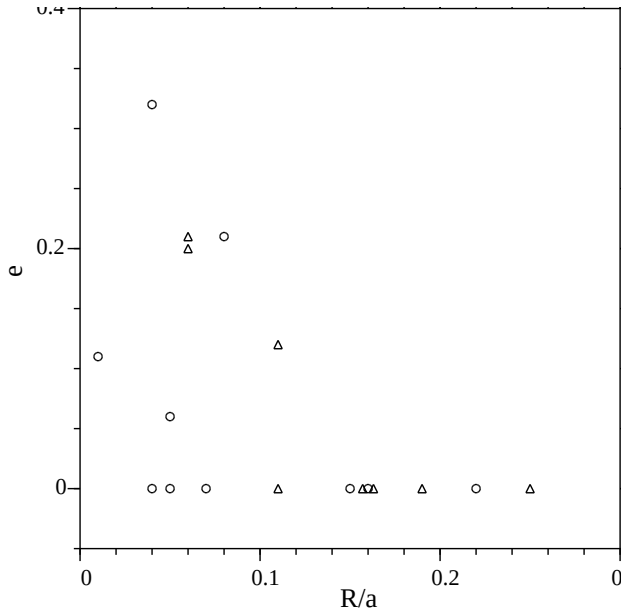

Figure II.20: Eccentricity versus the fractional radius R/a for this sample (circles) and for the systems of Paper V (triangles). From Carquillat et al. (2004).

II.5.11 Tidal effects: comparison with Zahn's theory

With the same theoretical description of radiative dissipation induced by tidal effects that we described in Sect. II.5.9, Zahn (1975) also predicted values for $t_{\rm sync}$, the characteristic synchronization time of binary systems. He obtained:

$$\frac{1}{t_{\rm sync}} = 5 \times 2^{5/3} \times \left(\frac{GM}{R^3}\right)^{1/2} q^2 \, (1+q)^{5/6} \, E_2 \, \frac{MR^2}{I} \, \left(\frac{R}{a}\right)^{17/2} \qquad \text{(II.10)}$$

where I is the momentum of inertia of the star.

Like for $t_{\rm circ}$ (Sect. II.5.9), we computed the values of $t_{\rm sync}$ using the tabulated E_2 and MR^2/I of Zahn (1975), with $q = 0.5$ for all systems, except for HD 126031 for which $q = 0.75$ was known. The corresponding values are displayed in Line 25 of Table II.10.

Here, the agreement with Zahn's radiative theory is better than for $t_{\rm circ}$ (see Sect. II.5.9):

- all systems for which KK-test is negative have $t_{\rm sync} \gg t_{\rm age}$, where $t_{\rm age}$ is the age of the star (Line 23 of Table II.10);
- for HD 199360, $t_{\rm sync} \ll t_{\rm age}$ and indeed this system is very likely to be synchronized (since KK-test is positive and the period is very short, $P = 1.99$ d);
- the agreement with Zahn's theory is marginal with $\log t_{\rm sync} \sim \log t_{\rm age}$ for HD 126031 (synchronized) and HD 155714 (very likely to be synchronized with a positive KK-test and a very short period).

The only clear possible disagreement is found for the systems HD 127263, 138406 and 195692 which have a positive KK-test and $t_{\rm sync} > t_{\rm age} \times 10^2$.

Hence the tidal effects seem more efficient for synchronizing binaries than what is expected from Zahn's theory of radiative dissipation. A possible explanation could be that synchronization by tidal effects starts from the upper layers of the star and then proceeds inwards to the center (J.-P. Zahn, 2003, private communication). As observational data (rotation velocity) concern the surface of the star, there is a possible bias of considering as synchronized stars objects for which synchronism state is not fully reached on the whole star. A theoretical problem would then be to derive the characteristic time $t_{\rm start}$ when the process starts in the surface and the typical duration $\Delta t_{\rm mig}$ of this migration process, from the surface to the center. For HD 127263, 138406 and 195692, this time would be very large with $t_{\rm start} \leq 10^{-2}\, t_{\rm sync}$ and $\Delta t_{\rm mig} \sim t_{\rm sync}$.

As a general conclusion of this section and Sect. II.5.9, the radiative dissipation of dynamical tides as presented by Zahn (1975) is not efficient enough to circularize and synchronize the binary systems we have studied. Two possibilities may partially account for this situation:

- Circularization of the orbit is performed with a greater efficiency by convective dissipation of tidal effects acting on the cool companion during the pre-main sequence stage.
- Synchronization of the radiative primaries is suggested by observations much earlier than the characteristic times indicate, since the process starts from the surface.

II.6 Paper VII: study of 7 new spectroscopic binaries, implications on tidal effects

In Carquillat et al. (2004) we presented the the results of a radial-velocity study of seven Am stars: HD 3970, 35035, 93946, 151746, 153286, 204751 and 224002. They were observed at Haute-Provence and Cambridge observatories with CORAVEL instruments. We find that these systems are single-lined spectroscopic binaries (SB1) whose orbital elements are determined for the first time. Among this sample, HD 35035 and HD 153286 have very long periods, of 2.8 yr and 9.5 yr, respectively, which is rather unusual for Am stars. Four systems have orbits with large eccentricities (with $e \geq 0.4$). Physical parameters have been inferred from this study for the primaries of those systems.
We then investigated the influence of tidal interaction which has already led to the synchronism of the primaries and/or to the circularisation of the orbits of some systems belonging to this sample. We extended this study to the list of 33 objects studied in this series of papers and derived values of the critical fractional radii $r = R/a$ for circularisation and synchronisation of Am-type binaries. We found that the stars with $r \gtrsim 0.15$ are orbiting on circular orbits and that synchronism is likely for all components with $r \gtrsim 0.20$.

II.6.1 Introduction

In this section, we report the results of a RV monitoring of the Am stars HD 3970, 35035, 93946, 151746, 153286, 204751 and 224002. Five stars of this group come from the *Third Catalogue of Am Stars with Known Spectral Types* (Hauck, 1986), the mean source of our sample, and two other stars originate from Bidelman (1988)'s list *(Miscellaneous Spectroscopic Notes)*. Those stars appeared as single-lined spectroscopic binaries (SB1) with CORAVEL. We obtained, for the first time to our knowledge, the orbital elements of those binary systems. In Carquillat & Prieur (2007c), that was the last of this series, we also gave the list and RVs of the sample stars for which we found a constant radial velocity.

II.6.2 Observations and derivation of orbital elements

All the observations were performed with CORAVEL instruments by our team with the 1-meter Swiss telescope at OHP and by R.F. Griffin who kindly observed some stars of our program with his own CORAVEL mounted on the 91-cm telescope at the Cambridge observatories.

The RVs were reduced to the system of the Geneva observatory data base (Udry, Mayor & Queloz 1999), via the observation of RV standard stars conjointly with the program stars. The RVs obtained by R.F. Griffin at Cambridge were also reduced to that system applying an appropriate offset. The observed RVs for the sample stars are reported in Tables 1 to 7 of Prieur et al. (2006b).

The spectroscopic orbital elements given in Table II.12 were obtained with our least-squares program `BS1.for` (see Sect I.4). The observed RVs were all weighted to unity.

The $(O - C)$ residuals are reported in Tables 1 to 7 of Prieur et al. (2006b) and the computed RV curves are displayed in Fig II.21. In all cases, the standard deviation of the residuals, $\sigma_{(O-C)}$, is consistent with the RV mean error, which indicates the absence of detectable spectroscopic third components in those systems.

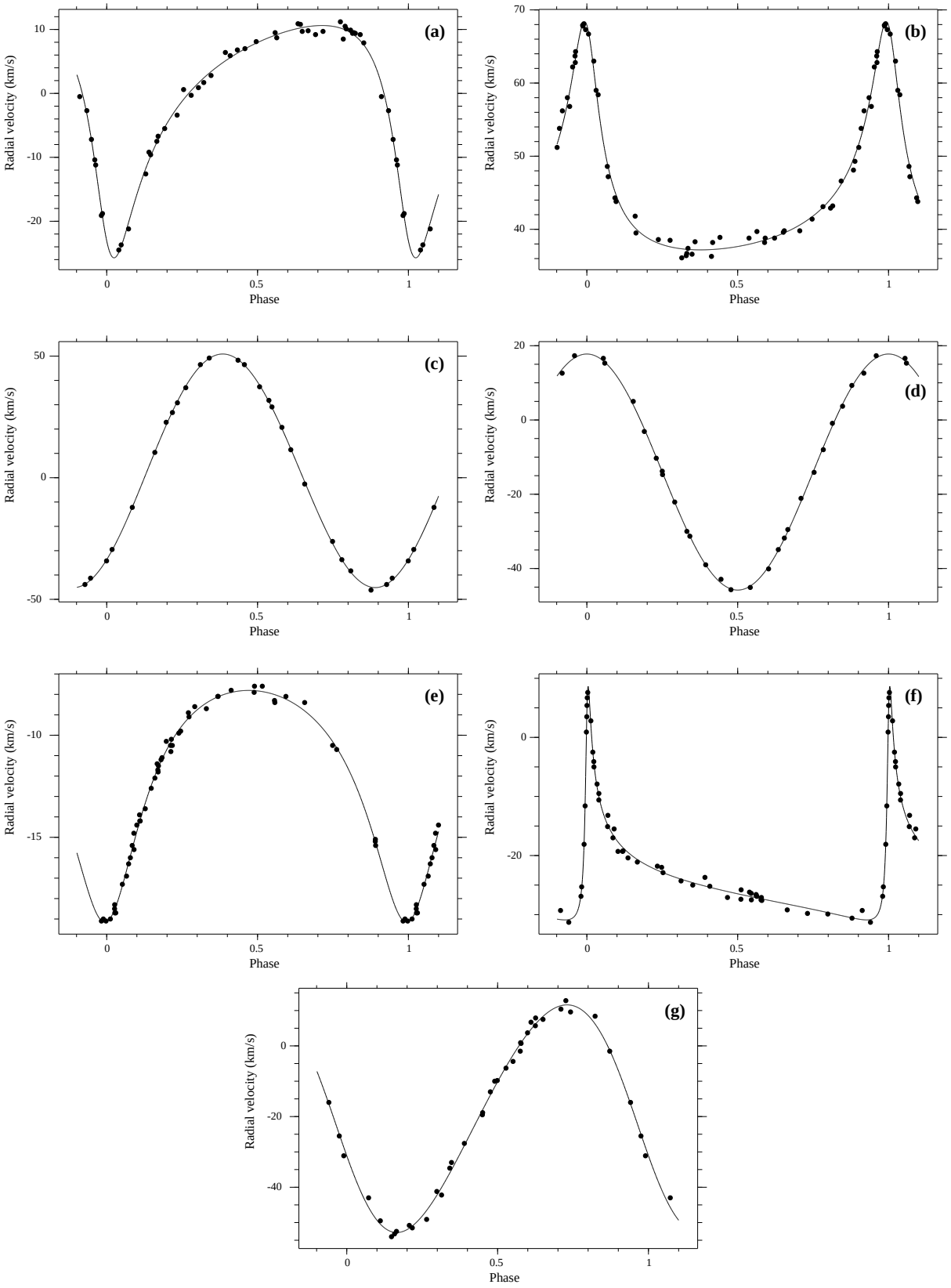

Figure II.21: RV curves computed with the orbital elements of Table II.12: (a) HD 3970, (b) HD 35035, (c) HD 93946, (d) HD 151746, (e) HD 153286, (f) HD 204751, and (g) HD 224002. For HD 151746 which has a circular orbit, the ascending node was taken as the origin of the phases. For the other systems, the origin of the phases corresponds to the periastron passage. From Prieur et al. (2006b).

Table II.12: Orbital elements of the spectroscopic binaries. In Col. 3 T_0 is the epoch of periastron passage, except for HD 151746 for which T_0 corresponds to the ascending node passage. From Prieur et al. (2006b).

HD	P (d)	T_0 (JD) 2400000+	ω (°)	e	K_1 (km.s^{-1})	V_0 (km.s^{-1})	$a_1 \sin i$ (Gm)	$f(m)$ ($M_\odot$)	$\sigma_{(O-C)}$ (km s^{-1})
3970	39.5743	48945.06	148.6	0.521	18.17	0.52	8.44	0.015	0.78
	± 0.0012	± 0.16	± 1.3	± 0.011	± 0.30	± 0.13	± 0.21	± 0.001	
35035	1025.21	49357.9	14.0	0.613	15.59	43.51	173.7	0.199	0.95
	± 0.67	± 2.4	± 1.6	± 0.009	± 0.25	± 0.16	± 4.4	± 0.015	
93946	3.55527	53091.29	220.5	0.014	48.02	3.36	2.347	0.0409	0.59
	± 0.00004	0.19	± 19.8	± 0.004	± 0.20	± 0.15	± 0.010	± 0.0005	
151746	4.83737	52826.205	—	0.0	31.78	−14.02	2.114	0.0161	0.57
	± 0.00006	± 0.008		(fixed)	± 0.19	± 0.12	± 0.013	± 0.0003	
153286	3458.18	49051.3	185.3	0.367	5.67	−11.41	251.0	0.053	0.22
	± 7.74	± 12.4	± 1.6	± 0.008	± 0.06	± 0.04	± 4.0	± 0.002	
204751	59.6993	52475.31	320.9	0.867	19.78	−24.44	8.08	0.0059	0.70
	± 0.0006	± 0.02	± 1.1	± 0.002	± 0.26	± 0.12	± 0.18	± 0.0004	
224002	19.8059	49657.33	109.0	0.107	32.21	−19.48	8.72	0.068	1.38
	± 0.0006	± 0.35	± 6.3	± 0.012	± 0.41	± 0.29	± 0.12	± 0.003	

For the short period systems HD 93946 and HD 151746, the Lucy & Sweeney (1971)'s test led us to consider as significant, although very small, the eccentricity of the HD 93946 orbit and to adopt a circular orbit for HD 151746. The systems HD 35035 and 153286 have long periods of 2.8 yr and 9.5 yr, respectively, which is unusual for systems involving an Am star. Note also the very eccentric orbit of HD 204751 ($e \approx 0.9$).

II.6.3 Notes on individual systems

In this section we report some information about the stars studied in Prieur et al. (2006b), in particular the origin of the Am classification and, when available, the classifications from the Ca II K line (k), hydrogen lines (h) and metallic lines (m). We give also previous information about the SB nature of the star when it was known.

HD 3970 (HIP 3331). The Am classification quoted in Hauck's catalogue originates from Abt (1984) who gave F2 (k), F0 (h), F4 (m). That is somewhat unusual because the type of the K lines is later than the type derived from the hydrogen lines. Olsen (1980) also proposed an Am classification from its Strömgren indices. Note that other and different classifications can be found in the literature: δ Del (Bidelman 1983) and F2 II (Sato & Kuji 1990). Fehrenbach et al. (1987) and Grenier et al. (1999) classified HD 3970 as a supergiant F2 Ib star and noted the variability of its RV.

HD 35035 (HIP 25160). Two classifications are reported in Hauck's catalogue: Am (A3 (k), F0 (m)), from Walther (1949) and Am (A2 (k), F4 (m)) from Zirin (1951). Strömgren photometry is available for this object, but there was no previous detection of RV variations.

Table II.13: Physical parameters derived from this study, and from the knowledge of m_v, $B-V$ and π. The subscripts 1 and 2 refer to the primary and secondary components, respectively. From citeAm-PaperVII.

HD	3970	35035	93946	151746	153286	204751	224002
HIP	3331	25160	53081	81757	82864	—	117856
m_V	7.20	7.56	8.65	6.82	7.03	7.93	7.99
$B-V$	0.34	0.31	0.28	0.22	0.31	0.33	0.31
E_{B-V}	0.04	0.08	0.00	0.00	0.00	0.03	0.06
$v_e \sin i$ (km.s^{-1})	29.1 ± 2.9	22.1 ± 2.2	25.3 ± 1.3	13.1 ± 2.6	7.3 ± 0.2	27.3 ± 2.7	38.8 ± 3.9
π (mas)	5.40 ± 0.81	5.33 ± 1.24	3.61 ± 1.15	8.26 ± 0.59	9.43 ± 0.60	12.0 ± 4.1	6.47 ± 0.86
d (pc)	185^{+33}_{-24}	188^{+56}_{-36}	277^{+130}_{-67}	121^{+9}_{-8}	106^{+7}_{-6}	83^{+44}_{-21}	155^{+23}_{-19}
$M_{V,1}$	0.83 ± 0.33	1.6 ± 0.5	1.52 ± 0.69	2.0 ± 0.2	1.98 ± 0.14	3.31 ± 0.74	1.94 ± 0.28
$T_{\rm eff}$ (K)	7400 ± 100	8000 ± 100	(7300 ± 100)	—	7500 ± 100	7300 ± 100	(7500 ± 100)
$\log g$ (cgs)	3.7	4.1	—	—	4.0	4.0	—
[Fe/H]	0.68	0.43	—	—	0.71	0.86	—
$\log(L/L_\odot)$	1.55 ± 0.13	1.25 ± 0.20	1.28 ± 0.28	—	1.09 ± 0.06	$0.73^{+0.13}_{-0}$	1.11 ± 0.11
M_1 ($M_\odot$)	2.2 ± 0.2	1.9 ± 0.2	1.9 ± 0.3	(~ 2)	1.80 ± 0.05	~ 1.6	1.8 ± 0.1
R_1 ($R_\odot$)	3.6 ± 0.6	2.2 ± 0.6	2.7 ± 0.9	(~ 2)	2.0 ± 0.2	~ 1.6	2.1 ± 0.3
$M_{2,\,\rm min}$ ($M_\odot$)	0.5	1.3	0.6	(~ 0.5)	0.7	~ 0.3	0.8
a ($R_\odot$)	71.5 ± 4.0	647 ± 20	14.3 ± 1.0	(17.5 ± 1.2)	1386 ± 85	89.5 ± 4.5	44.5 ± 2.5
$a(1-e)$ ($R_\odot$)	35 ± 2.0	250 ± 8	14.2 ± 1.0	—	863 ± 54	11.6 ± 0.6	39.6 ± 2.2
P (days)	40	1025	3.6	4.8	3458	60	20
$P_{\rm ps}$ (days)	16.62	238.14	—	—	1872.04	2.57	18.47
$v_{\rm sync}$ (km.s^{-1})	11.0	0.5	38.4	(21)	0.05	31.5	5.8
Synchronised?	no	no	likely	likely	no	likely	no
Circularised?	no	no	yes	yes	no	no	no
log age (yr)	$8.90^{+0.1}_{-0.1}$	$8.87^{+0.1}_{-0.1}$	$9.00^{+0.04}_{-0.10}$	—	$8.95^{+0.05}_{-0.05}$	< 8.95	$9.00^{+0.01}_{-0.05}$
log $t_{\rm sync}$ (yr)	13/10.6	23/20	8.4	(10)	26/25	17/10.0	14/13
log $t_{\rm circ}$ (yr)	17/13	29/25	10.7	(13)	33/31	22/12.5	17/16

HD 93946 (HIP 53081). The Am classification originates from Bidelman (1988)'s list. Here also, no previous information could be found about its RV.

HD 151746 (HIP 81757). This object was classified as Am by Bidelman (1988) who also mentioned it as SB. This star is the primary component of the close visual binary CCDM 16420+7353, for which Seymour et al. (2002) computed a preliminary visual orbit (with $P = 32$ yr and $a = 0.''17$) based on 15 speckle interferometry observations between 1978 and 1993. Therefore HD 151746 is a physical triple system.

HD 153286 (HIP 82864). The classification quoted in Hauck's catalogue, A3 (k), F5 (m), originates from Bertaud & Floquet (1967). The Am nature of HD 153286 was confirmed by Grenier et al. (1999) who gave the detailed classification A3 (k), A8 (h) and F4 (m). According to Babcock (1958) three spectra of this star indicate a magnetic field of *"significant intensity and negative polarity"*, which is not usual among Am stars. The SB nature was not previously mentioned. Strömgren photometry is available.

HD 204751 (TYC 4261–1731–1). The classification reported in Hauck's catalogue, A3 (k), F1 (h), F6 (m), is from Abt (1984). Olsen (1980) proposed also an Am classification from its Strömgren indices. This object is not listed in the HIPPARCOS Catalogue but it was observed by the TYCHO mission. The parallax given in Table II.13 was extracted from the TYCHO catalogue. No previous information was found about the RV of this star.

HD 224002 (HIP 117856). This star was first classified as Am by Cowley & Cowley

Table II.14: Strömgren photometry and derived data with Crawford (1975, 1979)'s calibration. From Prieur et al. (2006b)

HD	β	$b-y$	$E_{(b-y)}$	m_1	$(m_1)_0$	c_1	$(c_1)_0$	$(\delta m_1)_0$
3970	—	0.21	0.03	0.23	0.25	0.83	0.83	−0.06
35035	2.83	0.18	0.06	0.21	0.23	0.88	0.87	−0.03
153286	2.79	0.18	0.01	0.25	0.26	0.81	0.81	−0.06
204751	—	0.22	0.02	0.24	0.25	0.69	0.68	−0.07

(1965) and later by Bertaud (1970) who gives the classification A2 (k), F2 (m) that is quoted in Hauck's catalogue. More recently, Grenier et al. (1999) gave the detailed classification A3 (k), A7 (h), F3 (m) and noted the variability of the RV.

II.6.4 Physical parameters of the primaries

In what follows, we present the procedure we used to derive the physical parameters of the primaries stars of those systems, that are listed in Table II.13. They are mainly based on:

- the available data found in the literature: magnitudes, colour indices (in the UBV and Strömgren systems) and parallaxes;
- the orbital parameters of Table II.12;
- grids of models used to calibrate Strömgren photometry, and evolutionary models to infer the masses and ages from the location in the HR diagram.

The final aim is, when possible, to estimate the evolutionary status of the concerned components. For this purpose we must first estimate the colour excess for each system and examine the influence of the undetected companions.

Strömgren photometry

Four stars have been measured in the Strömgren photometric system, namely HD 3970, 35035, 153286 and 204751, according to Hauck & Mermilliod (1998). The corresponding data are displayed in Table II.14. When the β value was available (for HD 35035 and 153286) we estimated the effective temperatures, $T_{\rm eff}$ and $\log g$ (Table II.13, lines 10 and 11) using the grids, $(c_1)_0$ versus β, given by Moon & Dworetsky (1985). When β was not known, those parameters were obtained from the Relyea & Kurucz (1978) grids of $(c_1)_0$ versus $(b-y)_0$. The de-reddened indices $(b-y)_0$, $(c_1)_0$ and $(m_1)_0$ were computed either with Crawford (1975, 1979)'s formulae, when β was available, or via E_{B-V} with Crawford (1975)'s relation.

For the stars without Strömgren photometry, we estimated the effective temperatures (except for HD 151746, see below) from the $B-V$ values and Flower (1996)'s Tables. In this case, the temperature is given between brackets in Table II.13, line 10.

We also give an estimate of the metallicity [Fe/H] (Table II.13, line 12), using Cayrel's calibration as reported by Crawford (1975, Fig. 17 of this paper). The values we found are in agreement with the metallic-lined nature of the stars.

Colour excess

We estimated the reddening E_{B-V} from the Strömgren indices, when H_β measurement was available. Indeed, from the value of the β parameter (free of the effect of interstellar absorption) we can obtain $(b-y)_0$, the de-reddened value of $(b-y)$ (Crawford 1979), and then the colour-excess $E_{B-V} = E_{b-y}/0.73$ (see Crawford 1975). When β was unknown we used Lucke (1978)'s maps and the distance deduced from the parallax. The adopted values of E_{B-V} are quoted in Table II.13 (line 5).

Then we computed the absolute visual magnitudes of the systems using the HIPPARCOS parallaxes values (ESA 1997) and the apparent visual magnitudes m_V corrected, if needed, for the interstellar absorption: $A_V \approx 3\,E_{B-V}$.

II.6.5 Influence of the undetected companions

Except HD 35035, all systems studied here have small mass functions, i.e. $f(m) < 0.07$ M$_\odot$ (Table II.12) which gives an indication of a small mass ratio $\mu = M_2/M_1$ of the two components (see Sect. II.6.7). When taking the statistically most likely values: $M_1 \approx 2$ M$_\odot$, $i \approx 60°$ and $M_{V1} \approx 1.7$ (cf. North 1997), we find $M_2 < 1$ M$_\odot$ and $\Delta m_V > 3$. So it is likely that the companions of those systems are faint and that the photometric indices are not very affected by the presence of the companions.

We can then consider that the visual absolute magnitude M_{V1} of the primary of a given system lies between two limits, a minimum value $M_{V1,\,\min}$ that is the global magnitude of the system (when Δm_V is very large) and a maximum value $M_{V1,\,\max}$, corresponding to $\Delta m_V = 2$ (which is the average limit of detection of the secondary with CORAVEL). We will adopt $M_{V1} = (M_{V1,\,\min} + M_{V1,\,\max})/2$ (Table II.13, line 9). The case of HD 35035 with a larger mass function ($f(m) = 0.2$ M$_\odot$) is examined hereafter.

The case of HD 35035

For this system, the mass function of 0.2 M$_\odot$ implies a rather massive secondary. Indeed, assuming $M_1 \approx 2$ M$_\odot$, we would have $M_2 \geq 1.3$ M$_\odot$. This corresponds to a spectral type earlier than F6V and a magnitude difference of $\Delta m_V < 2$, according to Schmidt-Kaler (1982), which is small enough to make it detectable with CORAVEL. The absence of secondary dips in the CORAVEL correlation patterns indicates that the secondary is hot, without metallic lines in its spectrum.

Other constraints come from photometric measurements of the global system: $M_V = 1.0$ and $B-V = 0.23$, after correction of the interstellar absorption.

We can then tentatively propose the following composite model which satisfy all the constraints:

- primary: Am, $M_V \approx 1.6$, $B-V = 0.18$
- secondary: F0 IV, $M_V \approx 1.9$, $B-V = 0.30$

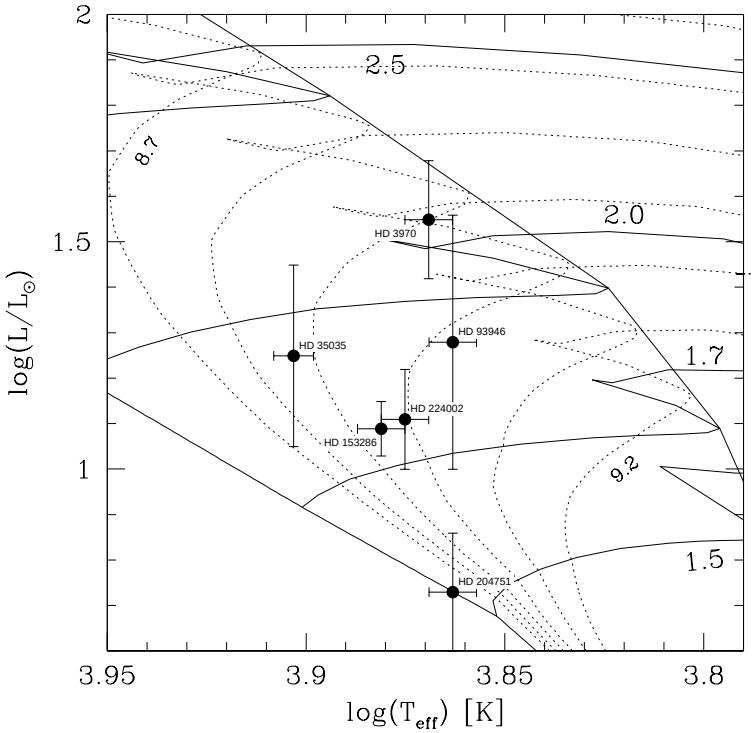

Figure II.22: Location of the primary components of the Am SB1 in the theoretical evolutionary HR diagram computed by Schaller et al. (1992) for $Z = 0.02$, with the isochrones (dotted lines) given by Meynet et al. (1993), for log age[years] varying from 8.7 to 9.2 by steps of 0.1. The solid lines correspond to the evolution tracks for mass values of 1.5, 1.7, 2.0 and 2.5 $M_\odot$. From Prieur et al. (2006b).

The case of HD 151746

For this close visual star, the CCDM Catalogue (Dommanget & Nys 1994) quotes $m_{V,A} = 7.3$ and $m_{V,B} = 7.6$. With $m_{V,A} = 7.3$, the visual absolute magnitude of the spectroscopic pair would be $M_{V,A} = 1.88 \pm 0.15$. A statistical correction for the unseen spectroscopic companion (see Sect. II.6.5) leads us to adopt $M_{V,1} = 1.96 \pm 0.15$. It is difficult to make a valid estimate of the effective temperature of the Am component in the absence of Strömgren photometry and other physical information about the visual companion. Nevertheless with a visual absolute magnitude of about 2 mag. the primary Am component must be a not very evolved dwarf star (Schmidt-Kaler 1982).

II.6.6 The evolutionary status, masses and radii

Using the estimates of $T_{\rm eff}$ and $\log(L/L_\odot)$ for six stars of the present sample, we can plot them in the theoretical HR diagram of Schaller et al. (1992) (see Fig. II.22) and derive the theoretical masses (Table II.13, line 14). We obtained the values of $\log(L/L_\odot)$ from the visual absolute magnitudes $M_{V,1}$ and the bolometric corrections tabulated by Flower (1996). For HD 204751 the TYCHO parallax, of poor quality, leads to a very faint luminosity which would set the star under the ZAMS in the HR diagram. Nevertheless, the error bars are rather large and we may assume that this component is on the ZAMS, i.e. with $\log L/L_\odot \approx 0.73$ (or $M_{\rm bol} \approx 2.9$) or even a little above the ZAMS.

From Fig. II.22, one sees that all the primaries have masses near 2 $M_\odot$, which is compat-

ible to what we assumed in Sect. II.6.5.

The isochrones from Meynet et al. (1993) reported in this HR diagram indicate ages lying between 500 millions and one milliard years, except perhaps HD 204751 that may be younger.

Using the Stefan radiation law as given by Schmidt-Kaler (1982): $\log(R/\mathrm{R}_\odot) = -0.2M_{\mathrm{bol}} - 2\log T_{\mathrm{eff}} + 8.47$, we computed the theoretical radius of those stars (Table II.13, line 15). HD 3970 appears as the most evolved star of the sample although it is not a supergiant. The classification as δ Del (i.e. evolved metallic-line star) proposed by Bidelman (1983) for this object seems realistic.

II.6.7 Minimum masses and separations of the spectroscopic companions

The mass function of a spectroscopic binary is defined as:

$$f(m) = M_1 \sin^3 i \, \mu^3/(1+\mu)^2 \tag{II.11}$$

where $\mu = M_2/M_1$ is the mass ratio of the components (1 = primary, 2 = secondary). When using for each system the mass M_1 quoted in line 14 of Table II.13, the relation (II.11) gives, with i = 90°, the minimum value of μ, from which we can derive $M_{2,\,\mathrm{min}}$, the minimum value of the mass of the companion (line 16 of Table II.13). For HD 151746, for which very few information was available (see Sect. II.6.5), we tentatively assumed a value $M_1 \approx 2\,\mathrm{M}_\odot$ that corresponds to an average mass value for Am stars (see Sect. II.6.6) and put all those mass estimates between brackets in Table II.13.

The mean linear separation a between the two components of a binary system is:

$$a = a_1(1 + 1/\mu) \tag{II.12}$$

where a_1 is the semi-major axis of the orbit of the primary relative to the center of mass of the system (Col. 8 of Table II.12). The relations (II.11) and (II.12) lead, for a given value of i, to an estimate of the separation a. Carquillat et al. (1982) brought to light that the values obtained in this way have a very small dependency on the value assumed for i. For the seven SBs of our sample we computed the values of a for $20° < i < 90°$ (range of 94% likelihood) with the constraint that $\mu < 1$, which sometimes reduces this range. The mean values and the corresponding ranges of uncertainties are given in Table II.13 (line 17).

Given their distances the mean angular separations of the two most detached systems, HD 35035 and 153286, are expected to be $0\text{”}016 \pm 0\text{”}004$ and $0\text{”}060 \pm 0\text{”}008$, respectively. For HD 35035, a separation with a multi-pupil interferometer should be possible, favoured by a faint Δm_V (see Sect. II.6.5). As for HD 153286, the rather large expected separation should permit a resolution with a speckle camera at the focus of a large telescope, provided the companion is not too faint.

II.6.8 Tidal effects: rotation-revolution synchronism

Because of energy dissipation induced by tidal effects, the orbit of a binary system evolves towards a circular orbit and the rotation of the components tends to be synchronised with the orbital motion, with a direction of spin perpendicular to the orbital plane. In such a case,

when a component of a binary system rotates in synchronism with the orbital motion and when the orbit and the equator of the star are coplanar, we have the following relation (see Sect. I.7.1):

$$R = P\ v_e = P\ v_e \sin i / \sin i \tag{II.13}$$

where R is the radius of the component, v_e its tangential equatorial velocity and P the orbital period.

Hut (1981) has shown that systems formed with highly eccentric orbits can reach a state close to synchronism, called *"pseudo-synchronism"* before the orbit is circularised. According to Hut, this state is characterised by a pseudo-period $P_{\rm ps}$ related to the orbital period P via the relation:

$$P_{\rm ps} = P\ \frac{(1 + 3\,e^2 + \frac{3}{8}\,e^4)\,(1 - e^2)^{3/2}}{1 + \frac{15}{2}\,e^2 + \frac{45}{8}\,e^4 + \frac{5}{16}\,e^6} \tag{II.14}$$

The parameter $v_e \sin i$ (projected equatorial velocity) can be obtained from the width of the CORAVEL correlation dip profiles, using Benz & Mayor (1981)'s calibration. The values are reported in line 6 of Table II.13. From relation (II.13) we derive $v_e \sin i = R \sin i / P$, which leads to:

$$v_e \sin i \leq v_{\rm sync} \quad \text{with} \quad v_{\rm sync} = R/P \tag{II.15}$$

Note that $v_{\rm sync} = 50.6\,(R/R_\odot)/(P/{\rm d})$ km.s^{-1}. For circular orbits, the inequality (II.15) can be used as a test of synchronism when i is unknown. Indeed, if a star rotates in synchronism, its value of $v_e \sin i$ should verify the relation (II.15). In the case of elliptic orbits, P should be replaced with the pseudo-period $P_{\rm ps}$ given in line 20 of Table II.13. Note in this table the big difference between P (line 19) and $P_{\rm ps}$ for the orbits with large eccentricities (e.g, HD 35035 and 204751).

We applied this test to the primary component of the seven systems. To do so, the primary radii were assumed to be equal to the theoretical values obtained with the Stefan law or, when not available (e.g. for HD 151746), we assumed the typical value $R \approx 2$ R$_\odot$ (see Table II.13, line 15). We thus obtained the equatorial velocity value for synchronism $v_{\rm sync}$, quoted in line 21 of Table II.13. This value could then be compared with the measured value of $v_e \sin i$ (line 6) and the result of the test is given in line 22. We see that the synchronism state has probably been reached for the two short-period circularised systems HD 93946 and HD 151746. This could be expected since the major axes are small for those two objects, which leads to strong tidal interaction. The same occurs for HD 204751 in terms of pseudo-synchronism. It is again not very surprising because, at periastron passage of this very eccentric orbit, the distance of the components is only 12 R$_\odot$.

II.6.9 Tidal effects: comparison with theoretical characteristic times

To account for tidal effects among early type stars, Zahn (1975, 1977) proposed that the main dissipative mechanism was radiative damping acting on the dynamical tide. We have presented this model in Paper VI, with the expressions of the characteristic times $t_{\rm sync}$ and $t_{\rm circ}$ relative to the synchronisation of the star rotation and the circularisation of the orbit, respectively. The values computed for the objects of this paper are given in Table II.13 (lines 25 and 26) using the same procedure as described in Paper VI. When a system has a non-circular orbit, we also give in this table (in the same line and column, but separated with a slash) the

value obtained with the minimum separation $a(1-e)$ corresponding to the periastron passage, where the tidal effects are the strongest and the most efficient. For a system with a large eccentricity, like HD 204751 with $e = 0.87$, the minimum separation is much smaller than the mean separation (a) and the corresponding values of $t_{\rm sync}$ and $t_{\rm circ}$ are also much smaller. It should be remembered that those theoretical values are only rough estimates, since they are based on a simplified modelisation of the internal structure of those stars which is poorly known.

We obtained some estimates of the ages for all the systems displayed in Fig II.22 by using the isochrones of Meynet et al. (1993) plotted in this figure as dashed lines. Those values are reported in Table II.13 line 24.

When taking into account the results of the synchronisation test given in line 22, we find a rather good agreement between the ages of the stars and the theoretical values of $t_{\rm sync}$:

- the estimated age of HD 93946 is larger than $t_{\rm sync}$, and indeed the synchronisation test is positive;
- the cases when this test is negative correspond to values of $t_{\rm sync}$ much larger than the estimated ages.
- for HD 204751, the agreement is marginal with the value of $t_{\rm sync}$ obtained with the minimum separation $a(1-e)$.

When considering $t_{\rm circ}$, the agreement is rather good (lines 24 and 26), the cases of non-circular orbits corresponding to values of $t_{\rm circ}$ much larger than the estimated ages. Nevertheless the circularised systems have ages much smaller than the values computed for $t_{\rm circ}$ with Zahn's model. Indeed, log age $= 9.00$ for HD 93946 and log age < 10.2 for HD 151746 (since this star is younger than the age of the universe). As already discussed in Paper VI, possible origins of this discrepancy for an SB1 binary system are:

- the unseen companion has a small mass and thus must have a convective envelope. Tidal interaction is much more efficient in this case and the cool companion alone can have circularised the mutual orbit (this circularisation has probably occurred in the Hayashi phase of the pre-main sequence).
- the binary system may have formed as circular.

II.6.10 Tidal effects: synchronisation and circularisation critical fractional radii

Zahn (1977) predicted a strong dependency of the strength of tidal effects with the *fractional radius* $r = R/a$, defined as the ratio of the star radius with the semi-major axis of the orbit. For stars with a convective core and a radiative envelope, $t_{\rm circ} \propto (R/a)^{-21/2}$ and $t_{\rm sync} \propto (R/a)^{-17/2}$. Hence the determination of the smallest component separations, or *critical fractional radii* $r_{\rm sync}$ and $r_{\rm circ}$, at which synchronism or orbit circularisation become mostly observed, is a valuable test for theoretical models.

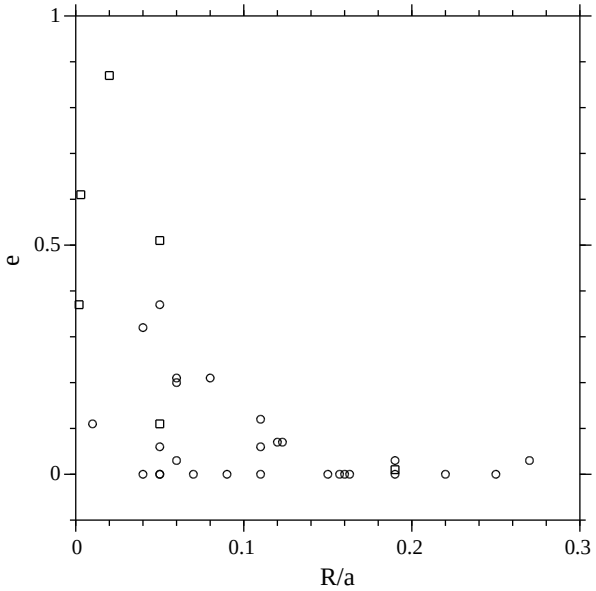

Figure II.23: Circularisation of the binary systems for this sample (squares), and for the systems from Paper I to Paper VI (circles). From Prieur et al. (2006b).

Determination from our whole sample of Am stars

The Figures II.23 and II.24 illustrate the influence of tidal interaction on the evolution of the 33 systems we have studied in the series of our papers devoted to Am spectroscopic binary systems (see Papers I to VI in the bibliography). Those figures were made by extracting all the relevant data contained in those papers.

Fig. II.23 clearly shows that all stars with $r \geq 0.15$ are orbiting on circular orbits.

In the diagram $\log(v_e \sin i/v_{\rm sync})$ versus r of Fig. II.24a, the synchronism test of the inequality (II.15) corresponds to imposing a threshold with the dotted line. This would lead to $r_{\rm sync} \approx 0.1$. We could also apply a stricter criterion involving the ratio $v/v_{\rm sync}$, where v is the true equatorial velocity. Indeed if we assume that the inclination has a uniform random distribution, the most probable value of $\sin i$ is 0.5, which corresponds to $i = 60°$ (dashed line). Hence the stricter test $v < v_{\rm sync}$ would lead to $r_{\rm sync} \approx 0.20$.

For the non-circular orbits, that are concerned with pseudo-synchronism only (see Fig. II.24b), we have plotted $\log(v_e \sin i/v_{\rm sync})$ versus $R/[a(1-e)]$, since the minimum separation is more relevant in this case. Indeed tidal interaction is much stronger in the portion of the orbit close to the periastron passage. From this plot it seems that the critical fractional radius, expressed as $R/[a(1-e)]$, is larger than 0.15, but the number of points is unfortunately too small to enable us to be more precise.

Discussion

Zahn (1977) computed the limiting separations *"for which the corresponding characteristic times are equal to one quarter of the main sequence life span"*, for circularisation and synchronism. For a population of relatively evolved primaries (i.e. stars that have already spent one fourth of their lifetime on the main sequence), those values are thus equal to the critical radii that can be deduced from the observations. From table 2 of Zahn (1977) we obtain

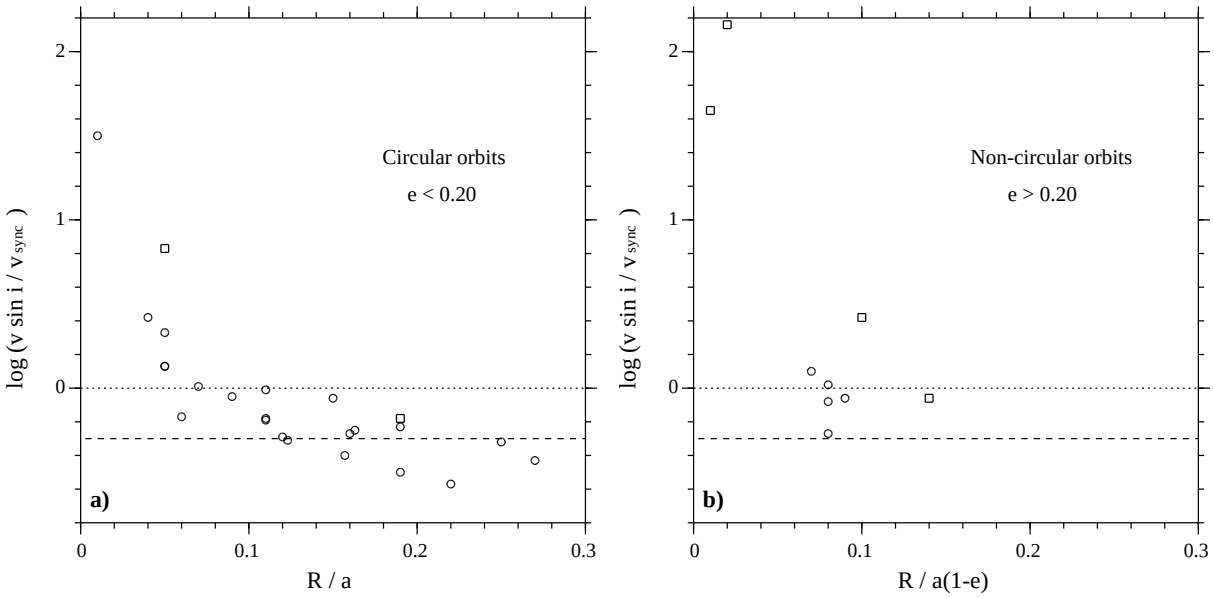

Figure II.24: Synchronisation of the binary systems belonging to this sample (squares), and to the whole list of Am stars studied from Paper I to Paper VI (circles). The dotted and dashed lines correspond to the synchronisation thresholds for $i = 0$ and $i = 60°$, respectively. From Prieur et al. (2006b).

$r_{\rm sync} \approx 0.14$ and $r_{\rm circ} \approx 0.20$, for binary systems with $M_1 = 2$ M$_\odot$ and $\mu = 1$. If we assume a smaller mass ratio, $\mu = 0.5$, which is generally more likely for single-lined spectroscopic binaries, those values become somewhat larger: $r_{\rm sync} \approx 0.17$ and $r_{\rm circ} \approx 0.24$.

With our sample of Am stars we find $r_{\rm sync} \approx 0.20$ which is very close to the predicted value. Concerning the circularisation, our determination of $r_{\rm circ} \approx 0.15$ is smaller than Zahn's expectations. Let us note however that Zahn assumed that the two stars forming the system had a radiative envelope, which is generally not the case for our systems. Indeed most of the objects studied in this series of papers are SB1 and the mass estimates of the unseen secondary stars are small (see e.g. Table II.13, line 16). Hence those stars must have convective envelopes. As mentioned in Sect. II.6.9, tidal effects acting on the companions are more effective in this case and may have led to the circularisation of the mutual orbits.

To our knowledge the only statistical study of early type stars that used the fractional radius r was made by Giuricin et al. (1984a,b). With early-type eclipsing binaries and double-lined spectroscopic binaries (SB2), they found $r_{\rm sync} \approx 0.15$ and $r_{\rm circ} \approx 0.25$, which is very close to Zahn (1977)'s predictions. The analysis of the light curves of eclipsing binaries can provide directly the values of the fractional radii r of both components and of the inclination i of the system. For the SB2 of their sample, they determined the r values with a procedure similar to ours. The value we find for $r_{\rm sync}$ is in good agreement with their value, but our determination of $r_{\rm circ} \approx 0.15$ is somewhat smaller than theirs. The sample of the 200 stars they used for determining $r_{\rm circ}$ (Giuricin et al., 1984a) is a compilation of many sources which include nearly main sequence detached eclipsing binaries (spectral types O, B, A) and short period SB2s ($P < 200$ d). A plausible explanation is that the fraction of low massive convective companions is larger in our sample. This is obvious for their group of SB2 constituted with systems with components of similar luminosities (and masses). It must also exist a high fraction of systems with comparable luminosities in the other group of the

eclipsing binaries, since such a property facilitates their detection. Hence the smaller value found for $r_{\rm circ}$ in our sample than in Giuricin's would support the argument that the presence of a convective companion plays a key role in the circularisation of close binary systems containing an early type star.

(Giuricin et al., 1984b) noticed that below $r_{\rm sync}$, there was a high fraction of synchronised stars, which was incompatible with Zahn's predictions. They concluded that *"tidal mechanisms in early-type close binaries are much more efficient in bringing stars to synchronism than is presently described by theory"*. Although we do not see this property in Fig. II.24 (which can be explained by our much smaller sample than theirs), our determination of $r_{\rm circ} \approx 0.15$, is smaller than Zahn's expectations. This would support Giuricin's conclusion about stronger tidal effects than predicted by the theory, for orbit circularisation also.

Zahn (1977) recognized that his theoretical predictions were rather imprecise, since they relied on many assumptions on the internal stellar structure, with very few observational constraints. He said that observations leading to the determination of the limiting separations, would be very helpful to revise the values of the tidal coefficients E_2, and precise the internal stellar structure. With those new values of $r_{\rm sync}$ and $r_{\rm circ}$, for Am-stars, we hope that this study will contribute to refining theoretical models.

Compared to the sample studied by Giuricin, our sample is limited to Am-type stars, which facilitates theoretical studies since it has a much more limited range of physical parameters (temperature, radius, mass).

II.7 Paper VIII, first part: study of 8 new spectroscopic binaries

I present in this section the study of eight new binaries we presented in Paper VIII: HD 32893, 60489, 109762, 111057, 113697, 204918, 219675 and BD+44°4512. We found that these objects are single-lined SBs whose orbital elements were determined for the first time. HD 32893 was found to be a triple spectroscopic system whose third body might be detected by speckle interferometry. Physical parameters were inferred for the primaries of those SBs. We then investigated the influence of tidal interaction and found that it has already led to the synchronism of the primaries and to the circularisation of the orbits of four of those systems.

In Section II.7.1, we present our observations and the orbital elements we derived, for the first time to our knowledge, for those eight systems. In Section II.7.2, we give some useful information that we found in the literature about the studied stars. In Section II.7.3, we derive some physical parameters of the primary components and examine their evolutionary status. We also estimate the minimum masses and separations of the unseen companions. In Section II.7.9, we examine the occurrence of tidal effects for the studied systems in terms of rotation-revolution synchronism of the primaries.

II.7.1 Observations and derivation of orbital elements

Most of the observations concerning the eight objects were performed at OHP, but additional observations were also carried out by R.F Griffin who kindly observed some stars of our programme with his own CORAVEL in Cambridge. CORAVEL is a spectrophotometer that allows measurements of heliocentric RVs by performing a cross-correlation of the stellar spectrum with a physical mask placed in the focal plane of the spectrograph (Baranne, Mayor & Poncet 1979). This instrument was initially conceived to study the stars cooler than the spectral type F4 but it was also found fit for use for slow-rotating ($v_e \sin i < 40$ km.s^{-1}) hotter stars when they exhibit metallic lines in their spectrum, like the Am stars. The precision of the RVs depends upon $v_e \sin i$, the projected rotational velocity of the star. The mean rms error varies from about 0.5 km.s^{-1} for the slowest rotators to about 1.5 km.s^{-1} for the maximum limit value of $v_e \sin i \approx 40$ km.s^{-1}.

The RVs obtained at OHP and in Cambridge were reduced to the system of the Geneva Observatory RV data base (Udry, Mayor & Queloz 1999). For HD 60489, we also used 4 RVs obtained with the AURELIE spectrograph at OHP by Künzli & North (1998) that were reduced to this system by applying an offset of $+1$ km.s^{-1}. The resulting RV measures of the eight new SBs are given in Tables 1 to 8 of Carquillat & Prieur (2007c).

The spectroscopic orbital elements given in Table II.15 were obtained from the observed RVs using a fully automatic sequence of programmes described in Paper VII. All the RVs obtained with CORAVEL (OHP and Cambridge) were weighted unity; those from the AURELIE spectrograph were weighted 1/4. For HD 32893, our usual least-squares programme "BS1", that fits orbital parameters to SB1 data (Nadal et al 1979), led to $O - C$ residuals much larger than the value expected from the RV errors, and not randomly distributed with time. This gave us a hint of the presence of an unseen third body in the system and the analysis of the residuals allowed us to estimate its period. The RVs were then successfully re-processed with our programme "BS4", that performs a least-squares minimization of the

Table II.15: Orbital elements of the eight new SB studied in Paper VIII. T_0: periastron passage epoch for eccentric orbits, ascending node passage epoch for circular orbits. Column 1, HD 32893: (s) short-period system, (ℓ) long-period system. From Carquillat & Prieur (2007c).

HD/BD	P (d)	T_0 (JD) 2400000+	ω (°)	e	K_1 (km.s^{-1})	V_0 (km.s^{-1})	$a_1 \sin i$ (Gm)	$f(m)$ ($M_\odot$)	$\sigma_{(O-C)}$ (km.s^{-1})
32893 (s)	2.175561	50747.305	—	0.0	49.84	var.	1.491	0.0280	0.55
	±0.000002	± 0.002			±0.13		0.004	± 0.0002	
" (ℓ)	1136.7	51173.2	185.0	0.848	9.76	14.21	81.0	0.0164	
	±1.5	±2.0	±2.7	±0.010	±0.27	±0.13	±4.8	±0.0029	
60489	67.9501	50495.89	100.6	0.422	13.71	43.56	11.62	0.0136	0.74
	±0.0088	±0.55	±4.8	±0.021	±0.43	±0.22	±0.50	±0.0017	
109762	34.1863	50850.25	65.5	0.135	26.29	−13.11	12.24	0.0627	0.71
	±0.0021	±0.35	±3.4	±0.009	±0.24	±0.18	±0.13	±0.0019	
111057	3.848018	53091.727	—	0.0	15.96	−1.72	0.8446	0.00162	0.45
	±0.000048	±0.009			±0.12	±0.09	±0.0066	±0.00004	
113697	539.9	46696.8	54.4	0.675	9.93	1.32	54.4	0.0220	0.97
	±1.4	±9.7	±3.1	±0.034	±0.52	±0.18	±5.3	±0.0063	
204918	5.04496	53262.446	—	0.0	18.21	−30.21	1.263	0.00316	0.79
	± 0.00017	±0.019			±0.22	±0.15	±0.015	±0.00011	
219675	531.40	49833.	88.3	0.197	4.56	10.20	32.7	0.00494	0.38
	±0.84	±15.	±8.9	±0.024	±0.13	±0.09	±1.1	±0.00049	
+44°4512	5.002094	50482.563	—	0.0	29.34	−5.51	2.018	0.01312	0.90
	±0.000025	±0.009			±0.24	±0.17	±0.017	±0.00032	

orbital elements of a triple hierarchical spectroscopic system to SB1 data (see Paper IV).

The computed RV curves for those eight systems are given in Figs. II.25 and II.26, and the $O-C$ residuals in Tables 1 to 8 of Carquillat & Prieur (2007c). For BD +44°4512, the bad repartition in phase of the observations is due to the value of the orbital period which is nearly equal to an integer number of days ($P = 5.002$ d).

II.7.2 Notes on individual systems

In this section we report the origin of the Am classification of those eight stars and some complementary information.

HD 32893 (HIP 24108). The Am classification originates from Abt (1985). The star is ADS 3723 A, the primary component of a wide visual pair. According to the CCDM catalogue (Dommanget & Nys 1994), the visual secondary is a faint star of tenth magnitude at ≈ 12 " of the A component. It is a new spectroscopic triple system (see Sect. II.7.1).

HD 60489 (HIP 36869, HR 2904). This star was classified Am by Bertaud & Floquet (1967) and A7 III by Cowley & Jaschek (1969). Künzli & North (1998) found it is an evolved metallic-line star and detected some light variations.

HD 109762. Two references for its Am nature are quoted in Hauck (1986)'s catalogue: Slettebak, Bahner & Stock (1961) and Slettebak, Wright & Graham (1968). Hill et al. (1976) confirmed its classification as Am and first noted the variability of its RV. This star was not observed by Hipparcos.

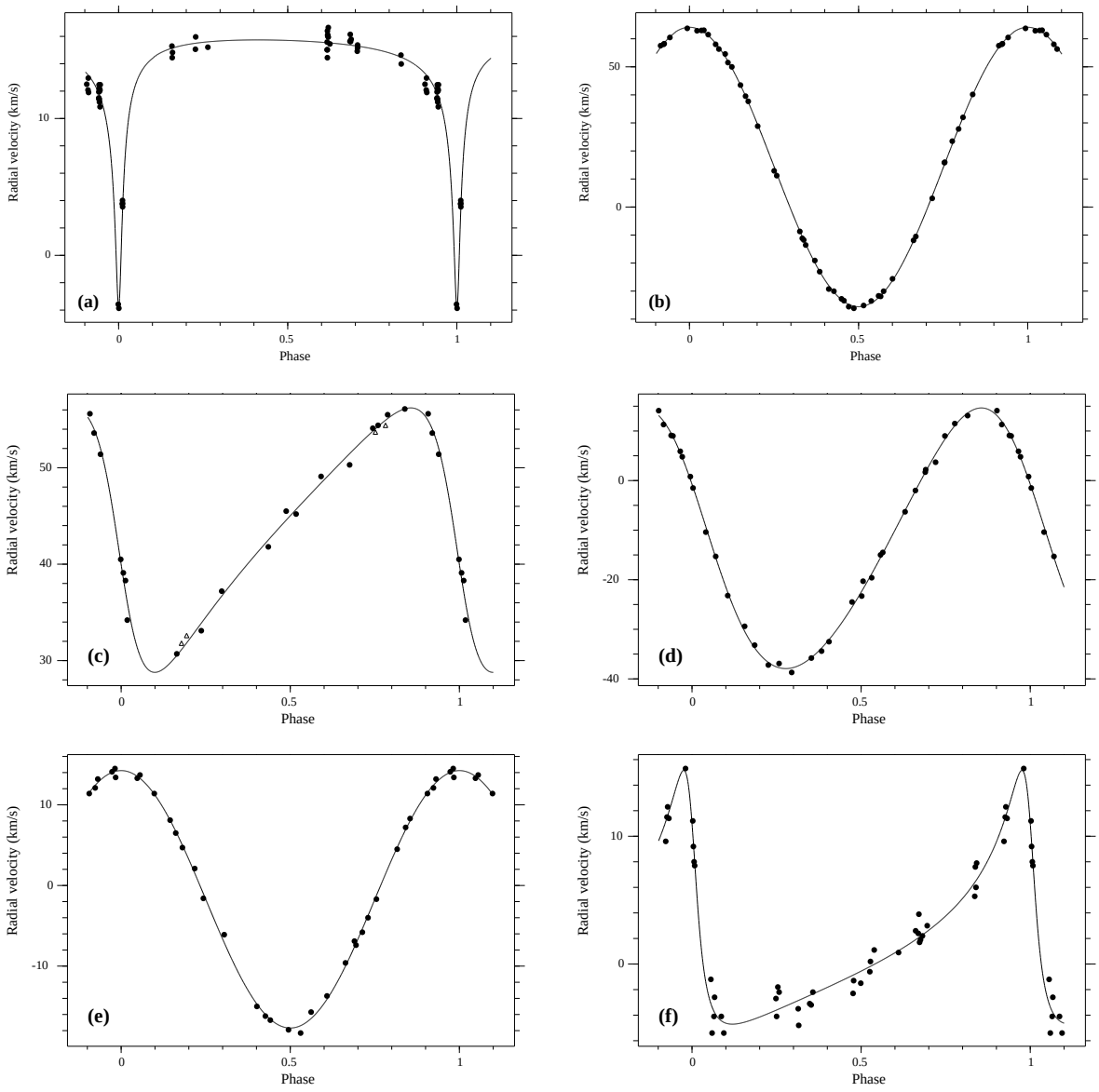

Figure II.25: RV curves (solid lines) computed with the orbital elements of Table II.15: (a) HD 32893 (long-period outer system), (b) HD 32893 (short-period inner system), (c) HD 60489, (d) HD 109762, (e) HD 111057 and (f) HD 113697. For HD 32893 (a) and HD 111057 that have a circular orbit, the ascending node was taken as the origin of the phases. For the other systems, the origin of the phases corresponds to the periastron passage. The CORAVEL measures are displayed with black dots. For HD 60489, the few AURELIE measures are reported with open triangles. From Carquillat & Prieur (2007c).

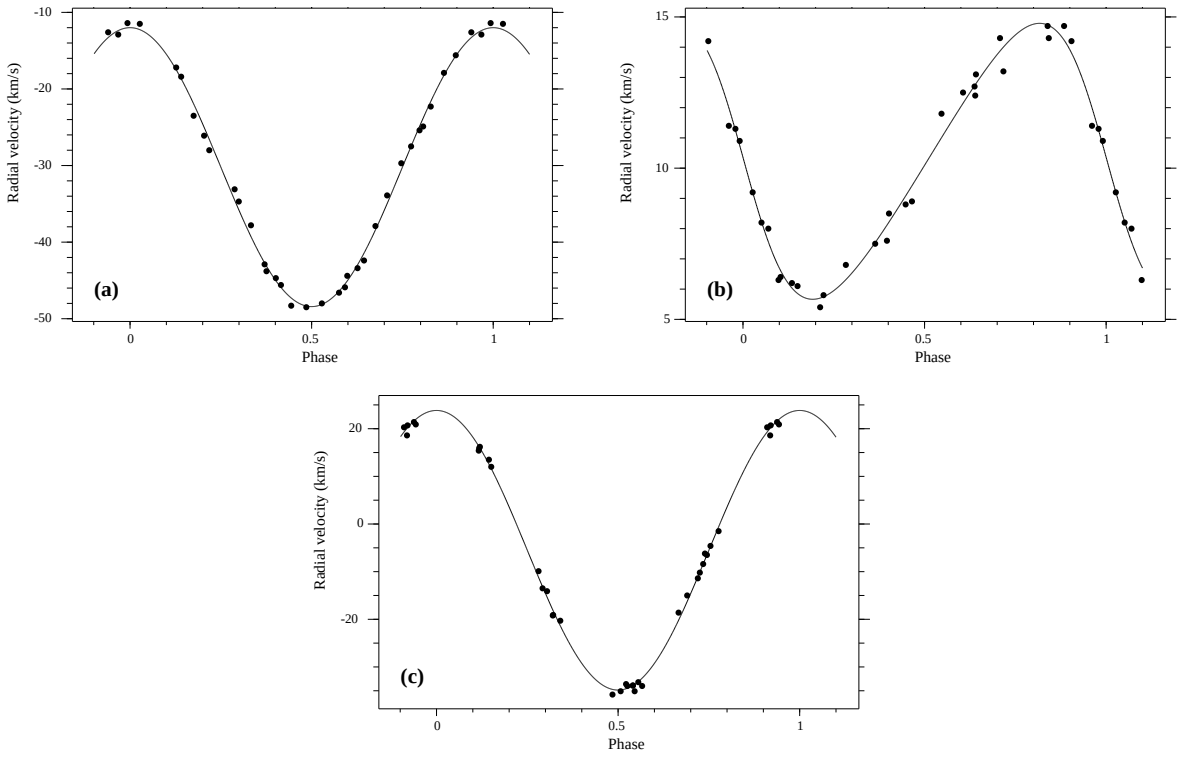

Figure II.26: RV curves computed with the orbital elements of Table II.15: (a) HD 204918, (b) HD 219675 and (c) BD $+44°4512$ The origin of the phases corresponds to the periastron passage. From Carquillat & Prieur (2007c).

HD 111057 (HIP 62341). The Am classification originates from Hill et al. (1976) and was confirmed by Bidelman (1988).

HD 113697 (HIP 63806). Hynek (1938) listed this star with "composite spectrum", but this was contradicted by our spectroscopic study in the near infrared region that led to a classification as Am (Ginestet et al. 1997). Our result is in agreement with the Henry Draper's Catalogue where this star is classified as A3 with a mention in the notes of the presence in the spectrum of *"several solar lines (too) strong for class A3"*. Grenier et al. (1999) gave the classification A5 III but this luminosity class is not in agreement with the visual absolute magnitude ($M_V = 2.4 \pm 0.3$) obtained from the trigonometric parallax (ESA 1997). This value of M_V corresponds to that of a dwarf A star, which is the typical luminosity class of the Am stars.

HD 204918 (HIP 106184). The Am classification quoted in Hauck (1986)'s catalogue originates from Abt (1984).

HD 219675 (HIP 115011). The Am classification originates from Abt (1985). This new SB belongs to the close visual binary ADS 16650 AB, for which Scardia et al. (2002) computed an orbit with $P = 173.7$ yr and $a = 0.41$". According to Fabricius & Makarov (2000), we have $\Delta m_V \approx 2$ for this visual pair. Therefore, HD 219675 is a true physical triple system.

BD$+44°4512$ The Am classification of this faint star listed in Hauck (1986)'s catalogue originates from Floquet (1975). This star was not observed by Hipparcos.

II.7.3 Physical parameters

Like for the previous papers of the series we now derive some physical parameters of those systems (reported in Table II.16) using the orbital parameters we have found, Strömgren photometry and other available data found in the literature.

II.7.4 Color excess and M_V deduced from Strömgren photometry

The Strömgren photometric indices β, $b-y$, m_1 and c_1, found in Hauck & Mermilliod (1998)'s catalogue for the studied objects are displayed in cols. 2, 3, 5 and 7 of Table II.17, respectively. Unfortunately, no Strömgren photometry data was found for BD $+44°4512$.

When β was available, the de-reddened indices $(b-y)_0$, $(m_1)_0$, $(c_1)_0$ and $(\delta m_1)_0$ were computed with Crawford (1975, 1979)'s formulae. The colour-excess was then derived with the relation $\mathrm{E}_{B-V} = \mathrm{E}_{b-y}/0.73$ (Crawford 1975). When β was not known, E_{B-V} was derived from Lucke (1978)'s opacity maps and the distance deduced from the parallax. Then the same relation allowed to retrieve E_{b-y} which we could use to correct the Strömgren indices for reddening effects. The values obtained for E_{b-y}, $(m_1)_0$, $(c_1)_0$ and $(\delta m_1)_0$ are reported in cols. 4, 6, 8 and 9 of Table II.17, respectively.

The values derived for E_{B-V} (line 5 of of Table II.16) were also used to correct the apparent visual magnitudes m_V (line 3) for the interstellar absorption $\mathrm{A}_V \approx 3\,\mathrm{E}_{B-V}$. When the Hipparcos parallaxes were available (line 7) those corrected magnitudes allowed the computation of the absolute magnitudes M_V (line 9).

For HD 109762, which has not been observed by Hipparcos, we estimated its absolute magnitude from the Strömgren photometry using the relation derived by North et al. (1997) for a sample of stars of types A and Am observed by Hipparcos:

$$M_V = 12.6 - 3.7\,\beta - 8.3\,(\delta c_1)_0 + 6.5\,(\delta m_1)_0 + 7.2\,10^{-6}\,(v_e \sin i)^2.$$

With the formulae of Crawford (1975), we obtained $(\delta c_1)_0 = 0.05$, which led to $M_V = 1.71$.

II.7.5 $T_{\rm eff}$, $\log g$ and [Fe/H] from Strömgren photometry

When β was known, the effective temperature $T_{\rm eff}$ and the gravity $\log g$ (lines 11 and 13 of Table II.16) were estimated from the grid of $(c_1)_0$ versus β given by Moon & Dworetsky (1985). In the other cases, those parameters were obtained from the Relyea & Kurucz (1978) grids of $(c_1)_0$ versus $(b-y)_0$.

The metallicity [Fe/H] (Table II.16, line 14) was derived from the δm_1 values, using Cayrel's calibration as reported by Crawford (1975, Fig. 17 of this paper). The positives values we found are in agreement with the metallic-lined nature of the stars. Note that the value [Fe/H] = 0.86 obtained for HD 219675 is probably slightly overestimated, because of the presence of a close cooler visual companion only two magnitudes fainter.

II.7.6 Influence of the unseen companions

The eight systems studied here have small mass functions, i.e. $f(m) < 0.063$ $\mathrm{M}_\odot$ (see Table II.15), which indicates that the companions have probably small masses. Indeed, if we assume that M_1, i and M_{V1} are equal to their statistically most likely values, $M_1 \approx 2$ $\mathrm{M}_\odot$,

Table II.16: Physical parameters derived from Strömgren indices, parallaxes, orbital elements and theoretical data. The indices 1 and 2 refer to the primary (Am) or the secondary stars, respectively.

(1)	HD (BD)	32893	60489	109762	111057	113697	204918	219675	$+44°4512$
(2)	HIP	24108	28432	—	62341	63806	106184	115011	—
(3)	V	6.74	6.55	8.58	8.46	8.47	6.77	6.73	10.19
(4)	$B-V$	0.30	0.23	0.27	0.23	0.34	0.31	0.37	0.32
(5)	E_{B-V}	0.03	0.01	0.00	0.00	0.00	0.04	0.00	—
(6)	$v \sin i$ (km.s^{-1})	10.0	24.0	20.5	10.6	23.8	11.4	21.3	18.9
		$\pm$1.0	$\pm$2.4	$\pm$1.5	$\pm$1.3	$\pm$2.4	$\pm$1.6	$\pm$2.1	$\pm$1.0
(7)	π (mas)	11.63	6.98	—	5.72	6.07	8.15	6.23	—
		$\pm$0.88	$\pm$0.83		$\pm$1.07	$\pm$0.95	$\pm$0.60	$\pm$1.31	
(8)	d (pc)	86	143	—	175	165	123	161	—
(9)	M_V	1.98	0.74	—	2.25	2.39	1.21	0.70	—
		$\pm$0.16	$\pm$0.26		$\pm$0.41	$\pm$0.34	$\pm$0.16	$\pm$0.46	
(10)	M_{V_1}	2.06	0.82	1.71	2.33	2.47	1.29	0.94	—
		$\pm$0.17	$\pm$0.26	$\pm$0.36	$\pm$0.41	$\pm$0.34	$\pm$0.17	$\pm$0.46	
(11)	$T_{\mathrm{eff}\,1}$ (K)	7900	7650	7500	7950	7200	7700	7200	—
		$\pm$100	$\pm$100	$\pm$100	$\pm$100	$\pm$100	$\pm$100	$\pm$100	
(12)	$\log(L_1/\mathrm{L}_\odot)$	1.064	1.560	1.200	0.956	0.900	1.372	1.512	—
		$\pm$0.068	$\pm$0.104	$\pm$0.144	$\pm$0.164	$\pm$0.136	$\pm$0.068	$\pm$0.184	
(13)	$\log g_1$ (cgs)	4.3	3.6	4.1	4.2	4.0	4.1	3.7	—
(14)	$[\mathrm{Fe/H}]_1$ (dex)	0.42	0.18	0.49	0.62	0.12	0.45	0.86	—
(15)	M_1 ($\mathrm{M}_\odot$)	1.80	2.20	1.85	1.70	1.60	2.00	2.15	$\approx$2
		$\pm$0.05	$\pm$0.10	$\pm$0.15	$\pm$0.10	$\pm$0.10	$\pm$0.05	$\pm$0.15	
(16)	R_1 ($\mathrm{R}_\odot$)	1.8	3.4	2.3	1.6	1.8	2.7	3.6	$\approx$2.5
		$\pm$0.2	$\pm$0.5	$\pm$0.4	$\pm$0.3	$\pm$0.3	$\pm$0.3	$\pm$0.9	
(17)	$M_{2\mathrm{min}}$ ($\mathrm{M}_\odot$)	0.5	0.5	0.8	0.2	0.5	0.3	0.3	0.4
(18)	a ($\mathrm{R}_\odot$)	10.0	103.1	64.3	13.1	381	16.8	388	17.6
		$\pm$0.8	$\pm$6.8	$\pm$4.0	$\pm$0.4	$\pm$28	$\pm$1.0	$\pm$20	$\pm$1.3
(19)	a (au)		0.48	0.30		1.8		1.8	
			$\pm$0.03	$\pm$0.02		$\pm$0.1		$\pm$0.1	
(20)	Synchronism?	Likely	No	No	Likely	No	Likely	No	Likely
(21)	log [age (yr)]	8.80 $^{+0.05}_{-0.10}$	8.88 $^{+0.04}_{-0.04}$	9.00 $^{+0.02}_{-0.04}$	< 8.82	9.05 $^{+0.05}_{-0.25}$	8.93 $^{+0.02}_{-0.02}$	8.93 $^{+0.07}_{-0.03}$	—

Table II.17: Strömgren photometry (subscript 0 refers to de-reddened indices).

HD	β	$b-y$	E_{b-y}	m_1	$(m_1)_0$	c_1	$(c_1)_0$	$(\delta m_1)_0$
32893	—	0.169	0.02	0.220	0.23	0.752	0.75	-0.02
60489	2.800	0.135	0.01	0.199	0.20	0.969	0.97	0.00
109762	2.778	0.164	0.00	0.224	0.22	0.791	0.79	-0.03
111057	2.828	0.125	0.00	0.249	0.25	0.836	0.84	-0.04
113697	2.745	0.196	0.00	0.175	0.18	0.724	0.72	0.01
204918	—	0.195	0.03	0.215	0.23	0.776	0.77	-0.03
219675	—	0.218	0.00	0.248	0.25	0.701	0.70	-0.07

$i \approx 60°$ and $M_{V1} \approx 1.7$ (cf. North 1997), we find $M_2 \lesssim 0.9$ M$_\odot$. This corresponds to a companion with spectral type cooler than G5 V and $\Delta m_V \gtrsim 3.4$ (Schmidt-Kaler 1982). So we may approximate, with only a minor error, the photometric indices of the primary components by the global values. The physical parameters derived from the global Strömgren indices in Sect. II.7.4 and II.7.5 can thus be affected to the Am primaries only.

For a given system, the visual absolute magnitude M_{V1} of the primary component lies between two limits, a minimum value corresponding to the global magnitude M_V of the system and a maximum value $M_{V1,\,\mathrm{max}}$, corresponding to $\Delta m_V = 2$ (which is the average limit of detection of the secondary with CORAVEL). We will adopt $M_{V1} = (M_V + M_{V1,\,\mathrm{max}})/2$, which is reported in line 10 of Table II.16. For the triple system HD 219675 we applied a double correction, taking also into account the presence of the close visual component (see Section II.7.2).

II.7.7 Evolutionary status, masses and radii

From the values of M_{V1} and the bolometric corrections tabulated by Flower (1996) we obtained the luminosity $L_1/\mathrm{L}_\odot$ given in line 12 of Table II.16. The stars could be then plotted on the theoretical HR diagram of Schaller et al. (1992) for solar metallicity (Fig. II.27). Like the other Am stars studied in the previous papers of the series, they are scattered within the whole width of the main sequence. This fact was also pointed out by Domingo & Figueras (1999) and is inconsistent with an older study of Gómez et al (1981) who found that the Am stars were located about 1 mag. above the main sequence.

We then derived the theoretical masses (line 15 of Table II.16) and ages (line 21) of the Am primaries using the isochrones from Meynet, Mermilliod & Maeder (1993) also displayed in Fig. II.27. The values found for masses are close to 2 M$_\odot$, which is in agreement to what we assumed in Section II.7.6. The isochrones indicate ages lying between 0.5 and 1 giga-years, except perhaps HD 111057 that may be younger.

Finally, using the Stefan radiation law: $\log(R/\mathrm{R}_\odot) = -0.2 M_{\mathrm{bol}} - 2 \log T_{\mathrm{eff}} + 8.47$ (Schmidt-Kaler 1982), we computed the theoretical radii of those stars (line 16). The rather large values we found for HD 60489 and HD 219675 are consistent with the evolved character of the primary components of those systems.

In the case of BD $+44°4512$ for which very few data were known, we simply assumed that $M_1 \approx 2$ M$_\odot$ and $R_1 \approx 2.5$ R$_\odot$, which are typical values for Am stars.

II.7.8 Minimum masses and separations of the spectroscopic companions

The mass function of an *SB1* can be defined as (see Sect. I.4.4):

$$f(m) = M_1 \, \sin^3 i \, \mu^3/(1+\mu)^2 \qquad \text{(II.16)}$$

where $\mu = M_2/M_1$ is the mass ratio of the components (1 = primary, 2 = secondary). When using for each system the mass M_1 quoted in line 15 of Table II.16, the relation (II.16) gives, with $i = 90°$, the minimum value of μ, from which we can derive $M_{2,\,\mathrm{min}}$, the minimum value of the mass of the companion (line 17 of Table II.16).

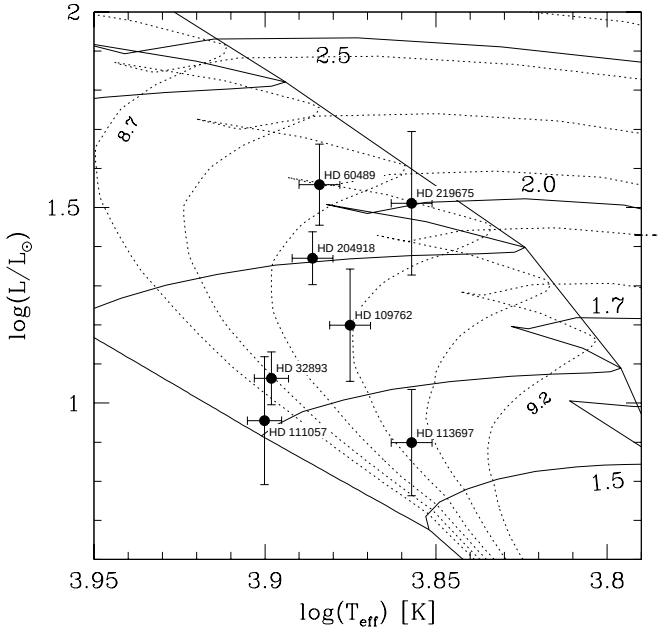

Figure II.27: Location of the primary components of the eight new SB1s in the theoretical HR diagram computed by Schaller et al. (1992) for $Z = 0.02$, with the isochrones (dotted lines) given by Meynet et al. (1993), for $\log$ age[years] varying from 8.7 to 9.2 by steps of 0.1. The solid lines correspond to the evolution tracks for mass values of 1.5, 1.7, 2.0 and 2.5 $M_\odot$.

The mean linear separation a between the two components of a binary system is:

$$a = a_1(1 + 1/\mu) = a_1 \sin i(1 + 1/\mu)/\sin i \qquad \text{(II.17)}$$

where a_1 is the semi-major axis of the orbit of the primary relative to the centre of mass of the system. The value of $a_1 \sin i$ can be derived from the orbital elements (col. 8 of Table II.15), but unfortunately the inclination i is unknown. The relations (II.16) and (II.17) can lead to an estimate of the separation a, provided that an assumption is made on the value of i. According to Carquillat et al. (1982) the values obtained in this way have a very small dependency on the value assumed for i. For the eight SBs of our small sample we computed the values of a for $20° < i < 90°$ (range of 94% likelihood) with the constraint that $\mu < 1$, which sometimes reduced this range. The mean values and the corresponding ranges of uncertainties are given in Table II.16 (lines 18 and 19).

The third body of the triple system of HD 32893 was also considered and we estimated its minimum mass $M_{3,\,\rm min}$ and its distance a' from the short-period system. In the formulae (II.16) and (II.17) we replaced M_1 with $(M_1 + M_2)$, the total mass of the short-period system, and we set $\mu = M3/(M1 + M2)$. The value of $M_{3\,\rm min}$ corresponds to the case when $i = 90°$ with $(M_1 + M_2)_{\rm min} = 1.8 + 0.5 = 2.3$ M$_\odot$ (see Table II.16, col. 2, lines 15 and 17). We thus found: $M_{3\,\rm min} = 0.5\ M_\odot$, which is similar to what we obtained for $M_{2\,\rm min}$. The maximum value corresponds to a mass ratio unity for the short-period system, i.e. $(M_1 + M_2)_{\rm max} = 3.6$ M$_\odot$. For a', we computed the mean of the two values obtained for a' when using the minimum and maximum values for $M_1 + M_2$, and found $a' = 3.5 \pm 0.5$ au. At 86 pc, which is the distance derived from the Hipparcos parallax, this value corresponds to an angular separation of 0.041 ± 0.009 " (taking also into account the error on the parallax). According to the high eccentricity of the orbit ($e \approx 0.85$), a separation near 0.075" could be reached at the apastron. Hence the third companion could be detected by speckle interferometry with a 2-meter class telescope, provided it is not too faint (i.e. $\Delta m_V < 3$ mag).

II.7.9 Rotation-revolution synchronism

In this section we test the occurrence for the studied systems of rotation-revolution synchronism that is the consequence of gravitational tidal effects. More details about this procedure can be found in Papers VI and VII.

For a circular orbit, the orbital period P of the system, the radius R of the considered component ant its equatorial rotational velocity v verify the relation $v = R/P$ when synchronism is reached. Using the following units: P in days, R in solar radii and v in km.s^{-1}, this relation becomes:

$$v = 50.6(R/\mathrm{R}_\odot)/P. \qquad \text{(II.18)}$$

Practically, we only have access to the projected equatorial velocity $v \sin i$. The relation (II.18) implies that:

$$v \sin i < 50.6\ (R/\mathrm{R}_\odot)/P \qquad \text{(II.19)}$$

This inequality constitutes a test for synchronism.

For the systems formed with highly eccentric orbits the evolution is much slower. Hut (1981) has shown that such systems reach first a state close to synchronism, called *"pseudo-synchronism"* before the orbit is circularised. The test of pseudo-synchronism uses also the

inequality (II.19) with a small change: P is replaced by the pseudo-period P_{ps} defined as:

$$P_{\rm ps} = P\,\frac{(1+3\,e^2+\frac{3}{8}\,e^4)\,(1-e^2)^{3/2}}{1+\frac{15}{2}\,e^2+\frac{45}{8}\,e^4+\frac{5}{16}\,e^6} \qquad \text{(II.20)}$$

We derived the values of $v_e \sin i$ for our eight systems from the width of the correlation dips obtained with CORAVEL (reported in Table II.16, line 6) using the calibration given by Benz & Mayor (1981). We thus applied the test (II.19) to the primary components of HD 32893, 111057, 204918 and BD $+44^\circ 4512$ which have circular orbits, and found that those velocities were compatible with the values of R_1 reported in line 16 of Table II.16. For the four other systems, HD 60489, 106762, 113697 and 219675 with an eccentric orbit, we found that P_{ps} are 31.1, 30.8, 94.4 and 430 d, respectively, which lead to negatives tests: the primaries still rotate too fast. Those results, reported in line 20 of Table II.16, are in agreement with what we have obtained in our series of papers: the Am primary stars belonging to SB systems with short periods ($P \lesssim 10$ d) and circular orbits verify the synchronism tests, whereas most of the primaries of the other systems with longer periods and eccentric orbits rotate too fast.

Chapter III

Statistical study

III.1 Paper VIII, 2nd part: statistical study of a sample of 91 Am-type stars.

I present in this section the statistical study we presented in the second part of Paper VIII. It was the eighth and last paper of a series (see Table I.1) devoted to the search for and the consequent study of spectroscopic binaries (SBs) in a sample of 91 Am stars, mainly constituted from the Third Catalogue of Am Stars with Known Spectral Types (Hauck, 1986) (see Sect. I.1).

In Paper VIII, we presented the main results of our whole programme and derived some statistical properties of Am stars. We built a recapitulating table of the orbital parameters found for the SBs of our whole sample and published the list of those for which no evidence for radial velocity variations could be found during our monitoring. Our study showed that at least 64% of Am stars were members of SBs. This rate is significantly greater than that of normal stars. Although some SBs may have been not detected, this study showed that a substantial fraction of Am stars do not belong to SBs: they are either isolated stars or members of wide binary systems.

We then presented some statistical properties of the orbital parameters of the SBs whose primary was an Am star, on an extended sample obtained by adding 29 Am SB orbits published by other authors. The corresponding e vs $\log P$ diagram shows a cutoff between the circular and the eccentric systems at $P \approx 5.6 \pm 0.5$ d, which indicates that a typical age of 0.5–1 $\times 10^9$ yr for the Am stars, which is in agreement with the values found in our previous detailed studies. A Monte-Carlo analysis showed that the distribution of the mass function values $f(m)$ was compatible with a power-law distribution $N(m) \propto m^{-\alpha}$ of the masses m of the companions with $\alpha = 0.3 \pm 0.2$ or with a Gaussian distribution centered on 0.8$\pm$0.5 $M_\odot$, which indicates that the companions of Am SBs are mostly dwarf stars of type G-K-M.

In Section III.1.1, we recall the final results of the RV survey of our sample of 91 stars and some related statistics about the frequency of Am belonging to SBs. In Section III.1.3, we present the properties of the orbital systems of an extended SB sample of Am stars with 89 orbits and derive some constraints on the distribution of the masses of companions.

III.1.1 Final results of our RV survey of 91 Am stars

In this section we present the final results of the RV survey of our sample of 91 Am stars, whose full list can be found in Tables III.1 and III.2.

III.1.2 Presentation of the data

When we started this study in the mid-1980's, none of the stars belonging to our sample had known SB orbital elements. We are now able to present in Table III.1 the orbital elements of 53 double or multiple spectroscopic systems from this sample. The references of the corresponding papers are indicated in the last column. Most of the data come from this series of papers (see Table I.1), but additional references were used for:

- HD 66068/9, 83270/1, 177390/1: for historical reasons, the orbits of those objects were published in our series of papers devoted to composite-spectrum stars, because those Am objects were misclassified;

Table III.1: Orbital elements obtained of our list of Am stars (begin.). T_0: periastron passage for elliptic orbits, ascending node passage for circular orbits. For triple spectroscopic systems, (l) and (s) in col. 1 indicate long and short period systems, respectively.

HD (BD)	P (days)	T_0 (JD) 2400000+	ω (°)	e	K_1 K_2 (km.s^{-1})	V_0 (km.s^{-1})	$a_1 \sin i$ $a_2 \sin i$ (Gm)	$M_1 \sin^3 i$ $M_2 \sin^3 i$ ($M_\odot$)	$f(m)$ ($M_\odot$)	$v_1 \sin i$ $v_2 \sin i$ (km.s^{-1})	R N
341	6.24268	48941.63	299.1	0.010	32.46	−3.19	2.79		0.0221	11.7	F
3970	39.5743	48945.06	148.6	0.521	18.17	0.52	8.44		0.015	29.1	F
7119 (s)	6.761504	48945.35	7.7	0.028	42.48	var	3.945	0.262	0.054	12.8	F
					46.81		4.350	0.237		7.8	S
" (l)	1867	50684.4	—	0.0	3.00	−10.94	69.61		0.0047	—	s
19342	42.6301	49323.630	—	0.0	26.80	6.16	15.71		0.0853	9.9	F
19910	15.41418	49325.46	67.2	0.059	45.77	11.64	9.68		0.1526	14.1	F
32893 (s)	2.175561	50747.305	—	0.0	49.84	var.	1.491		0.0280	10.0	T
" (l)	1136.7	51173.2	185.0	0.848	9.76	14.21	81.0		0.0164	—	s
35035	1025.21	49357.9	14.0	0.613	15.59	43.51	173.7		0.199	22.1	F
36360	216.54	49129.1	116.1	0.112	12.37	13.90	36.60		0.0417	20.0	F
41724/5	2.887679	46337.619	—	0.0	71.7	10.9	2.85		0.111	25.0	C
43478	5.464086	47000.176	—	0.0	86.48	−6.63	6.498	1.777	0.367	28.1	N
					95.03		7.14	1.617		20.6	V
51565/6 A	6.766301	47995.05	280.8	0.027	44.76	−11.20	4.163		0.06293	14.0	C
51565/6 B	4.48131	48160.45	11.0	0.0	16.54	−13.18	1.019		0.00212	—	c
55822	5.12294	48673.60	70.6	0.122	40.20	30.87	2.81		0.0338	21.0	F
60489	67.9606	50495.07	94.6	0.400	13.35	43.30	11.43		0.0129	24.0	T
61250	2.23024	48939.29	—	0.0	25.37	−5.43	0.78		0.00378	25.2	F
66068/9	7.747993	47600.690	341.1	0.418	56.07	−21.06	5.425	0.776	0.106	27.3	C
					75.06		7.265	0.580		9.1	
67317	4.43324	49321.05	—	0.0	33.23	6.37	2.03		0.0169	12.6	F
67911	12.50736	49998.763	—	0.0	40.01	−1.15	6.881	0.896	0.083	11.7	C
					63.90		10.992	0.561		3.9	C
73174 (s)	5.97012	49996.23	—	0.009	41.73	var	3.410		0.0444	7.3	F
" (l)	2878	45931	203.8	0.417	4.60	35.56	165.6		0.0221	—	s
73045	435.57	49722.0	28.8	0.320	11.89	35.20	68.01		0.0662	14.1	F
81976	5.655750	49785.941	341.4	0.061	61.68	19.85	4.788	0.5875	0.137	14.7	F
					63.84		4.956	0.5676		14.4	
83270 (s)	5.821433	45343.878	—	0.0	44.24	var	3.54		0.0523	—	C
" (l)	635.4	45464.5	135.4	0.149	9.37	10.84	80.9		0.0524	—	s
93946	3.55527	53091.29	220.5	0.014	48.02	3.36	2.347		0.0409	25.3	F
93991	3.20858	48675.01	—	0.0	16.46	−15.33	0.73		0.00149	26.2	F
96391	4.915427	45234.242	—	0.0	84.69	−1.67	5.724	1.408	0.310	23.5	N
					90.19		6.10	1.322		18.0	
98880	14.20783	48682.883	—	0.0	42.47	2.40	8.298	0.6091	0.113	10.6	F
					49.16		9.604	0.5262		9.2	
100054B (s)	12.79430	49781.19	137.0	0.028	18.69	var	3.29		0.0087	5.6	F
" (l)	874.2	49377.0	172.0	0.097	5.30	−13.52	63.4		0.013	—	s
102925	16.43718	49798.439	—	0.0	26.62	−0.89	6.02		0.0322	8.0	F
105680	70.0795	45991.19	192.6	0.380	30.75	−5.13	27.42		0.1676	13.9	C
109762	34.1863	50850.25	65.5	0.135	26.29	−13.11	12.24		0.0627	20.5	T
111057	3.848157	53091.716	—	0.0	15.83	−1.72	0.8374		0.00158	10.6	T
113697	539.9	46696.8	54.4	0.675	9.93	1.32	54.4		0.0220	23.8	T
125273	7.482664	48665.660	355.3	0.071	49.82	−17.42	5.113	0.412	0.095	11.0	F

Table III.1: Orbital elements obtained for our list of Am stars. T_0: periastron passage for elliptic orbits, ascending node passage for circular orbits (cont.).

HD (BD)	P (days)	T_0 (JD) 2400000+	ω (°)	e	K_1 K_2 (km.s^{-1})	V_0 (km.s^{-1})	$a_1 \sin i$ $a_2 \sin i$ (Gm)	$M_1 \sin^3 i$ $M_2 \sin^3 i$ (M$_\odot$)	$f(m)$ (M$_\odot$)	$v_1 \sin$ $v_2 \sin$
177390/1	8.00802	46335.165	—	0.0	27.8	−19.9	3.06	0.085	0.018	8.0
					30.3		3.34	0.078		9.0
187258	25.8048	49628.91	165.9	0.370	17.36	−34.76	5.72		0.011	11.4
195692	11.292249	48138.102	—	0.0	39.92	−25.49	6.20		0.0746	9.6
199360	1.9986874	49640.743	—	0.0	11.74	4.90	0.323		0.000336	13.5
204751	59.6993	52475.31	320.9	0.867	19.78	−24.44	8.08		0.0059	27.3
204918	5.04496	53262.446	—	0.0	18.21	−30.21	1.263		0.00316	11.4
208132	8.30344	50039.24	72.9	0.194	21.80	7.61	2.442		0.00843	14.0
219675	531.40	49833.	88.3	0.197	4.56	10.20	32.7		0.00494	21.3
224002	19.8059	49657.33	109.0	0.107	32.21	−19.48	8.72		0.068	38.8
224890	9.54640	48971.19	85.6	0.214	10.89	−8.02	1.40		0.00119	11.9
225137	4.33346	49326.559	—	0.0	56.42	0.94	3.36		0.0808	19.1
BD+44°4512	5.002094	50482.563	—	0.0	29.34	−5.51	2.018		0.01312	18.9

- HD 43478, 51565 A and B, 67911, 73045, 73174, 96391: their orbits were published in collaboration with colleagues of Cambridge or Geneva;
- HD 105680, 140122 A and B, 208132: their orbits were published by other authors before the end of our investigation.

Table III.2 contains the RV data we have collected about the remaining 38 stars. When the RVs can be considered as constant, the average value and its estimated error is given in col. 7. Otherwise the mention "var" indicates it is variable. For each object, we give the number N of observations in col. 5 and the range of epochs concerned in col 6. When N is small or RVs are variable, we give the individual measures separately (Table III.3). This is indicated with an asterisk in col. 5.

The analysis of this data have led to the following conclusions:

- 31 stars have not shown significant RV variations during our observing runs.
- 3 stars (HD 40602, 101393 and 151235) were found as having a variable RV but with an insufficient number of observations for deriving an orbit;
- 3 stars (HD 104957, 112431 and 154392) do not show significant RV variations but the small number of observations precludes us from deriving any conclusion;
- one star (HD 200407) is perhaps variable in RV, but here also more observations are needed for confirmation.

III.1.3 Rate of Am stars belonging to SB systems

Among our sample of 91 Am stars observed with CORAVEL, 58 objects have been identified as SBs: the 55 entries of Table III.1 and three other stars (HD 40602, 101393 and 151235)

Table III.2: Other stars of the whole Am sample. For the stars with an asterisk in Col. 5, individual RVs are displayed in Table III.3.

HD	HIP	V	$B-V$	N	Epoch	RV (km.s^{-1})	Notes
1714	1722	8.50	0.35	9	1993...2005	5.6±0.4	
1732	1748	7.75	0.33	10	1992...2005	5.3±0.6	
5128	4212	6.27	0.19	12	1992...2005	−2.4±0.6	ADS 735 A
13929	10690	7.45	0.25	12	1992...2006	−3.0±0.5	
15385	11578	6.19	0.16	10	1992...2005	22.0±0.7	
16763	12540	6.99	0.27	14	1992...2005	24.5±1.0	ADS 2050 AB
16932	—	8.2	—	11	1997...2005	5.9±0.5	
18460	14013	8.44	0.36	10	1994...2005	−11.3±0.3	
21437	16143	6.72	0.45	9	1993...2005	−9.1±0.3	ADS 2546 AB
29193	21465	7.35	0.32	10	1993...2005	4.3±0.4	ADS 3329 AB
40602	28432	7.90	0.37	11	1992...2004	var	Now studied by R. Griffin
56820	35735	6.36	0.28	15	1992...2005	5.0±1.1	ADS 5995 AB. Wide dip.
62257	37898	7.54	0.19	8	2004...2006	13.2±0.5	
76461	43976	6.99	0.27	9	1993...2005	33.9±1.0	Wide dip
90931	51457	6.86	0.32	11	1992...2005	0.5±0.7	
95190	53727	7.24	0.25	10	1997...2006	1.1±0.5	ADS 8003 AB
101393	56940	9.05	0.29	9*	2004...2006	var	
104957	58937	8.87	0.26	4*	2005...2007	−17.3±0.8?	
105601	59271	7.38	0.29	10	1992...2005	−59.8±0.9	High proper−motion star
105702	59309	5.72	0.35	10	1992...2005	−6.2±0.7	11 Vir
105967	59451	6.93	0.15	9	1997...2006	−1.8±0.5	
109764	61579	6.59	0.25	8	1995...2005	−1.4±0.2	
109782	61584	7.67	0.40	10	1992...2005	−4.1±0.5	ADS 8611 AB
110248	61851	7.65	0.30	10	1992...2005	−9.1±0.5	Variable star
112431	63135	8.93	0.21	4*	2005...2007	−5.0±0.4?	
124587/8	69523	6.80	0.34	10	1992...2005	−8.3±0.9	ADS 9174 AB. Wide dip
144999	79010	7.74	0.23	8	2003...2006	−25.2±0.4	ADS 9930 AB
151235	81929	8.97	0.28	4*	2005	var	Wide dip
154392	83445	8.65	0.25	4*	2005...2007	−52.1±1.3?	Wide dip
158116	85327	7.68	0.29	9	1993...2005	−24.5±0.5	ADS 10553 A
158251	85434	7.24	0.28	10	1993...2006	−15.2±0.7	ADS 10560 AB
188593	—	8.52	0.28	8	1994...2005	−25.9±0.5	
190145	98357	7.56	0.26	8	2003...2005	−16.4±0.7	
190401	98728	7.00	0.35	8	1994...2005	−29.3±1.0	
200407	103779	6.74	0.31	7*	2004...2005	var ?	ADS 14560 AB. Wide dip.
201033	104051	8.04	0.26	8	1994...2005	−25.2±0.3	
222770	117010	7.63	0.30	11	1992...2006	−11.8±0.4	
223247	117360	8.13	0.30	17	1992...2006	−3.8±1.0	Wide dip

Table III.3: Individual RVs for HD 101393, 104957, 112431, 151235, 154392 and 200407.

HD	Date (JD) 2400000+	RV (km.s^{-1})	σ_{RV} (km.s^{-1})
101393	53088.47	10.4	0.5
"	53089.44	10.8	0.9
"	53090.53	11.8	0.8
"	53091.43	10.7	0.5
"	53343.73	11.9	0.5
"	53446.47	8.6	0.4
"	53447.56	8.4	0.5
"	53704.72	4.6	0.8
"	53747.54	5.8	0.5
104957	53447.63	−16.4	0.4
"	53448.52	−17.1	0.4
"	53746.70	−18.2	0.7
"	54134.74	−17.5	0.5
112431	53446.53	−5.3	0.4
"	53447.57	−5.2	0.5
"	53448.60	−4.5	0.9
"	54134.73	−5.1	0.5
151235	53447.62	−36.5	0.7
"	53448.63	−33.0	0.8
"	53627.31	−0.7	0.9
"	53628.30	−4.9	1.0
154392	53446.61	−51.6	0.6
"	53447.69	−53.1	0.7
"	53626.31	−50.4	0.8
"	54209.58	−53.1	0.7
200407	53260.41	−5.0	0.8
"	53261.47	−6.0	0.5
"	53262.42	−6.3	0.4
"	53344.26	−4.3	0.5
"	53345.27	−3.7	0.4
"	53626.34	−3.7	0.5
"	53706.29	−3.0	0.5

recognized as having a variable RV (see Table III.2). This number of SBs corresponds to a rate of 64%, which is significantly larger than the rate of $47 \pm 3\%$ found by Jaschek & Gómez (1970) for a sample of 295 normal A-type stars. Note that they find that the rate of SBs is constant along the main sequence with a total value of $47 \pm 5\%$ for their whole sample of 746 normal main sequence stars.

We reach the same conclusion when comparing with the investigation of Duquennoy & Mayor (1991) who studied a sample of 164 nearby solar-type stars and concluded that "only about one third of the G-dwarf primaries may be real single stars". Since their estimation also included visual binaries, we should now consider, for comparison, the total number of binaries in our sample. When adding the 12 visual binaries that have not been detected as SBs of Table III.2 to the 58 SBs that we have found, it appears that 70 Am stars at least are binaries. We conclude that at least 77% of the Am stars of our sample belong to binary systems. This is again larger than the proportion of 2/3 found by Duquennoy & Mayor (1991).

As for the distribution between double-lined (SB2) and single-lined (SB1) among the 58 SBs in the sample, we count only 12 SB2s (21% of the SBs, or 13% of the sample). Note that this value should be considered as a minimum estimate since the detection as SB1 or SB2 strongly depends upon the used instrument. For example, HD 67911 and HD 126031 are quoted as SB2s (Table III.1) because of the contribution to our observations of the ELODIE spectrometer (Baranne et al. 1996) mounted on a 2-m telescope, which permitted the detection of the secondary.

In Table III.4 we give, for the SB2s of our sample, the values obtained for the mass ratio $\mu = M_2/M_1$ of the two components (col. 2) and the estimates i_0 of the inclinations of those systems (col. 3), derived when assuming that $M_1 = 2 \pm 0.4$ $M_\odot$. For the eclipsing binaries HD 43478 and HD 126031, we give instead the more accurate values found for the inclination i and the mass M_1 derived by fitting the light curves. In the third column, the values of i_0 show that a necessary condition for detecting SBs seems to be $i \gtrsim 10°$. When the inclination is smaller than $10°$, the orbital motion is undetected by spectroscopic observations.

There are 60 orbits reported in Table III.1, although the number of concerned Am stars is only of 53. This is explained by the presence of multiple systems in our sample: 5 triple spectroscopic systems (HD 7119, 32893, 73174, 83270/1 and 100054 B) and 2 quadruple systems that both include 2 SBs (HD 51565/6 and 140122). Note also that 5 other SBs belong to close visual pairs (with $\rho < 1$"): HD 61250, 151746, 155714, 195692 and 219675.

In Table III.2, we see that 31 Am stars seemed to have a constant RV, which represents 34% of our sample. We find a similar proportion in the other sample of 60 bright Am stars studied by Abt & Levy (1985). This rate should be considered as a maximum value of the fraction of the single stars present in those samples, because some SBs may have not been detected, either because they have a long period and a very eccentric orbit, or because their inclination is too small with $i \lesssim 10°$. The latter possibility has nevertheless a negligible influence on the observed rate since the probability to see a system near "pole-on" with $i < 10°$ is only 1.5 %.

Note that 12 stars among those 31 objects belong to visual binary systems (see Table III.2, col. 8).

Table III.4: SB2s of our program Am stars: mass ratio $\mu = M_2/M_1$ in col. 1 and inclination estimates i_0 in col. 2, assuming that $M_1 = 2 \pm 0.4$ M$_\odot$ (except for the eclipsing binaries (EB) HD 43478 and HD 126031).

HD	μ	i_0 (degrees)	Notes
7119	0.905	31^{+2}_{-2}	
43478	0.910	74^{+16}_{-9}	EB: i=79°, $M_1 = 1.88$ M$_\odot$
66068/9	0.747	47^{+5}_{-4}	
67911	0.626	50^{+6}_{-4}	
81976	0.966	42^{+4}_{-3}	
96391	0.939	63^{+10}_{-6}	
98880	0.864	42^{+4}_{-3}	
125273	0.961	36^{+4}_{-2}	
126031	0.747	68^{+22}_{-7}	EB: i=83°, $M_1 = 1.64$ M$_\odot$
140122A	0.60	14^{+1}_{-1}	
151604	0.984	72^{+18}_{-8}	EB: still in study
177390	0.92	20^{+2}_{-1}	

III.1.4 Statistics on a sample of 89 SB orbits of Am stars

In this section we examine some properties of the orbital elements of the SBs whose primary is an Am star. To improve the validity of those statistics, we have added to our sample some Am stars studied by Abt & Levy (1985). From their initial sample of 35 Am stars in SB systems (table 3 of their paper), we have selected 29 objects for which the quality of the orbit was good enough, and discarded the stars for which the orbital elements were qualified by the authors of "uncertain" or "marginal". In this way our sample of 60 orbits (Table III.1) could be extended to 89 SB orbits involving 82 Am stars. In what follows, this set will be called "extended SB sample".

III.1.5 Distribution of the orbital periods

The histogram of the periods P smaller than 100 d is plotted in Fig. III.1a with a step of 2 d and the histogram of $\log P$ of the extended SB sample in Fig. III.1b. Both distributions show a well-marked peak at $P \approx 5$ d. Note also that most of those binary stars have a small period: 2/3 of the sample systems have a period smaller than 20 d. This result is in agreement with those of past investigations (Abt 1961, Ginestet et al. 1982): the Am binaries are mostly encountered in tight SBs. This puts to light the key role played by tidal effects through the spin-orbit synchronism that reduces the axial rotation of the stars in such systems which in turn triggers the formation of Am-stars, according to the generally admitted theory (see Sect. I.2). Indeed, in his pioneering comparative study of normal and Am stars, Abt (1965) found two main differences concerning the equatorial velocities and orbital periods: normal

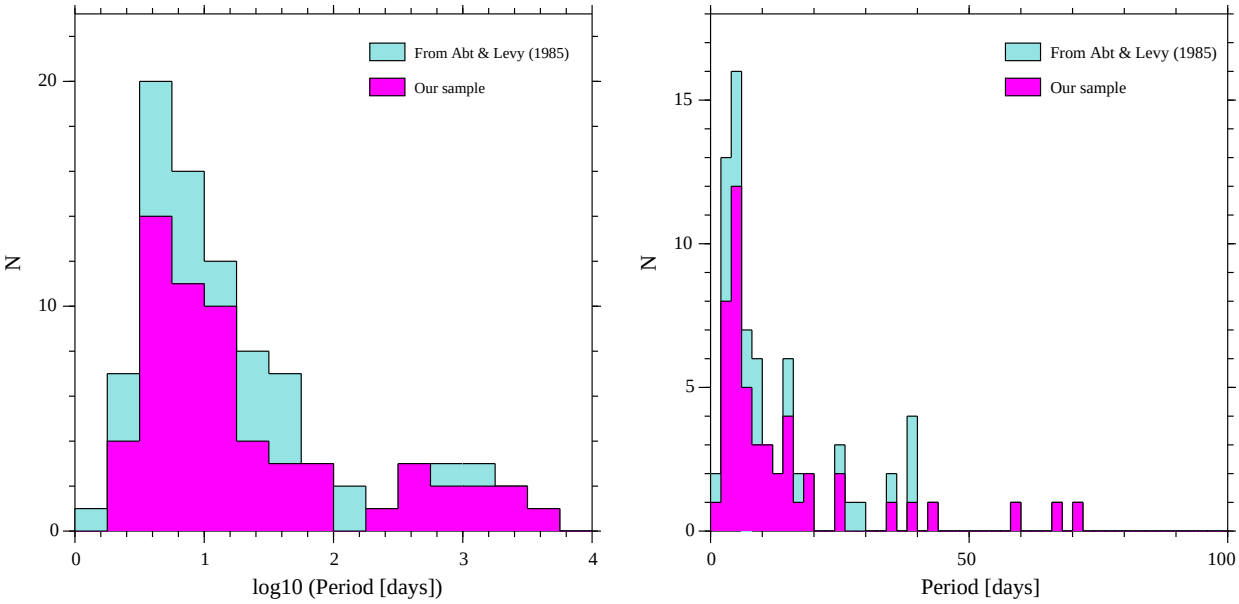

Figure III.1: Distribution of the orbital period P for the extended SB sample of Am stars. Histograms of $\log(P)$ (left) and of P (right) limited to $P < 100$ d.

A stars rotate more quickly, with $v \sin i$ in the range 50-250 km.s^{-1} and belong to long-period systems, with $P > 100$ d. This absence (or strong deficit) of A stars in systems with $P < 100$ d was confirmed by subsequent studies (Abt & Bidelman 1969, Ginestet et al. 1982), who showed that the domain with 2.5 d $< P <$ 100 d mutually excludes A and Am binaries.

Another feature of the Am stars clearly visible in our sample (see Table III.1, col. 2) is the lack of systems with very short periods (i.e., less than 1.3 d). This property is also the consequence of the same phenomenon. Indeed, assuming for instance $R = 2.5$ R$_\odot$ for the radius of the star and $i = 90°$, a period shorter then 1.3 d implies that $v \sin i > 100$ km.s^{-1} which corresponds to the generally admitted superior limit for producing an Am star (Abt & Levy 1985).

In the long-period side of the distribution, we note 12 orbits (13 % of the sample) with $\log P > 2.5$ (i.e. $P \gtrsim 300$ d). Five of those are the long-period orbits of triple spectroscopic systems, but the others are not tightly bound to another star. Hence it appears, as previously pointed out by Abt (1965) and Ginestet et al. (1982) that some Am stars (i.e. 7 in our sample) also belong to long-period SBs, like normal A-type stars.

III.1.6 $\log P/e$ diagram

The e vs $\log P$ diagram plotted in Fig. III.2 presents the general features of those of other star families, but it differs by the value of the critical period, $P_c = 5.6 \pm 0.5$ d, that separates the domains of eccentric and circular orbits. For comparison, other studies have found shorter values, with $P_c \approx 3.2$ d for Ap binaries (North et al. 1998b) and only $P_c \approx 0.6$ d for normal A stars (Gerbaldi, Floquet & Hauck 1985), whereas a longer value of about 11 d was found by Duquenoy & Mayor (1991) for nearby G dwarfs.

The value of P_c is linked to the time necessary for the tidal effects to circularize the orbits:

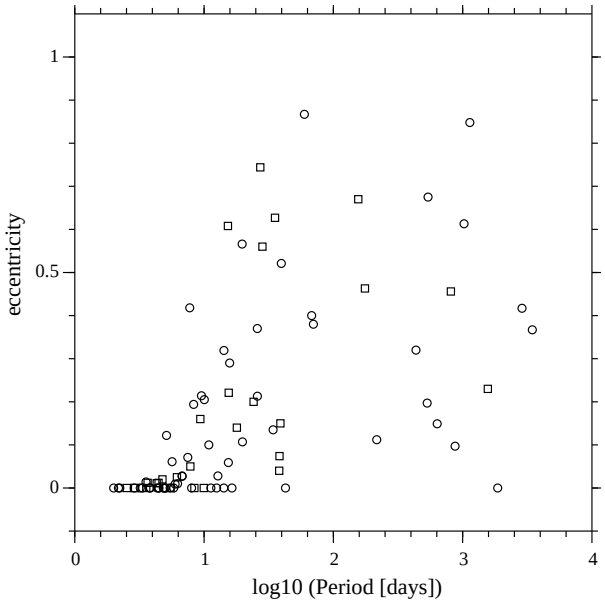

Figure III.2: Diagram e vs $\log P$ for all the SBs of our sample of Am stars (circles) and the selection from Abt & Levy (1985) (squares).

as time goes by, more and more systems are circularized. As a consequence P_c increases with time. For a given sample of stars P_c is an indicator of the age of this sample. From the calibration table of Duquenoy & Mayor (1991) derived from observations of stellar clusters, the typical age of the Am stars of our programme is found to be about 0.5–1 $\times 10^9$ yr. This is in agreement with the values obtained with the theoretical isochrones in the HR diagram (see Sect. II.7.7 and the papers of this series).

III.1.7 Distribution of $f(m)$ and incidence on the mass distribution of the companions

In Sect. I.4.4, we have seen that our observations of *SB1* lead to the determination of the mass function defined as (Eq. I.3):

$$f(m) = M_1 \sin^3 i \, \mu^3/(1+\mu)^2$$

Although the values of M_1 and i are unknown for each system, we have some knowledge about their statistical distribution ($M_1 \approx 2 \pm 0.4$ M$_\odot$ and uniform orientation of the orbits). From the distribution of the 89 values of $f(m)$ obtained for the extended SB sample, it is thus possible to derive some constraints on the mass distribution of the companions.

We have studied this problem with a Monte-Carlo-type method, by writing and using specially-designed programmes. We first implemented a procedure to generate simulated samples of $f(m)$ compatible with the two theoretical mass distributions we wanted to test: a power-law distribution for which the number $N(m)$ of stars of mass m is proportional to $m^{-\alpha}$ and a Gaussian law $N(m) \propto \exp[-(m-m_0)^2/2\sigma_m^2]$ so that we could estimate the average mass m_0 of the companions from our study.

This procedure was based on the following steps:

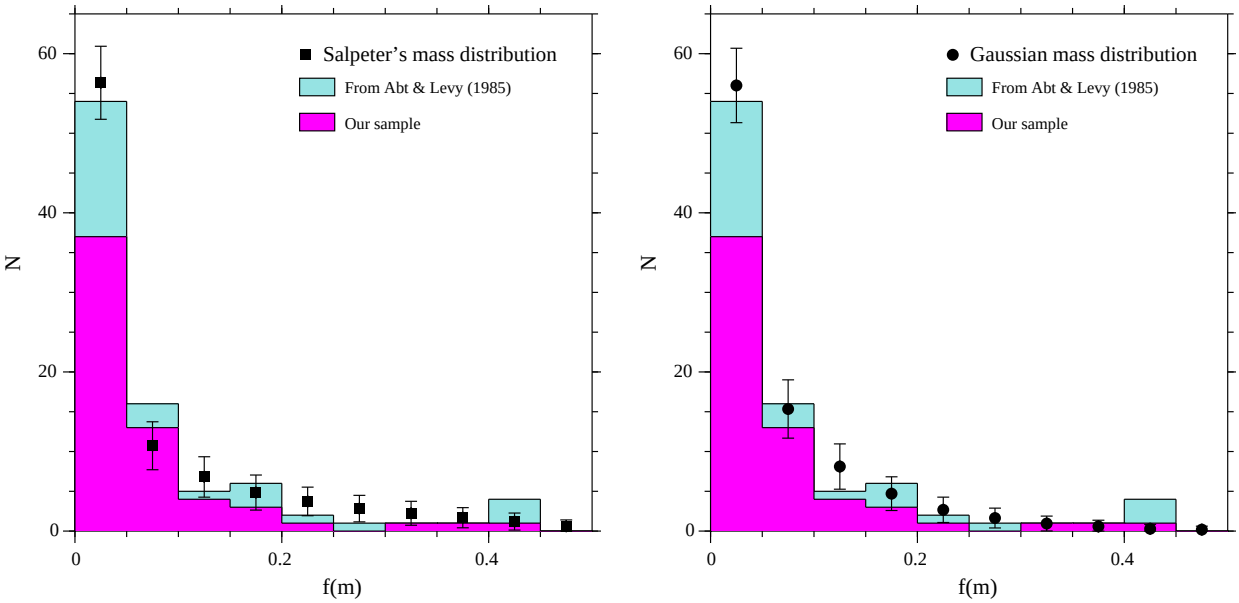

Figure III.3: Histogram of f(m) for 89 Am SBs and comparison with two models assuming that the distribution of the masses of the companions is a power-law in $m^{-\alpha}$ with $\alpha = 0.3$ (left) or a Gaussian centered on 0.8 ± 0.5 $M_\odot$ (right).

- Generation of random samples of companions with masses following power-law or Gaussian distributions, and truncated to 2 $M_\odot$ (since the companions are assumed to be less massive than the Am primary stars).

- Generation of a random inclination for each companion, corresponding to a uniform orientation of the axes of the orbits in three dimensions.

- Computation of the corresponding $f(m)$ for each companion, using Eq. (I.3) and assuming $M_1 = 2$ $M_\odot$.

We were thus able to generate simulated samples whose distribution functions of $f(m)$ could be compared with the observed distribution of our extended SB sample of Am spectroscopic binaries. We then determined the best parameters for the power-law and Gaussian distributions by minimizing the corresponding residuals. We obtained $\alpha = 0.3 \pm 0.2$ for the power-law and $m_0 = 0.8$ $M_\odot$ with $\sigma_m = 0.5$ $M_\odot$ for the Gaussian distribution. The corresponding fits are displayed in Fig. III.3. They are both in good agreement with the observed distribution within the error bars that we computed from a series of simulated samples with the same number of orbits than that of the extended SB sample (i.e., 89). Note that the small bump at $f(m) \approx 0.42$ $M_\odot$ can be explained by a selection effect favouring the study of eclipsing binaries (in Abt & Levy's sample).

We finally performed statistical tests to check the consistency of the two models with the observed sample of $f(m)$. This was done both with a χ^2-test which compares the distributions of $f(m)$ and with a Kolmogorov-Smirnov test which operates on the cumulative functions. The two tests led to the same conclusion: the sample is not significant at the 5% level for the two models. Hence both the power-law and the Gaussian distributions are compatible with the observed $f(m)$ distribution.

We also tested the influence of the truncation at around $i \approx 10°$, due to the lower detection threshold for the SBs (see Table III.4), and found that this effect was negligible for the distribution of $f(m)$.

The typical mass of $M_2 = 0.8 \pm 0.5$ M$_\odot$ found for the companions favours a spectral type of G-K-M V. This is in agreement with the small number of SB2 found in our sample (21% of the SBs in Sect. III.1.3) and indicates that the contribution of the secondaries can be generally considered as negligible for the global photometric indices (e.g. $B - V$ and Strömgren indices). Those indices can thus, in most cases (like in Sect. II.7.6), be affected to the primary components only, with a good approximation.

Since we have assumed that $M_1 = 2 \pm 0.4$ M$_\odot$, the typical mass found for $M_2 = 0.8 \pm 0.5$ M$_\odot$ corresponds to a mass ratio $\mu = 0.40 \pm 0.33$. This value is consistent with the value $\mu = 0.23 \pm 0.42$ found by Duquenoy & Mayor (1991) for their sample of main sequence solar-type stars. This would support the conclusions of those authors that most binaries are "formed by random association of stars from the same initial mass function". Am binaries seem to follow this rule, too.

III.1.8 Discussion on the mass distribution found for the companions

In his pioneering work, Salpeter (1954) found that the initial mass function (or IMF) of the stars between 0.4 and 10 M$_\odot$ could be approximated with a power-law $N \propto m^{-\alpha}$ with $\alpha = 2.35$. Subsequent observational studies have then shown that this law seemed rather universal, but with some possible variations of the value of this coefficient α according to the mass range. In a recent review, Kroupa (2001) finds that the available observational constraints are compatible with multi-part power-law IMF for single stars with values of α equal to 1.3±0.5, 2.3±0.3 and 2.3±0.7 for mass values such that $m \in [0.08, 0.5]$, $m \in [0.5, 1.0]$ and $m > 1.0\ M_\odot$, respectively.

To derive the IMF from an observed mass function (MF), one should take into account the number of stars that have evolved off the main sequence. In our case, all the Am stars that we have studied in our series of papers are located in the main sequence. Their companions that are less massive have thus not left the main sequence: their observed MF can be thus assimilated to their IMF.

From a statistical study of a sample of 60 Am stars Abt & Levy (1985) obtained a negative exponent for the power-law accounting for the mass distribution of the companions, with $N \propto m^{0.60}$. Statistical tests show that this value of $\alpha = -0.60$ is incompatible with our data at 0.01% level.

The value of $\alpha = 0.3 \pm 0.2$ that we have derived from the $f(m)$ distribution of our sample in Sect. III.1.7 is in better agreement with the values found by Kroupa (2001) for single stars with similar masses, but still at about 2σ from his values. In the scenario of co-eval formation of the two components of the binary system, this would indicate that the stars formed close to Am stars are globally more massive than isolated stars, possibly because of the proximity of the Am star (?). Indeed higher temperatures of the star-forming clouds seems to favour higher masses (Larson 1998). In the capture formation scenario, which assumes that binary stars formed in star clusters, this small excess of large masses in the MF could be explained with the dynamical history of those systems. The most massive stars have spent more time in the cluster than less-massive stars that were lost earlier due to energy equipartition within the cluster (mass segregation). As a consequence, Am-type stars would have preferentially

accreted more massive companions.

III.2 Conclusion

Paper VIII concluded the series of papers devoted to the radial velocity study of a sample of 91 Am stars. Our work has responded to our initial objectives that were presented in Sect. I.1. The statistics about the circularisation of the orbits and spin-orbit synchronism of Am systems have already been largely discussed in Papers VI and VII. Let us now summarize the main results obtained in the second part of Paper VIII:

In our sample of 91 Am stars, which were initially not known as binaries, 58 were found to be new SBs. The rate of SBs among Am stars in our sample is therefore at least 64 %, which is significantly greater than that of normal stars. It is likely that some genuine binaries with a very small inclination ($i < 10°$, see III.1.3) have not been detected by spectroscopic observations. Nevertheless it seems that a significant fraction of Am stars (around 30%) do not belong to SBs: they are either isolated stars or members of wide binary systems (Sect. III.1.3). This is in agreement with the previous conclusions of the statistical study of Am stars of Abt & Levy (1985). They suggested that another mechanism than tidal effects in a tight binary system had to be envisaged as an alternative (e.g. evolutionary expansion of a single star) for reducing the rotational velocity of an A-type star, which seems a necessary (and maybe also sufficient) condition to convert it into an Am star (Michaud al., 1983; Abt, 2000; Talon et al., 2006).

The statistical study of the orbital elements of the SBs containing an Am star has led to the following results (Carquillat & Prieur, 2007c):

- The distribution of the periods with $P < 100$ d (Sect. III.1.5) is compatible with the theoretical models that explain the origin of Am stars as a consequence of the slowing down of the axial rotation of A-type stars produced by the rotation-revolution synchronism due to tidal effects. But the presence of long-period systems with $P > 100$ d shows that some Am stars were not produced by this mechanism.

- The cutoff separating the circular and the eccentric systems in the e vs $\log P$ diagram is $P_c \approx 5.6 \pm 0.5$ d. Let us recall that this value is linked to the time necessary for the tidal effects to circularize the orbits: as time goes by, more and more systems are circularized. As a consequence P_c increases with time. For a given sample of stars P_c is an indicator of the age of this sample. From the calibration table of Duquennoy & Mayor (1991) derived from observations of stellar clusters, the typical age of the Am stars of our programme is found to be about 0.5–1 $\times 10^9$ yr. This is in agreement with the values obtained with the theoretical isochrones in the HR diagram (see Sect. II.7.7 and the papers of this series).

- Our Monte-Carlo analysis shows that the distribution of $f(m)$, the mass function values, is compatible with a power-law distribution $N(m) \propto m^{-\alpha}$ for the masses m of the companions with $\alpha = 0.3 \pm 0.2$ (which is smaller that what is generally found for single stars), or with a Gaussian distribution with an average mass of 0.8 ± 0.5 $M_\odot$ which indicates that the companions of *SB1*'s are typically dwarf stars of type G-K-M.

In Paper VIII, we finally presented the list of radial velocity measurements of the remaining objects from the original sample (38 stars in Table III.2), for which the small number of observations prevented us either from computing an orbit or, in other cases, from concluding to the probable constancy of the radial velocity. We hope that this list will be used by other

colleagues for future investigations. We can also provide the source code of the programs quoted in this series of papers (see Sect. A).

Bibliography

The frequency of binaries among metallic-line stars
Abt H.A., 1961, ApJS, 6, 37

The frequency of binaries among normal A-type stars
Abt H.A., 1965, ApJS, 11, 429

Improved study of metallic-line binaries
Abt H.A., Levy S.G., 1985, ApJS, 59, 229

Does rotation alone determine whether an A-type star's spectrum is abnormal or normal?
Abt H.A., 2000, ApJ, 544, 933

CORAVEL - A new tool for radial velocity measurements
Baranne, A., Mayor, M., Poncet, J.L. 1979, Vistas in Astronomy, Vol 23, p. 279-316

Remarques préliminaires sur quelques propriétés de la discontinuité de Balmer dans les spectres stellaires
Barbier, D., Chalonge, D., 1939, Ann. d'Astroph. 2, 254

A new method for determining the rotation of late spectral type stars
Benz W., Mayor M., 1981, A&A 93, 235

Orbital elements of six spectroscopic binary stars,
Bopp B.W., Evans D.S., Laing J.D., Deeming T.J., 1970, MNRAS, 147, 355

Spectroscopy of HR 4665 - A bright long-period RS CVn system
Bopp, B.W., Fekel, Jr., F., Griffin, R.F., et al, 1979, AJ, 84, 1763

Les étoiles binaires spectroscopiques. Inventaire des données de l'observation
Carquillat, J.-M., Ginestet, N., Pédoussaut, A., 1971, Sciences, Tome II, No 4, 251 (Association Française pour l'Avancement des Sciences)

Contribution à l'étude des spectres composites. III. Les binaires spectrales, classe intermédiaire entre les binaires visuelles et les binaires spectroscopiques ?
Carquillat, J.-M., Nadal, R., Ginestet, N., Pédoussaut, A., 1982, A&A, 115, 23 (CS-PaperIII)

Contribution à l'étude des étoiles à spectre composite et des binaires spectroscopiques
Carquillat, J.-M., 1983 Thèse de doctorat d'état, Université Paul Sabatier

Contribution à l'étude des binaires des types F, G, K, M. II. Eléments orbitaux des binaires spectroscopiques à raies simples HD 69148 et HD 85091.
Carquillat, J.-M., Nadal, R., Ginestet, N., Pédoussaut, A., 1983, A&AS 54, 187 (FGKM-PaperII)

Contribution à l'étude des spectres composites. IV - Eléments orbitaux des binaires spectroscopiques de type Am HD 41724-5 et HD 177390-1
Carquillat, J.-M., Ginestet, N., Pédoussaut, A., 1988, A&AS 75, 305 (CS-PaperIV)

Contribution à l'étude des spectres composites. VI. HD 66068-9
Carquillat, J.-M., Ginestet, N., Duquennoy, A., Pédoussaut, A., 1994 A&AS 106, 597 (CS-PaperVI)

Contribution à l'étude des spectres composites. VII. HD 16646
Carquillat, J.-M., Griffin, R.F., Ginestet, N., 1995 A&AS 109, 173 (CS-PaperVII)

Contribution à l'étude des binaires des types F, G, K, M. VII. HD 147395, une géante M binaire spectroscopique.
Carquillat, J.-M., Ginestet, N.: 1996, A&AS 117, 445 (FGKM-PaperVII)

Contribution à l'étude des binaires des types F, G, K, M. VIII. HD 195850 et HD 201193, binaires spectroscopiques à raies doubles.
Carquillat, J.-M., Ginestet, N.: 2000, A&AS 144, 317 (FGKM-PaperVIII)

"Contribution to the search for binaries among Am stars. II. HD 81876 and HD 98880, double-lined spectroscopic binaries."
Carquillat J.-M., Ginestet N., Prieur J.-L., 2001, Astron. & Astrophys., 369, 908–914

"Contribution to the search for binaries among Am stars. III. HD 7119, a double-lined spectroscopic binary and a triple system"
Carquillat J.-M., Ginestet N., Prieur J.-L., Udry S., 2002, MNRAS, 336, 1043–1048

Contribution to the study of composite spectra. IX. Spectroscopic orbital elements of ten systems.
Carquillat J.-M., Prieur J.-L., Ginestet N., 2003a, MNRAS, 342, 1271–1279

"Contribution to the search for binaries among Am stars. V. Orbital elements of eight short-period spectroscopic binaries"
Carquillat J.-M., Ginestet N., Prieur J.-L., Debernardi Y., 2003b, MNRAS, 346, 555–564.

"Contribution to the search for binaries among Am stars. VI. Orbital elements of ten new spectroscopic binaries, implications on tidal effects"
Carquillat J.-M., Prieur J.-L., Ginestet N., Oblak E., Kurpinska-Winiarska M., 2004, MNRAS, 352, 708–720.

Contribution to the study of F-G-K-M binaries. X. HD 54901, HD 120544 and HD 123280, three nearby F-type spectroscopic binaries.
Carquillat J.-M., Prieur J.-L., Udry S., 2005a, Astron. Nach., 326, 1, 31–37

Contribution to the study of composite spectra. X. HD 3210/1, 27395, 39847, 70826, and HD 218257/8, five new spectroscopic binaries in multiple systems.
Carquillat J.-M., Prieur J.-L., Ginestet N., 2005b, MNRAS, 360, 718–726

Spurious spectroscopic binaries in the GCRV
Carquillat, J.-M.: 2007, CDS Contributions 2

Contribution to the study of composite spectra. XI. Orbital elements of some faint systems,
Carquillat J.-M., Prieur J.-L., 2007a, Astron. Nachr., 328, 1, 46–54

Contribution to the study of composite spectra. XII. Spectroscopic orbits of eight southern stars,
Carquillat J.-M., Prieur J.-L., 2007b, Astron. Nachr., 328, 6, 527–535

"Contribution to the search for binaries among Am stars. VIII. New spectroscopic orbits of 8 systems and statistical study of a sample of 91 Am stars"
Carquillat J.-M., Prieur J.-L., 2007, MNRAS, 380, 1064–1078

Contribution to the study of F-G-K-M binaries. XII. Orbital elements of seven new spectroscopic binaries,
Carquillat J.-M., Prieur J.-L., 2008, Astron. Nach., 329, 1, 45–54

Circularization and synchronization times in Main-Sequence of detached eclipsing binaries II. Using the formalisms by Zahn
Claret A., Cunha N.C.S., 1997, A&A, 318, 187

Observation des étoiles doubles visuelles,
Couteau P., 1978, Flamarion.

Photo-electric $H\beta$ and $uvby$ photometry
Crawford D.L., 1966, *Spectral classification and multicolour photometry* Proc. IAU Symp. no 24, Ed. K. Loden, Academic Press, London, p. 170

Empirical calibrations of the ubvy,beta systems. I. The F-type stars.
Crawford D.L., 1975, AJ, 80, 955

Empirical calibrations of the uvby,beta systems. III. The A-Type Stars
Crawford D.L., 1979, AJ, 84, 1858

Erratum - Empirical calibrations of the uvby,beta systems. III. The A-Type Stars
Crawford D.L., 1980, AJ, 85, 621

Multiplicity among solar-type stars in the solar neighbourhood. II. Distribution of the orbital elements in an unbiased sample
Duquennoy, A., Mayor, M., 1991, A&A, 248, 485

On the surface gravitives of Am stars
Dworetsky, M.M., Moon T.T., 1986, MNRAS, 220, 787

Hipparcos and Tycho Catalogues
ESA 1997, ESA SP-1200.

Transformations from theoretical Hertzsprung-Russell diagrams to Color-Magnitude diagrams: effective temperatures, B-V colors, and bolometric corrections
Flower P.J., 1996, ApJ, 469, 355

Contribution à l'étude des spectres composites. I. Révision de l'échantillon des étoiles brillantes des listes de Hynek.
Ginestet, N., Pédoussaut, A., Carquillat, J.-M., Nadal, R., 1980, A&A, 81, 333 (CS-PaperI)

Contribution à l'étude des spectres composites. II. Binaires spectroscopiques A, Am et Ap.
Ginestet, N., Jaschek, M., Carquillat, J.-M., Pédoussaut A., 1982, A&A 107, 215 (CS-PaperII)

Contribution à l'étude des binaires des types F, G, K, M. III. Eléments orbitaux des binaires spectroscopiques à longue période HD 102928 et HD 145206.
Ginestet, N., Carquillat, J.-M., Pédoussaut, A., Nadal, R., 1985, A&A 144, 403 (FGKM-PaperIII)

Contribution à l'étude des spectres composites. V- HD 83270-1, étoile Am et système triple spectroscopique.
Ginestet, N., Carquillat, J.-M., Pédoussaut A., 1991, A&AS, 91, 265 (CS-PaperV)

Atlas de spectres stellaires
Ginestet, N., Carquillat, J.-M., Jaschek, M., Jaschek, C., Pédoussaut, A., Rochette, J., 1992, Centre Régional de Documentation Pédagogique de Toulouse

Spectral classifications in the near infrared of stars with composite spectra. I. The study of MK standards.
Ginestet, N., Carquillat, J.-M., Jaschek, M., Jaschek, C., 1994, A&AS 108, 359

Contribution à l'étude des binaires des types F, G, K, M. VI. HD 79968, binaire spectroscopique à raies doubles.
Ginestet, N., Carquillat, J.-M.: 1995, A&AS 111, 255 (FGKM-PaperVI)

Spectral classifications in the near infrared of stars with composite spectra. II. Study of a sample of 180 stars
Ginestet, N., Carquillat, J.-M., Jaschek, C., Jaschek, M., 1997, A&AS 123, 135

"Contribution à l'étude de la binarité des étoiles de type Am: I. HD 125273, binaire spectroscopique à raies doubles"
Ginestet N., Carquillat J.-M., 1998, A&AS 130, 415

Spectral classifications in the near infrared of stars with composite spectra. III. Study of a sample of 137 objects with the Aurelie spectrograph
Ginestet, N., Carquillat, J.-M., Jaschek, C., 1999a, A&AS, 134, 473

Contribution à l'étude des spectres composites. VIII. HD 174016-7, une étoile Ap associée à une géante G.
Ginestet, N., Griffin, R.F., Carquillat, J.-M., Udry, S., 1999b, A&AS 140, 279 (CS-PaperVIII)

Spectral classification of the hot components of a large sample of stars with composite spectra, and implication for the absolute magnitudes of the cool supergiant components.
Ginestet N., Carquillat J.-M., 2002, ApJS, 143, 513

"Contribution to the search for binaries among Am stars. IV. HD 100054 B and HD 187258"
Ginestet N., Prieur J.-L., Carquillat J.-M., Griffin R.F., 2003, MNRAS, 342, 61–68.

Orbital circularization in early-type detached close binaries
Giuricin G., Mardirossian F., Mezetti M., 1984a, A&A, 134, 365

Synchronization in early-type spectroscopic binary stars
Giuricin G., Mardirossian F., Mezetti M., 1984b, A&A, 135, 393

Composite spectra. XII. o Leonis: an evolving Am binary
Griffin R.E., 2002, AJ, 123, 988

Contribution à l'étude des binaires des types F, G, K, M. IX. HD 191588, nouvelle binaire spectroscopique à raies simples de type RS Cvn, système triple.
Griffin, R.F., Ginestet,N., Carquillat, J.-M., 2003, RoAJ 13, 31

Fourth Catalog of Interferometric Measurements of Binary Stars
Hartkopf W.L., Mason B.D., Wycoff G.L., McAlister H.A., 2014
http://ad.usno.navy.mil/wds/int4.html

Third catalogue of AM stars with known spectral types
Hauck B., 1986, A&AS, 64, 21

Uvbybeta photoelectric photometric catalogue
Hauck B., Mermilliod J.-C., 1998, A&AS, 129, 431

Stability of tidal equilibrium
Hut P., 1980, A&A, 92, 167

Tidal evolution in close binary systems
Hut P., 1981, A&A, 99, 126

A survey of stars with composite spectra.
Hynek J.A., 1938, Contr. Perkins Obs. n° 10

Contribution à l'étude des étoiles doubles spectroscopiques
Imbert, M.: 1975, Thèse de doctorat d'état, Observatoire de Marseille, Université de Provence.

Revision and calibration of MK luminosity classes for cool giants by HIPPARCOS parallaxes
Keenan, P.C., Barnbaum, C., 1999, ApJ 518, 859

Statistical study of Am stars in spectroscopic binary systems
Kitamura, M., Kondo M., 1978, Ap&SS, 56, 341

The distribution of color excesses and interstellar reddening material in the solar neighborhood
Lucke, P.B., 1978, A&A 64, 367

Duplicity in the solar neighborhood. I - A new spectroscopic orbit for BY Draconis
Lucke, P.B., Mayor, M., 1980, A&A 92, 182

Spectroscopic binaries with circular orbits
Lucy, L.B., Sweeney, M.A., 1971, AJ, 76, 544

Eccentric Orbits in Samples of Circularized Binary Systems: The Fingerprint of a Third Star
Mazeh, T., 1990, AJ, 99, 675

New dating of galactic open clusters
Meynet, G., Mermilliod, J.-C., Maeder, A., 1993, A&AS, 98, 477

The astrophysical context of diffusion in stars
Michaud G., 1980, AJ, 85, 689

Diffusion, meridional circulation, and mass loss in Fm-Am stars
Michaud G., Tarasick D., Charland Y., Pelletier C., 1983, ApJ, 269, 239

Atomic diffusion and o Leonis
Michaud G., Richer J., Richard O., 2005, ApJ, 623, 442

Grids for the determination of effective temperature and surface gravity of B, A and F stars using uvby-beta photometry
Moon, T.T., Dworetsky, M.M., 1985, MNRAS, 217, 305

64 Piscium, a double line spectroscopic binary - Discussion on orbital elements
Nadal, R., Ginestet, N., Carquillat, J.-M., Pédoussaut, A., 1979, A&AS, 35, 203

Absolute magnitudes of chemically peculiar stars
North P., Jaschek C., Hauck B., Figueras F., Torra J., Künzli M., 1997, in Battrick B., ed., Proc. ESA Symp. Hipparcos–Venice'97, ESA SP–402, p. 239

Contribution à l'étude des binaires des types F, G, K, M. I. Eléments orbitaux des binaires spectroscopiques à raies doubles HD 47415 et HD 210763
Nadal, R., Carquillat, J.-M., Pédoussaut, A., Ginestet, N., 1983, A&AS, 52, 293 (FGKM-PaperI)

Binaires spectroscopiques - 12ème catalogue complémentaire.
Pédoussaut, A., Carquillat, J.-M.: 1973, A&A Suppl. 10, 105

Contribution à l'étude des binaires des types F, G, K, M. IV. Eléments orbitaux de la binaire spectroscopique HD 23838.
Pédoussaut, A., Carquillat, J.-M., Ginestet, N.: 1987, A&A 175, 136 (FGKM-PaperIV)

Contribution à l'étude des binaires des types F, G, K, M. V. Eléments orbitaux de la binaire spectroscopique HD 189578.
Pédoussaut, A., Carquillat, J.-M., Ginestet, N.: 1989, A&AS 78, 441 (FGKM-PaperV)

A Stellar Spectral Flux Library, 1150 – 25000 Å
Pickles A.J., 1998, PASP 110, 863

Speckle measurements of composite spectrum stars: observations with PISCO in 1993-1998,
Prieur J.-L., Koechlin L., Ginestet N., Carquillat J.-M., Aristidi E., Scardia M., Arnold L., Avila R., Festou M.C., Morel S., Pérez J.-P., 2002b, ApJ Suppl., 142, 95–104

Speckle observations of composite spectrum stars: II. Differential photometry of the binary components,
Prieur J.-L., Carquillat J.-M., Ginestet N., Koechlin L., Lannes A., Anterrieu E., Roques S., Aristidi E., and Scardia M. 2003, ApJ Suppl., 144, 263–276

Contribution to the study of F-G-K-M binaries. XI. Orbital elements of three red-giant spectroscopic binaries: HR 1304, HR 1908 and HD 126947,
Prieur J.-L., Carquillat J.-M., Griffin R.F., 2006a, Astron. Nach., 327, 7, 686–692

"Contribution to the search for binaries among Am stars. VII. Spectroscopical orbital elements of seven new spectroscopic binaries, implications on tidal effects"
Prieur J.-L., Carquillat J.-M., Imbert M., 2006b, MNRAS, 372, 703–714

The Evolution of Am Fm Stars, abundance anomalies, and turbulent transport
Richer J., Michaud G., Turcotte S., 2000, ApJ, 529, 338

Ekman circulation and the synchronization of binary stars
Rieutord, M., 1992, A&A 259, 581

Ekman pumping and tidal dissipation in close binaries: a refutation of Tassoul's mechanism
Rieutord, M., Zahn, J.-P., 1997, ApJ 474, 760

Numerical Data and Functional Relationships in Science and Technology,
Schmidt-Kaler Th., 1982, in K. Schaifers, H.H. Voigt (eds.): Landolt-Börnstein, New Series, Group VI, Vol.2-B, (Springer-Verlag Berlin), p. 1

New grids of stellar models from 0.8 to 120 solar masses at Z = 0.020 and Z = 0.001
Schaller G., Schaerer D., Meynet G., Maeder A., 1992, A&AS, 96, 269

An analysis of variance test for normality (complete samples)
Shapiro, S.S., Wilk, M.B., 1965, Biometrika, vol. 52, No 3-4, p. 591

Fundamental stellar parameters derived from the evolutionary tracks
Starizys, V., Kuriliene, G., 1981, Astroph. & Space Science, 80, 353

Two-dimensional spectral classification of F stars through photoelectric photometry with interference filters
Strömgren, B., Vistas in Astron., 2, 1336

Am Fm stars as a test of rotational mixing models
Talon S., Richard O., Michaud G., 2006, ApJ, 645, 634

Tassi, P., 1989, *Méthodes statistiques*, Economica.

On synchronization in early-type binaries
Tassoul J.-L., 1987, ApJ, 322, 856

A comparative study of synchronization and circularization in close binaries
Tassoul J.-L., Tassoul M., 1992, ApJ, 395, 259

An introduction to Statistical Communication Theory,
Thomas J., 1969, John Wiley & Sons, New York

General Catalog of Stellar Radial Velocities
Wilson, R.E., 1953, Carnegie Institution, Washington, Publ. 601

Les marées dans une étoile double serrée
Zahn, J.-P., 1966, Ann. Astroph., 29, 313

The dynamical tide in close binaries
Zahn, J.-P., 1975, A&A, 41, 329

Tidal friction in close binary stars
Zahn, J.-P., 1977, A&A, 57, 383

Tidal evolution of close binary stars. I - Revisiting the theory of the equilibrium tide
Zahn, J.-P., 1989, A&A 220, 112

Tidal evolution of close binary stars. II - Orbital circularization of late-type binaries
Zahn, J.-P., Bouchet L., 1989, A&A 223, 112

Etude d'étoiles doubles visuelles et spectroscopiques
Prieur, J.-L., 2014, Annexe B de ma thèse d'HDR (Habilitation à Diriger les Recherches)
http://userpages.irap.omp.eu/~jprieur/docb.pdf.

Appendix A

Programs written for the study of Am stars

A.1 [Fe/H] and M_V from Strömgren photometry

Two programs are dedicated to Strömgren photometry in the case of A or F stars: `indices_Astars.for` and `indices_Fstars.for`. They process photometric measurements and compute reddening correction and various parameters (δm_1, δc_1) in order to estimate the metallicity ([Fe/H]) and the absolute magnitude M_V. The program for F-type stars was written by E. Oblak, and kindly sent to me in January 2004 by this author. I used this program to create a new version dedicated to A-type stars: `indices_Astars.for`, that was used to prepare Carquillat et al. (2004).

The input files containing the Strömgren photometry measurements have the same format for both programs. They are ASCII files, whose lines contain the HD number follwed by the $b-y$, m_1, c_1 and β measurements. Here is an example of the file `photom_AM-VI.dat` that was used for Carquillat et al. (2004):

```
# HD    b-y    m1     c1     beta
19342  0.310  0.198  0.772  2.733
19910  0.190  0.200  0.730  2.810
36360  0.162  0.235  0.812  2.802
126031 0.202  0.230  0.663  2.740
127263 0.135  0.282  0.800  2.826
155714 0.230  0.189  0.675  2.72
195692 0.164  0.207  0.760  2.78
199360 0.183  0.252  0.739  2.81
```

The underlying theory and the method I used in `indices_Astars.for` are presented in Sect. I.5.

The output file `table_AmVI.txt` corresponding to this example is given below. It is commented and presented the corresponding LaTeX version in Table I.4.

```
  HD     beta    b-y    E(b-y) m1    (m1)0   c1    (c1)0
 19342  2.733   0.310   0.10  0.198   0.23  0.772   0.75
```

```
 19910 2.810  0.190  0.04 0.200  0.21 0.730  0.72
 36360 2.802  0.162  0.01 0.235  0.24 0.812  0.81
126031 2.740  0.202 -0.01 0.230  0.23 0.663  0.67
127263 2.826  0.135 -0.01 0.282  0.28 0.800  0.80
155714 2.720  0.230  0.01 0.189  0.19 0.675  0.67
195692 2.780  0.164  0.00 0.207  0.21 0.760  0.76
199360 2.800  0.183  0.02 0.252  0.26 0.739  0.74
```

A.2 Characteristic circularisation and synchronization times (tidal effects)

`tsync_tcirc.c` computes the characteristic times, $t_{\rm sync}$ and $t_{\rm circ}$ for orbit synchronization and circularisation in the case of radiative envelope. It uses the formulae and interpolates the tabulated E_2 and MR^2/I of Zahn (1975), More information can be found in Sect. I.7.

Syntax: `tsync_tcirc M q R a` where `M` is the stellar mass of the primary (in $M_\odot$), `q` the mass ratio of the two components (less than unity), `R` the radius of the primary (in $R_\odot$), and a is the semi-major axis of the orbit (in $R_\odot$).

A.3 Photometry of individual components from global photometry

`compagnon.c` computes the $(B-V)$ and $T_{\rm eff}$ of each component using the global measured values, and the ratio $T_{\rm eff,2}/T_{\rm eff,1}$ derived from our study. This program uses the calibration tables of (Flower 1996, ApJ 469, 355). It was written in Carquillat et al. (2004). to estimate the influence of a companion of an Am star on the global photometry.

Here is an example of input file `compagnon.dat` that was used for Carquillat et al. (2004):

```
# HD, B-V global, Delta V, T1, T2/T1
126031 0.34 1.41 7200 0.87
```

The corresponding output file `compagnon.log` is given below:

```
   HD      B-V   T2/T1   T1      T2      (B-V)1  (B-V)2
 126031  0.340 0.87 7365.5 6408.0  0.307   0.470
```

A.4 Projected periastron distance

`compute_periastron.c` computes the projected periastron distance d_p from $a\sin i$ and e for large data sets:

$$d_p = a\sin i \times (1-e)$$

This program was written to prepare Carquillat & Prieur (2007c).

A.5 Simulation of masses and mass functions $f(m)$, assuming Salpeter's law or a Gaussian function for the mass distribution

`simu_mass.c` This program was written to prepare Carquillat & Prieur (2007c). The theoretical aspects are described in Annexe B. The purpose is to simulate distributions of stellar masses following a Salpeter's law or a Gaussian law, and generate the corresponding histograms of the spectroscopic orbit mass functions $f(m)$. In a subsequent stage, those histograms can be compared with those obtained experimentally with the orbits derived from CORAVEL observations, using statistical tests (see Annexe B).

Syntax:
`simu_mass S,alpha out_histogram out_list`
or:
`simu_mass G,alpha out_histogram out_list`
where `S` and `G` stand for Salpeter or Gaussian distributions, respectively.
The output list file is made of (mass, $f(m)$) couples, which are very numerous (100000 in the present version). This list has been used for debugging purposes, but it is no longer used.

Syntax examples:

- For Salpeter's law with $M^{-0.3}$:
  `simu_mass.exe S,-0.3 histo_M03.dat list_M03.dat`
- For Gauss with mean=0.8 $M_\odot$ and sigma=0.5 $M_\odot$:
  `simu_mass.exe G,0.8 histo_G08.dat list_G08.dat`

Index